# Effect of Rapid Laser Deconsolidation on Intimate Contact Development

Tom Bussink

MSc. Thesis
Aerospace Engineering

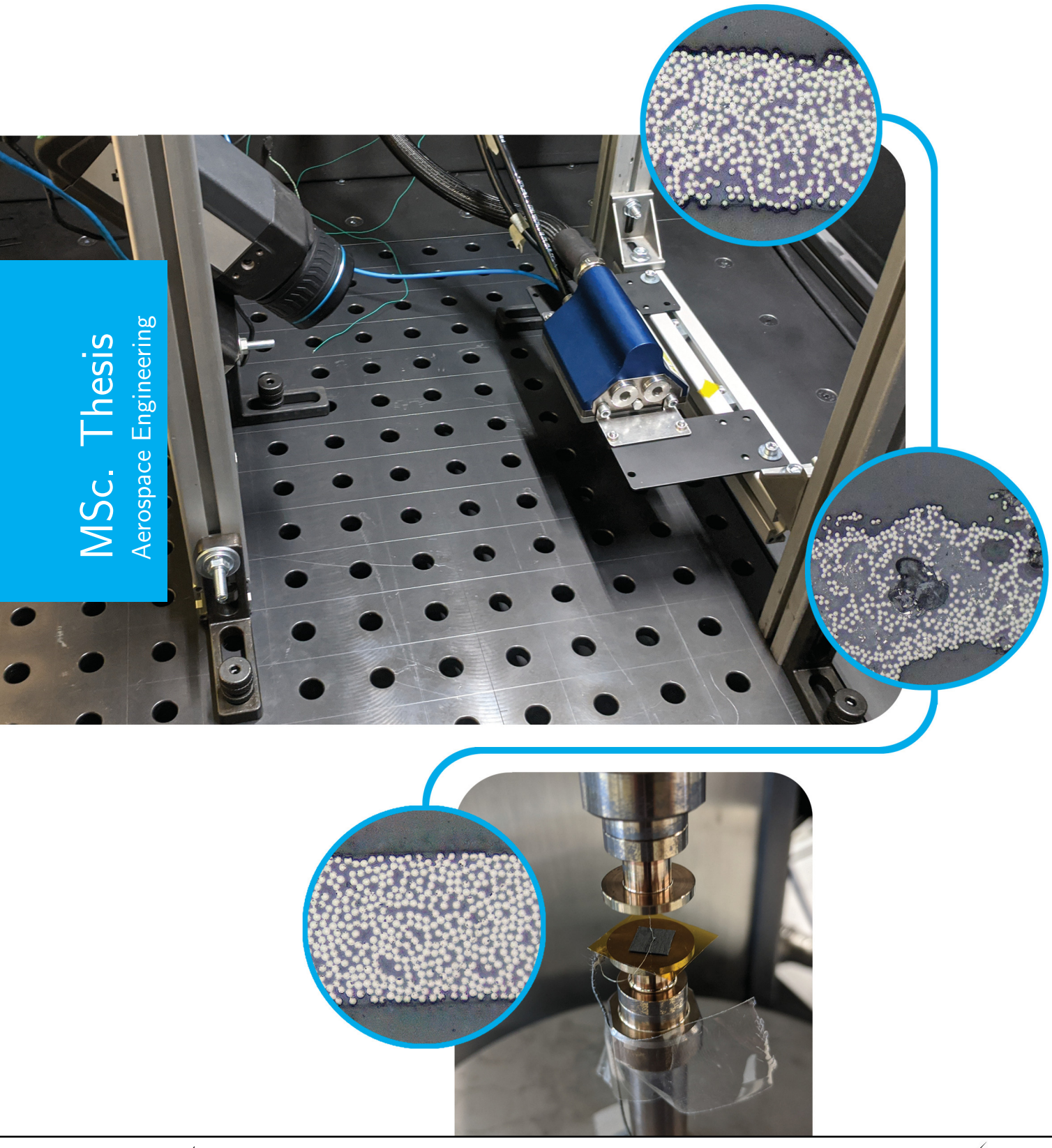

TU Delft Delft University of Technology

July 8, 2021

# Effect of Rapid Laser Deconsolidation on Intimate Contact Development

Master of Science Thesis

For obtaining the degree of Master of Science in Aerospace Engineering
at Delft University of Technology

Tom Bussink

8 July 2021

Faculty of Aerospace Structures & Materials · Delft University of Technology

Delft University Of Technology
Faculty of Aerospace Engineering
Department of Aerospace Manufacturing Technologies

**GRADUATION COMMITTEE**

Dated: 8 July 2021

Chair holder: _____
prof. C. A. Dransfeld

Supervisor: _____
dr.ir. J. J. E. Teuwen

External department: _____
dr.ir. D. M. J. Peeters

Second supervisor: _____
O. Çelik, MSc.

# Summary

Laser-Assisted Fiber Placement (L-AFP) is able to place composite tapes in very precise directions, thereby allowing tailored stiffness designs. The laser is used to heat the thermoplastic matrix material to temperatures above its melting point. Carbon Fiber Reinforced PEEK Thermoplastic Composite (CF/PEEK) is a popular choice for aerospace grade structures due to the high structural performance and high glass transition and melting temperatures. Current L-AFP research is driven by the desire to produce Out-of-autoclave (OOA) laminates with a performance comparable to autoclave level. This will remove manual, labor intensive, and energy consuming steps, leaving a repeatable and automated process that is more predictable.

A key phase for the performance of a laminate during L-AFP is the development of intimate contact. Recent research showed the effects of thermal deconsolidation due to rapid laser heating and questioned the current practice of characterizing the surface of the composite tape material for the intimate contact development models: instead of characterizing the pristine tape surface, the laser deconsolidated surface should be characterized. Additionally, another dominant physical mechanism, driving the intimate contact development was proposed based on the observations of thermal deconsolidation. These ideas are novel and require more extensive understanding of what thermal deconsolidation due to rapid laser heating is, how it affects intimate contact development.

The effects of rapid laser deconsolidation were studied by performing (1) a rapid laser deconsolidation experiment where CF/PEEK samples were prepared and (2) an intimate contact development experiment where the specimens were compressed under constant pressure while being subjected to a temperature profile. Three degrees of deconsolidation were manufactured with the laser set-up: (1) zero deconsolidation by using the as-received tape directly as specimens, (2) slightly laser deconsolidated tapes which experienced maximum temperatures between the glass transition and melting region, and (3) highly laser deconsolidated tapes that experienced temperatures above the melting point. All samples were characterized on void content, roughness, and waviness; all of which significantly increased which showed that the state of the tape right before the nip-point during L-AFP is significantly different than the pristine state of the CF/PEEK tape.

The intimate contact development experiment was carried out with pressure levels of 10, 50, 100, and 300 kPa reaching maximum temperatures of 363 °C. Decreasing the degree of deconsolidation or increasing the pressure resulted in better consolidation. At 10 kPa, most of the characterization showed very little difference from a pristine tape, but a significant amount of Degree of Effective Intimate Contact (DEIC) was developed, with 36 % for the highly laser deconsolidated tape to 46 % for the as-received degree of deconsolidation. At the highest pressure of 300 kPa, no significant difference between the degrees of deconsolidation was observed as the average DEIC values are between 85 to 87 %. Additional intimate contact development temperature settings below melt showed that no intimate contact was developed below the melting temperature. During the glass transition, a significant compaction occurred which eliminated most of the void content. Between the glass transition and melting temperature, however, void content, thickness, and roughness all remained constant. At the melting point, a second thickness compaction occurred together with the development of DEIC and decrease of roughness which appeared to also relates with resin percolation.

# Contents

# List of Figures

# List of Tables

# List of Abbreviations

**AFP** Automated Fiber Placement.

**ASR** As-received tape: to label the zero degree of deconsolidation, thus the specimens that were not subjected to the laser.

**ATL** Automated Tape or Tow Laying.

**ATP** Automated Tape or Tow Placement.

**CF/PA6** Carbon Fiber Reinforced Polyamide-6 Thermoplastic Composite.

**CF/PEEK** Carbon Fiber Reinforced PEEK Thermoplastic Composite.

**CF/PEKK** Carbon Fiber Reinforced PEKK Thermoplastic Composite.

**DEIC** Degree of Effective Intimate Contact.

**DMTA** Dynamic Mechanical Thermal Analysis.

**DSC** Differential Scanning Calorimetry.

**GMT** Glass Mat reinforced Thermoplastic(s).

**HLD** Highly Laser Deconsolidated: the severely deconsolidated specimens which were subjected to temperatures above the melting temperature of the tape.

**ILSS** Inter-Laminar Shear Strength.

**IR** Infrared light.

**L-AFP** Laser-Assisted Fiber Placement.

**LSCM** Laser Scanning Confocal Microscope.

**OHC** Open-Hole-Compression.

**OOA** Out-of-autoclave.

**PEEK** Polyether Ether Ketone.

**PEI** Polyetherimide.

**SLD** Slightly Laser Deconsolidated: the middle degree of deconsolidation which were heated by the laser to temperatures between the glass transition and melting point.

**VCSEL** Vertical-Cavity Surface-Emitting Laser.

# Chapter 1

# Introduction

Fiber reinforced composite structures have been a topic of interest for a long time in the aerospace sector and beyond. Usage of composites increased from 15% in the Airbus A320 and 25% in the Airbus A380 [9] to 50% composite weight ratio in the Airbus A350 XWB and Boeing 787 Dreamliner [10, 11]. Current manufacturing processes for composites rely on an autoclave step to cure the thermoset epoxy or to fully consolidate the thermoplastic plies while decreasing the void content to less than 1% [12]. The autoclave step is expensive as it consumes a lot of energy, time, and manual labour. A promising solution to make thermoplastic composite manufacturing more competitive is by adapting Out-of-autoclave (OOA) techniques. Automated Fiber Placement (AFP) is a production process where thermoplastic carbon fiber tapes are first heated above melting temperature and then placed on top of each other by a robot; allowing to produce geometrically contoured parts, while controlling stiffness direction properties. Additionally, this method produces much more consistent quality than manual lay-up by hand, thus less performance variation, resulting in lower design margins. Yet, after lay-up these parts are often vacuum bagged and further consolidated in an autoclave. By means of in-situ consolidation, a thermoplastic tape above its melting temperature can be fully consolidated onto the previous layers with enough pressure and consolidation time. While autoclave and press-consolidated processed thermoplastic composite parts are already used in aircraft production, OOA AFP laminates require mechanical performance closer to autoclave processed parts at industry desired lay-up speeds in order to satisfy aerospace performance demands and economical viability [13]. Current developments focus on laser heating to elevate the composite tape temperature

This thesis aims to contribute to the understanding of the physical mechanisms that play a role during L-AFP by investigating the effect of the laser heating phase on the subsequent development of intimate contact which plays an essential role in the final laminate quality and performance properties.

First, Chapter 2 provides a general overview of the L-AFP process which will then elaborate on the importance of intimate contact development and the leaser heating phase on the laminate quality. Based on the literature assessment, Chapter 3 identifies a gap and formulates the research questions and hypotheses. Chapter 4 describes the material, experimental set-ups and characterization methods that are employed. The preparatory rapid laser deconsolidation results are presented in Chapter 5 and the intimate contact development results are discussed in Chapter 6. The research will be concluded in Chapter 7. Finally, Chapter 8 suggests improvements of the current study and other potential directions that can be pursuit to further advance knowledge about the effects of the laser heating phase and intimate contact development.

# Chapter 2

# Literature Review

This chapter dives deep into the state of the current literature. Section 2.1 provides an overview of the L-AFP process. Section 2.2 explains why bonding is both a prerequisite and key driver to achieve interlaminar strength. Intimate contact developments, which is the first phase of bonding, is discussed in Section 2.3. One of the aspects that is often not taken into account in L-AFP simulation models, is the effect of the laser heating on the composite material. Section 2.4 provides a review of the conventional thermal deconsolidation literature and the differences with the thermal deconsolidation during rapid laser heating. Section 2.5, then explains a novel intimate contact theory that was proposed based on observations of thermal deconsolidation due to rapid laser heating. In the last section, Section 2.6, main points are concluded which also serves as a prelude to the research framework that is presented in the next chapter.

## 2.1 Laser-Assisted Fiber Placement

Two common processes are present for automated lay-up; AFP which defines narrow tapes that are able to lay-up double curved parts and Automated Tape or Tow Laying (ATL) aimed to wider tapes, thereby able to lay-up a bigger area than a single tape, but only able to operate single curved parts. Automated Tape or Tow Placement (ATP) is often used to refer to both processes. Neglecting curvature and tape steering, all these processes are fundamentally the same. This thesis study will stick to the AFP terminology, but the findings can be applied to any form of tape laying.

**Heat Source** To achieve in-situ consolidation, a heat source is required to heat up the thermoplastic matrix above its melt temperature. Various heating sources have been used and proposed in literature as one of the most used conventional methods [14, 15]. However, advancements in laser technology led to comparisons favoring L-AFP for its heating efficiency and response time [16, 17]. Early research with $CO_2$ lasers was positive [18], but there is interest in Infrared light (IR) spectrum lasers, such as VCSEL, where the matrix is transparent to the laser, enabling to directly heat the fibers and reducing matrix oxidation and burning.

**Process Description** An illustration of all the components is given in Figure 2.1, this paragraph discusses the components involved. A laser is directed towards the nip-point, where the incoming tape and substrate merge, and heats both incoming tape and substrate. Process settings determine the heated lengths of the tape and substrate and the angle of incidence of the laser affects how close the laser light can approach the nip-point. At the nip-point, the incoming tape shall be above melting temperature in order to allow bonding between the incoming tape and substrate. Figure 2.2 shows tape and substrate temperatures as well as the applied pressure during the process. The thin tape dissipates its energy via convection to the surrounding air while the substrate, probably consisting of multiple layers, is also in contact with the tool it is layed on. Towards the nip-point it is harder to heat the tape since the tape aligns more and more parallel to the laser beam. Additionally, close to the

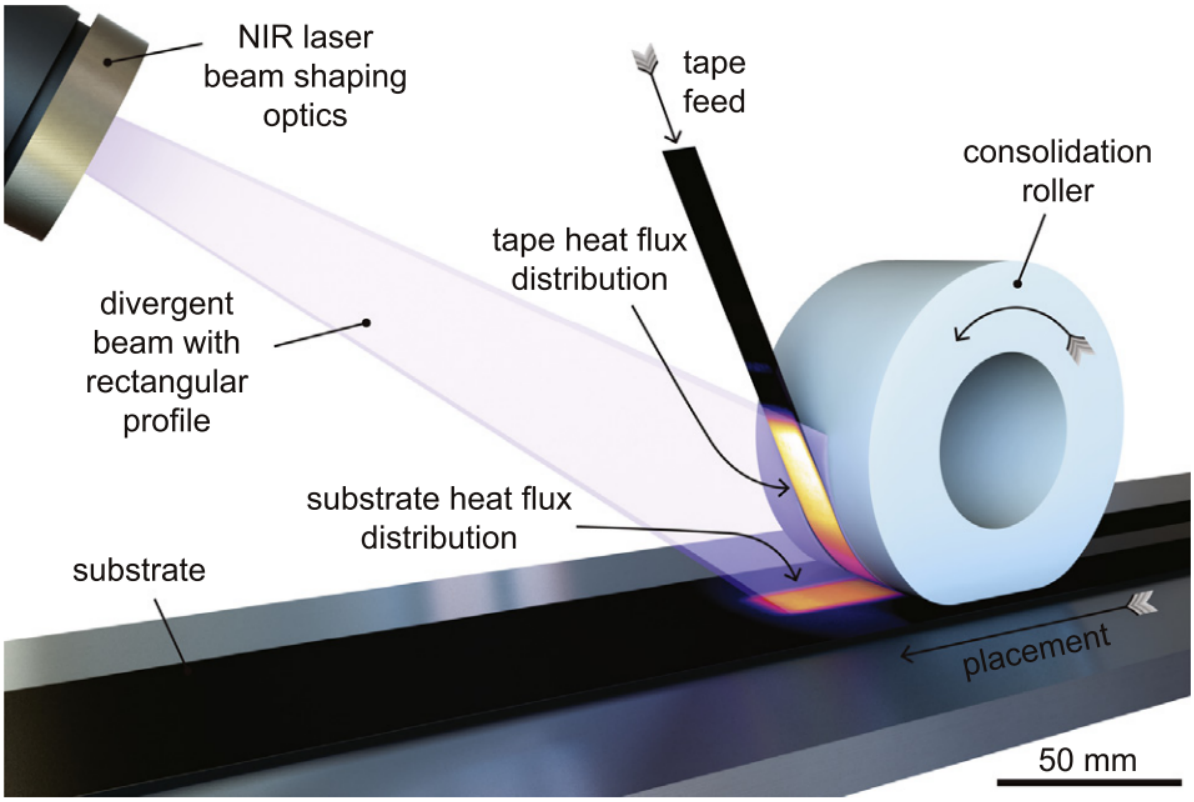


Figure 2.1: L-AFP process configuration. Figure from [1].

nip-point there is a shadow region where the laser will not reach the tape and substrate. Hence, the maximum temperature is achieved before the nip-point. At the nip-point, the tape and substrate make contact and their temperatures merge to a single temperature. At the same time, the consolidation roller quickly starts to apply pressure and bonding can occur. After the consolidation roller has passed, the pressure is released and temperature keeps decreasing as there is no heat applied any more after reaching the laser shadow area in front of the nip-point.

When the molten tape and substrate make initial contact, the pressure will deform the material to align with each other. The process of geometric deformation of the tape to align with the substrate or tool is called intimate contact development. Figure 2.3 (a) illustrates two polymeric mediums that developed full intimate contact with a dashed line representing the interface that is still apparent. In the next step, Figure 2.3 (b), the polymer chains of the matrix between the two mediums start to intermingle which is called autohesion. Finally, provided that the polymer chains had enough mobility, applied pressure and time to diffuse, the interface will disappear as there is full intermingling of the polymer chains between both sides of the interface as is seen in Figure 2.3 (c). Thus the tape and substrate will be fully bonded. The lay-up speed and contact area of the consolidation roller determine the amount of consolidation time for the intimate contact development and subsequent autohesion. The autohesion process occurs above the glass transition temperature for amorphous polymers and scales with the chain mobility, thus at higher temperatures the autohesion occurs faster. The required pressure is less important as the required pressure to compact the fiber bed is much higher [3]. During this process, temperature has an important impact on the material characteristics, such as viscosity, and the also final laminate properties for example relating to the crystal lattice structure are affected by the processing window of the L-AFP process.

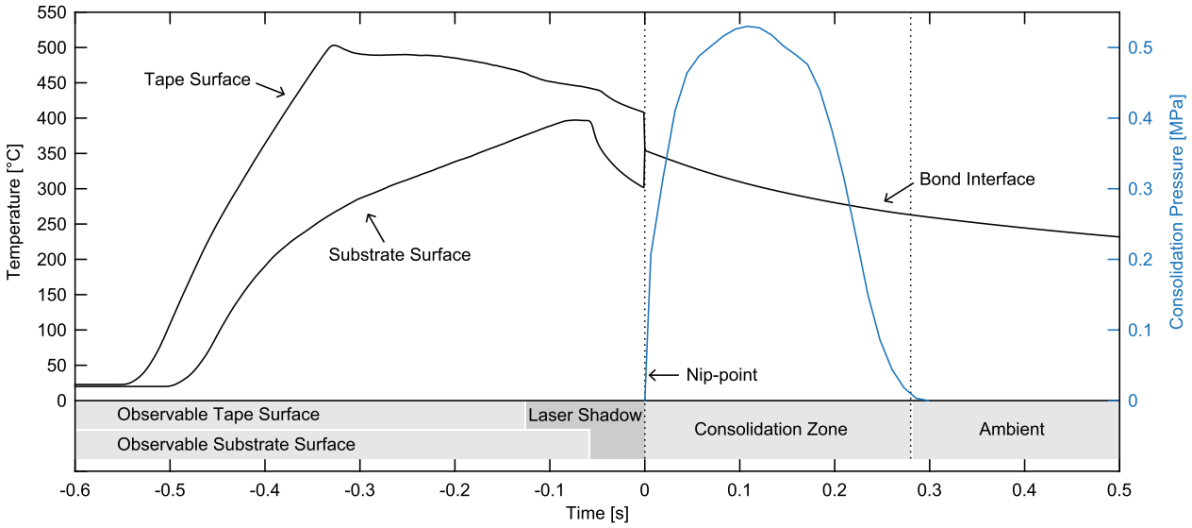


Figure 2.2: Temperature and pressure measurements during L-AFP lay-up. Figure from [2].

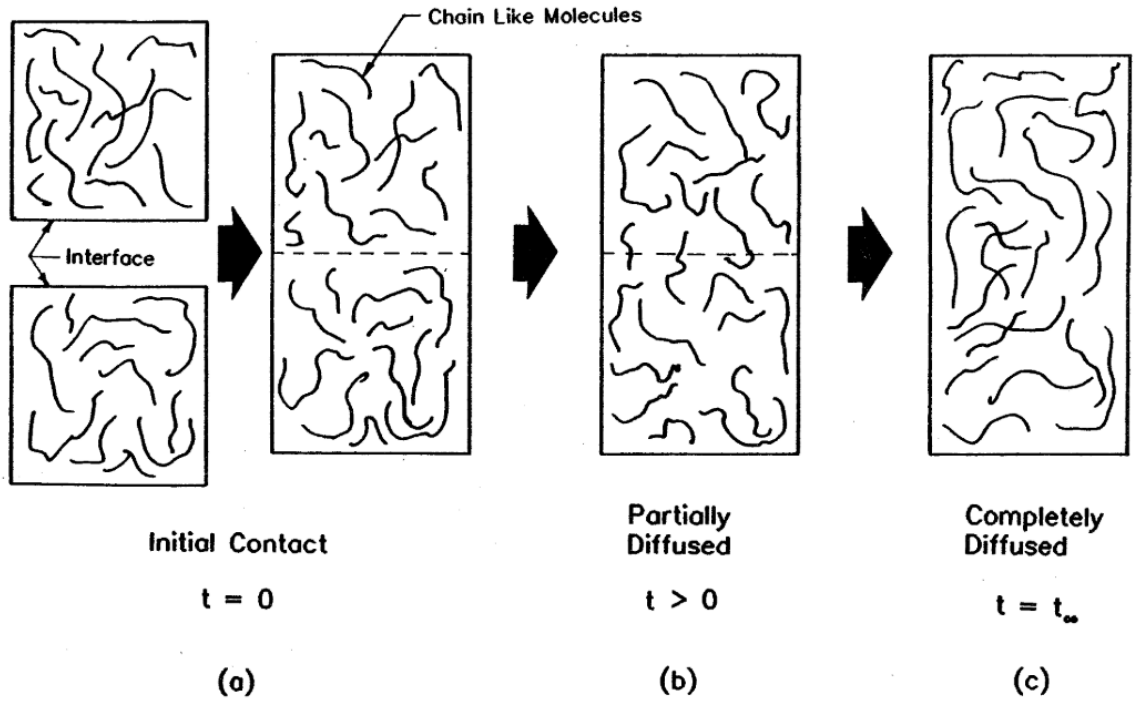


Figure 2.3: Autohesion of polymer chains. Figure from [3].

## 2.2 L-AFP Laminate Performance and Quality

One of the main goals is to achieve laminate performance comparable to autoclave quality at lay-up speed desired by industry. The latter is relative and depends on the industry and purpose of the produced part. This section will look at the mechanical performance of L-AFP produced laminates versus conventionally produced laminates such as press-consolidation and autoclave.

OOA CF/PEEK L-AFP laminates performed worse than autoclave consolidated laminated ones in flexural strength and stiffness, Inter-Laminar Shear Strength (ILSS) and Open-Hole-Compression (OHC) experiments due to more interlaminar voids present between the plies [13]. The interlaminar voids represent areas between the plies where no bonding has been achieved. Interestingly, in the same research [13], the OOA L-AFP laminates performed better in wedge peel strength performance. More plastic deformation of the matrix was possible due to the highly amorphous morphology of the polymer whereas the autoclave laminate exhibits a stronger fiber-matrix interface than matrix-matrix performance. Bonding between two plies is a prerequisite to achieve any interlaminar strength. The degree of bonding, $D_b$, is a key driver to predict the interlaminate bond strength [19, 20].

## 2.3 Squeeze Flow Based Intimate Contact Development

This section introduces intimate contact development in general. Starting with its relation and importance with respect to the laminate quality by discussing bonding in Section 2.3.1. The physical mechanism is presented by discussing the well established modeling approaches based on concept of squeeze flow of surface asperities in Section 2.3.2. Note that some of the findings in Section 2.4 question this squeeze flow of surface asperities theory and Section 2.5 presents a different an approach involving the physical mechanisms related to the flow through a permeable medium. Sections 2.3.3 and 2.3.4 present the approaches to characterize the material viscosity and tape surface representation. Section 2.3.5 discusses various methods to measure the developed intimate contact.

### 2.3.1 Bonding

As explained by Dara and Loos [3], bonding can be decomposed into the development of intimate contact where two surfaces conform their geometry and, subsequently, the autohesion process during which the polymer chains diffuse across the interface resulting the interface to disappear (no microscopic distinction can be observed) between both sides. During autohesion, the bond strength is developed [3, 19–22]. A simplified expression for the degree of bonding is provided by Mantell and Springer [23],

$$D_b = D_{ic} D_{ah} \tag{2.1}$$

where $D_{ic}$ is the degree of intimate contact and $D_{ah}$ is the degree of autohesion. A nonisothermal autohesion model of Yang and Pitchumani is often used [19, 20], however for the purpose of simplifying the equations or longer processing times, one can assume instantaneous autohesion $D_{ah} = 1$ [23] which emphasizes the importance of the intimate contact description

$$D_b \approx D_{ic}, \tag{2.2}$$

hence this section focuses purely on the intimate contact development due to its importance to the laminate strength.

### 2.3.2 Simulation Models

Dara and Loos [3] also proposed an intimate contact development model wherein the tape surface is represented as a statistical distribution of rectangle sizes that flatten under the applied force. Also, only half (top or bottom surface side) of a single tape is modeled which is then subjected to compression by a rigid surface, this is equivalent to two mirrored tapes that have the exact same surface asperity distribution that are being pressed onto each other. This principle of squeeze flow of surface asperities became the standard for intimate contact development model in thermoplastic composite AFP research.

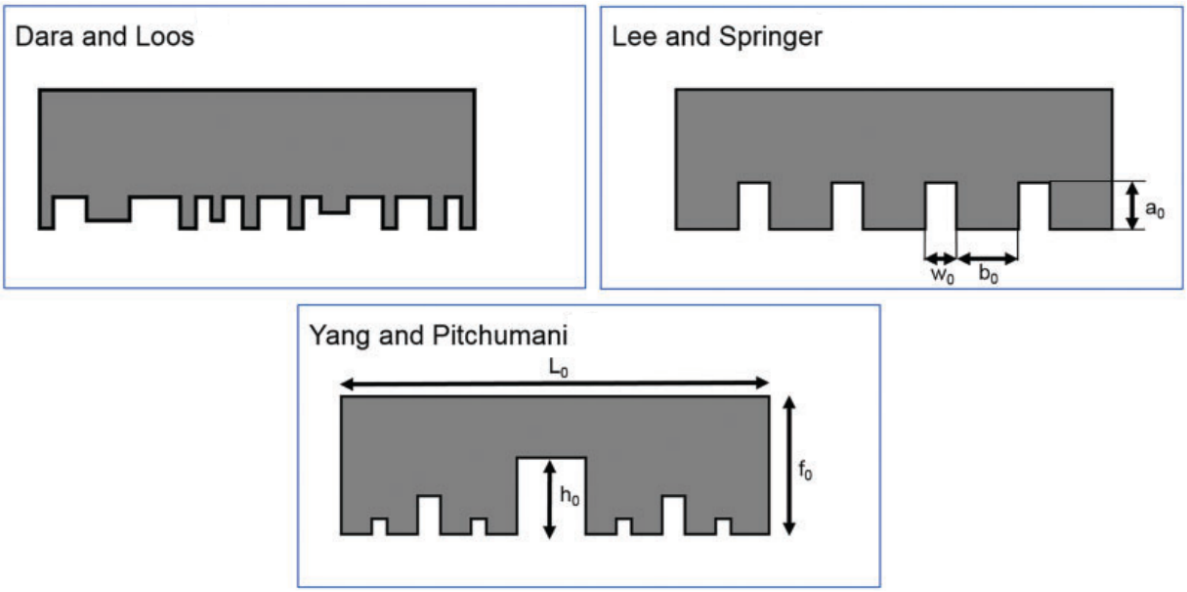


Figure 2.4: 2D surface representations for the intimate contact models from: Dara and Loos [3], Lee and Springer [4] and Yang and Pitchumani [5]. Figure from [6].

Lee and Springer [4] simplified the model to equally sized rectangles, and Mantell and Springer [23] slightly reformulated the formula to allow for time dependent pressure and viscosity

$$D_{ic} = \frac{1}{1+\frac{w_0}{b_0}}\left[1+5\left(1+\frac{w_0}{b_0}\right)\left(\frac{a_0}{b_0}\right)^2\int_0^{t_C}\frac{P}{\mu_{mf}}\mathrm{d}t\right]^{\frac{1}{5}}, \tag{2.3}$$

with ratios $\frac{w_0}{b_0}$ and $\frac{a_0}{b_0}$ describing the width and aspect ratio of the rectangular elements (see Figure 2.4), $P$ the applied pressure, $\mu_{mf}$ the fiber-matrix viscosity, the latter two integrated over the consolidation time $t_C$. Figure 2.4 depicts the difference between the surface representations of Dara and Loos [3] and Lee and Springer [4]. This formulation and a simplified version [23] have been widely used in literature to simulate and validate intimate contact development [14, 24–31].

Another model, by Yang and Pitchumani [5], based on the squeeze flow of surface asperities makes use of surface roughness measurements to represent the surface as a fractal cantor set

$$D_{ic}^{(n)} = \frac{1}{f^n}\left[\frac{5}{4}\left(\frac{h_0}{L_0}\right)^2\frac{f^{\frac{2nD}{2-D}+n+4}}{(f+1)^2}\int_{t_{n+1}}^{t}\frac{P}{\mu_{mf}}\mathrm{d}t+1\right]^{\frac{1}{5}}, \tag{2.4}$$

calculating the degree of intimate contact, $D_{ic}$, for each generation $n$ between $t_{n+1} \leq t \leq t_n$, with $D$ and $f$ the fractal dimension and scaling factor that represent the surface and are obtained together with the geometrical parameters of the first generation $f_0$, $h_0$, and $L_0$ (see Figure 2.4 for an illustration) via surface characterization. Being based on actual profile measurements and incorporating asperity feature the sizes spanning multiple orders of magnitude, see Figure 2.4 for an illustration incorporating three fractal iterations, this model has also been widely used [1, 20, 32–37].

### 2.3.3 Viscosity

Even though the aforementioned models have been widely adopted by literature, there exists a lack of consensus regarding the viscosity. The authors of the aforementioned intimate contact models [4, 5, 23, 24] and others following their approach [15, 38, 39], use the fiber-matrix viscosity in the direction perpendicular to the fibers, which can be argued by fact that the squeeze flow behavior extends the tape width and, therefore, the modeled rectangular surface asperities as well. Fiber-matrix viscosity and has been characterized by many researchers via the squeeze flow method [34, 40–44] as well as other methods such as off-centered oscillatory rheometry [45, 46], a picture-frame experiment [47], and

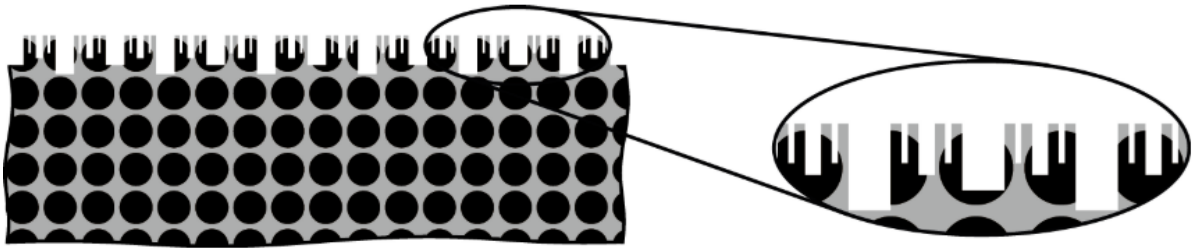

Figure 2.5: Illustration of surface asperity size of Yang and Pitchumani's [5] fractal surface representation with respect to carbon fiber size for the purpose of chossing between matrix and fiber-matrix viscosity. Picture from [7].

a fiber pull-out set-up [48]. However, the resulting CF/PEEK viscosity values, from one publication to another, range up to 2 orders of magnitude [46].

However, other researchers apply only the matrix viscosity without further reasoning [29, 31], base their decision on the observation of a resin rich surface or areas [6, 7, 14], or argue that the surface asperity size is smaller than the diameter of a carbon fiber and it is the matrix that needs to flow in order to achieve development of intimate contact [7] which as Figure 2.5 depicts is not physically possible for the fiber-matrix medium.

### 2.3.4 Surface characterization

All intimate contact models require a surface representation. These can are measured from the tape, but sometimes they are also obtained by fitting the material parameters of the intimate contact development model. This section provides a brief overview of machines used to characterize the surface directly. A 2D surface profile can be extracted from cross-sectional microscopy images [4, 7, 30]. To obtain a 3D surface, contact profilometry can be used [5, 6], where Schaefer [6] also used atomic force microscopy to supplement his fractal model with more detailed data. Nowadays, non-contact profilometry via confocal microscopy allows to measure fine details without touching and potentially damaging the sample [29, 39, 49, 50].

### 2.3.5 Intimate Contact Measurement

It is difficult to measure the developed degree of intimate contact. Often, the degree of intimate contact characterization methods only measure the degree of bonding or the bonding is assessed via structural performance of the laminate. This section will not cover methods that work via mechanical testing. Ultrasonic C-scans have been used to detect whether the layers in a laminate form a continuous medium or if an interface is detected [3, 5]. Cross-sectional microscopy can also be used to quantify the voids between two layers of a laminate, these areas can than be considered to not be in intimate contact [7, 30, 50, 51]. Another method, presented more recently is via X-ray computed tomography [6].

All the aforementioned methods require bonding of two layers of tape. Çelik et al. [39] proposed a method two quantify the degree of intimate contact for a tape being layed onto a flat rigid tool, applying Otsu's threshold on the optical grayscale measurement of the surface. Instead of intimate contact, the concept Degree of Effective Intimate Contact (DEIC) was introduced as the method only quantifies flattened resin rich surface area. An advantage of this characterization is that it can be more relevant considering resin is required for autohesion to occur, hence only DEIC area can perform polymer reptation across the interface of two thermoplastic composite tapes. Additionally, intimate contact models also simulate the deformation of a single tape onto a rigid surface, the experiment is, therefore, more comparable to the intimate contact models than L-AFP experiment laying a tape onto a substrate.

## 2.4 Thermal Deconsolidation

Deconsolidation does not have an exact definition and is often used to describe the state of the interface between two tapes. However, deconsolidating can also occur for a single ply or carbon fiber tape. Ye et al. [52] describes thermal deconsolidation of a thermoplastic composite as a negative impact on the meso-structure or macro-performance induced by a heating cycle and also introduces the term 'degree of deconsolidation' to describe the severity of the deconsolidation.

### 2.4.1 General Thermal Deconsolidation Mechanisms

Mechanisms that affect deconsolidation are [53]:

1. "Decompaction of the fiber reinforcement network
2. Void expansion of the interlaminar and intralaminar voids due to thermal gas expansion and internal void pressure
3. Void shrinkage and coalescence of smaller voids into larger voids due to surface tension
4. Thermal expansion and viscoelastic behavior of the composite matrix"

Because void content can be quantified it is often used as an indication to express the degree of deconsolidation [52, 54, 55]

An intralaminar void model in AFP research is based on the concept of deconsolidation in conjunction with Darcy's law [56]. Khan et al. [15] applied this void model and relates the heating phase of the tape with deconsolidation, which is then reversed under the pressure of the compaction roller, but another deconsolidation increase takes place when the compaction roller leaves the tape while being above the glass transition temperature. The deconsolidation, observed by Khan [15], occurs above the glass transition temperature is due to the lack of pressure. Increasing pressure results in less deconsolidation [57] until a certain minimum consolidation pressure is reached [55]. Due to the various mechanisms at play, different values for minimum pressure have been found ranging from 20 kPa [40] to 200 kPa [54] for certain CF/PEEK compositions.

### 2.4.2 Rapid Laser Deconsolidation

The research from the previous section is based on slow heating rates when compared to the L-AFP process; Comer et al. [13] measured temperature rates of 442 °C/s and Figure 2.2 from Stokes-Griffin and Compston [58] shows a tape reaching 500 °C in less then 0.2 s and only another ∼0.3 s later the consolidation roller applies pressure to the tape. Hence, the time-frame in L-AFP deconsolidation is much smaller which can have a significant effect on for example void development which can takes place in in order of seconds [59]. Similarly, observations regarding the springback effect in deconsolidation that is evaluated over a time span in the order of minutes [60] cannot directly be assumed to hold true for the process conditions in L-AFP.

For the purpose of this thesis, the definition 'Rapid Laser Deconsolidation' is introduced in order to distinguish the thermal deconsolidation experienced by a tape during L-AFP from the more general or less specifically defined term (thermal) deconsolidation.

**Definition: Rapid Laser Deconsolidation**

*Thermal deconsolidation of a thermoplastic composite tape due to rapid laser heating from room temperature to temperatures above the glass transition within a second.*

In 2018, Kok [7] presented research about the effects of rapid laser deconsolidation using an L-AFP set-up and constraining the minimum gap length that the unidirectional CF/PEEK tapes could consolidate. Key mechanisms that were observed are fiber bed decompaction via fibers popping out of the fiber bed which also leave cavities with voids behind and an increase in void size which suggests void expansion and merging of smaller migrating voids. These observations are similar to the mechanisms from more traditional thermal deconsolidation research [52, 53] discussed in the previous sub-section.

Slange et al. [61] compared the deconsolidation mechanisms of L-AFP and press consolidated produced blanks from unidirectional CF/PEEK tape material and found that these have different key drivers. Where thermal expansion of dissolved moisture was found to be most crucial for the press consolidated blanks, L-AFP produced blanks deconsolidated to a greater extend due to other mechanisms related to frozen-in fibers stresses.

A design of experiments study of the main mechanisms of rapid laser deconsolidation via a VCSEL of CF/PEEK tapes by Choudhary [49] confirmed fiber decompaction as a mechanism and to be related to residual stresses which, together with void growth due to absence of applied pressure, cause a thickness of the tape. Also, large local temperature variations of ±100 °C were observed and related to the out-of-plane deformation. Minimizing the degree of deconsolidation is not straightforward as shorter heating times did cause less surface roughness, void content and thickness increase, but the out-of-plane deformation and width of the tape were affected to a greater extend.

### 2.4.3 Effect of Rapid Laser Deconsolidation on Intimate contact Development

The intimate contact models based on the squeeze flow of surface asperities from Section 2.3 have all been applied with characterization input from a pristine tape surface. Kok [7] was the first to consider the effects of rapid laser deconsolidation on the application of the intimate contact development models. The degree of intimate contact obtained from L-AFP experiments was compared simulation results of Yang and Pitchumanis [5] model evaluated for both as-received and rapid laser deconsolidated tapes. The rapid laser deconsolidated tape fractal surface representation exhibited wider and higher asperity size than the as-received tape which caused the rapid laser deconsolidated simulation to yield higher degrees of intimate contact that were closer to the experimental results. Here the model favors the rougher surface representation whereas literature assumes that smoother tapes promote intimate contact development [62].

Kok [7] also showed that the rapid laser deconsolidated surface was more fiber rich than the as-received state. Resin is required for bonding to occur and resin rich surface tapes are generally assumed to promote the development of intimate contact [6, 14, 62, 63]. Fiber rich bundles can potentially prevent local void filling by the matrix and fiber rich through the thickness bundles can limit further thickness reduction of the tape as a whole [62]. In another investigation, Slange et al. [64] showed better consolidation of stamped L-AFP produced blanks with a resin rich surface than the blanks without a resin rich surface.

## 2.5 Fiber Re-impregnation Based Intimate Contact Development

Based on the fiber rich surface observations due to rapid laser deconsolidation, Kok [7] proposes another intimate contact development mechanism: instead of the squeeze flow of surface asperities, Kok argues that fiber re-impregnation is needs to take place in order to achieve intimate contact of dry fiber area.

As basis, Kok uses the 1D fiber impregnation model used in Glass Mat reinforced Thermoplastic(s) (GMT) research [65] where fiber impregnation is described by Darcy's law, expressing the flow velocities of liquid matrix, $u_l$, and solid fiber network, $u_s$, as

$$u_l - u_s = -\frac{K}{\mu\,(1 - V_f)}\frac{\partial P}{\partial z} \tag{2.5}$$

with, the permeability of the fiber network $K$ as a function of the fiber volume density $V_f$, matrix viscosity $\mu$, and the pressure gradient along the thickness direction $\frac{\partial P}{\partial z}$. Kok only considers the tape half that makes contact with the tool or substrate, as the roller acts as heatsink thereby quickly increasing the local tape viscosity. Figure 2.6 illustrates such a control volume. Initially, a large part of the 1D control volume is already impregnated, denoted by the distance $Z_I$, and has an initial fiber volume content $V_{f0}$. While $Z_D$ is the distance of dry fibers due to the rapid laser deconsolidation. Kok found a dry fiber bed thickness of about 8 µm for most part of the tape and a maximum of 20 µm for his rapid laser deconsolidated tapes. When pressure is applied, the dry fiber bed first 'instantaneously' compacts and then the matrix flows through the fiber bed described by Darcy's law, wetting the dry fiber area.

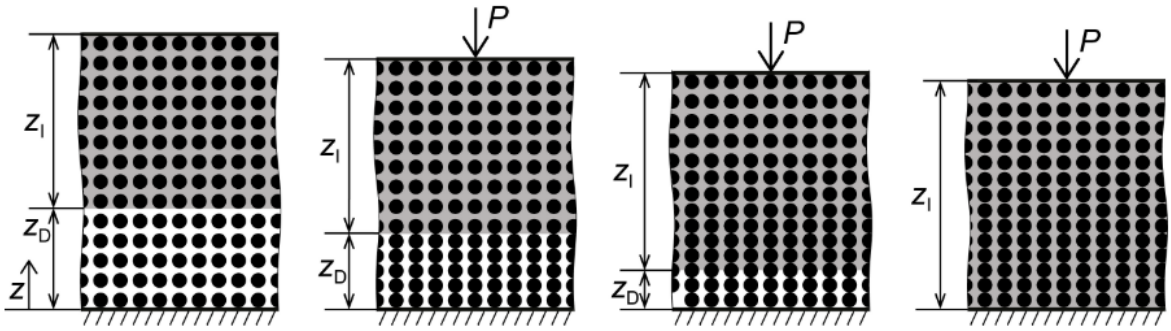


Figure 2.6: Illustration of 1D fiber impregnation model described by Darcy's law. Figure from [7].

Intimate contact is reached for a control volume when there is no dry fiber bed over to be impregnated, $Z_D = 0$. Via cross-sectional microscopy, a tape cross-section is divided into 50 partitions along the width, each partition is then modeled as a control volume by extracting the volume fractions of the fibers and matrix along the thickness direction of the partition. The sum of control volumes that reached full re-impregnation of the dry fiber bed after a set time over the total amount of control volumes is developed intimate contact.

After subjecting Equation (2.5) to conservation of mass of the liquid and solid mediums and relating the pressure gradient to the fiber compaction stress $\sigma_c$, Kok ends up with the following formulation

$$\frac{\partial V_f}{\partial t} + \frac{\partial}{\partial z}\left(-\frac{K\, V_f}{\mu}\frac{\partial \sigma_c}{\partial V_f}\frac{\partial V_f}{\partial z}\right) = 0. \tag{2.6}$$

The fiber volume fraction, $V_f$, input is obtained from the cross-sectional microscopy analysis of deconsolidated tapes which leaves the need for material models of the matrix viscosity $\mu$, fiber bed permeability $K$, and fiber bed compaction stress $\sigma_c$.

Darcy's law describes the flow of a liquid with a certain viscosity through a permeable medium. Hence, it is clear that matrix viscosity is required and the fiber-matrix viscosity is not relevant to the 1D flow which is not that straight forward for the squeeze flow models discussed in Subsection 2.3.3. Kok used a temperature dependent Arrhenius law, which is regularly used in thermoplastic processing [4, 14, 31, 35], to describe Polyether Ether Ketone (PEEK) viscosity as a Newtonian fluid.

Several approaches exist to describe the permeability of a unidirectional fiber bed as a function of the fiber volume fraction. Kok seems to have used the modified Carman-Kozeny model from Gutowski et al. [66]

$$K\left(V_f\right) = \frac{r_f^2}{4k_0}\frac{\left(\sqrt{\frac{V_a}{V_f}} - 1\right)^3}{\frac{V_a}{V_f} + 1}, \tag{2.7}$$

the physical fiber radius $r_f$ is straightforward, the available fiber volume fraction $V_a$ allows to tune the fiber volume fraction value at which the fiber bed becomes impermeable and can either be based on perfect geometrical packing density or by fitting the model with data [66–69], and the Carman-Kozeny constant $k_0$ which is determined based on fitting. Unfortunately, Kok [7] did not provide the value used for the Carman-Kozeny constant. Instead of semi-empirical Carman-Kozeny based formulations, Gebart [68] presented a purely geometrical input dependent model based on the Navier-Stokes equations. With these different formulations and variance in literature reported values, predicting permeability is not straightforward and varies based on assumptions and estimations.

From semi-empirical models that conceptualize carbon fibers as bending beams between the contact points with their neighboring fibers, Kok estimated the fiber bed compaction stress using Gutowski and Dillons [70] formulation

$$\sigma_c\left(V_f\right) = \frac{3\pi E_f}{\beta^4}\frac{\left(1 - \sqrt{\frac{V_f}{V_0}}\right)}{\left(\sqrt{\frac{V_a}{V_f}} - 1\right)^4} \tag{2.8}$$

which depends on the Youngs modulus $E_f$ of the fibers, a parameter $\beta$ that represents a waviness defined by the fiber contact points with its neighboring fibers along its length, and the fiber volume fraction $V_0$ which describes the state when no pressure would be applied and can be estimated via the available fiber volume fraction $V_a - V_0 = 0.38$ which Kok did. Equation 2.8 is somewhat arbitrary [66] and Gutowski also uses slightly different formulations of the fiber volume fractions to match their data [67].

Potential improvements of the fiber re-impregnation as basis for intimate contact development consist of expanding the model to take transverse flow into account, allowing filled control volumes to further wet neighboring control volumes or applying a more general 2D formulation. Pressure distribution might be affected by the local thickness and amount of developed intimate contact. Additionally, the material models might be better characterized for the conditions of a rapid laser deconsolidated tape such as optimizing the fit of the models for the fiber volume range that is present in the tape laying process.

## 2.6 Conclusion

L-AFP was first introduced and the desire for OOA production due to increased repeatability, decreased production cost, and less energy consumption was made clear. Currently achievable CF/PEEK laminate quality reports from literature showed that laminates can already exhibit performance properties close to autoclave level. However, to reach industry desired lay-up rates, there are still significant improvements to be made.

Bonding, or more specifically the prior development of intimate contact, was shown to be a prerequisite for any interlayer load transfer. Increasing the developed intimate contact will increase ILSS and other laminate performance properties. Currently, intimate contact development models are based on the concept of squeeze flow of surface asperities and are the standard for simulations and input of other mechanisms such as thermal contact resistance are dependent of the in-situ degree of intimate contact. However, there is less unity regarding the fiber-matrix viscosity input for these models, values found in literature range up to two orders of magnitude. Additionally, different opinions exist whether to use fiber-matrix or only the matrix viscosity.

The definition of 'Rapid Laser Deconsolidation' was proposed: thermal deconsolidation due to rapid laser heating. Literature evidence of the effects of rapid laser deconsolidation on roughness, fiber-matrix composition, fiber network decompaction, and void content was presented. Taking the rapid laser deconsolidation induced roughness increase into account increased current squeeze flow based intimate contact development models.

Based on the fiber decompaction observations, more specifically the dry fiber bed resulting from rapid laser deconsolidation, Kok [7] proposed an intimate contact model based on re-impregnating the dry fiber bed. This fiber re-impregnation model was further discussed and the input material models were briefly reviewed.

# Chapter 3

# Research Framework

The previous chapter showed several gaps in the current literature. A selection of these gaps are summarized and presented in Section 3.1 to form the basis for this thesis. A framework is set-out in Section 3.2 to conceptualize a plan to investigate the research gap. With the research gap and framework in mind, the reader can put the posed research questions in Section 3.3 into context. Derived from these research questions, the research will be subjected to the set of hypotheses formulated in Section 3.4.

## 3.1 Research Gap

Before Kok [7], rapid laser deconsolidation was not considered when characterizing the surface for intimate contact development models. Instead, all widely accepted intimate contact development models [3–5, 23] are purely set-up with the as-received state of a tape in mind. Several researchers further explored some aspects of rapid laser deconsolidation [49, 61], others considered it in their observations [63, 64, 71]. However, it is not yet widely recognized as the concept of thermal deconsolidation is also fully ignored in the context of, for example, a very recent overview from 2020 about mechanical performance of L-AFP produced laminates [72]. This shows there is a clear need for better understanding and agreement of the effects of rapid laser deconsolidation on intimate contact development. Consensus regarding the tape surface characterization in squeeze flow based intimate contact models and insight of the physical mechanisms at play will benefit from further research into this topic.

## 3.2 Framework

The approach is to decouple the rapid laser deconsolidation and intimate contact development phases of the L-AFP process as illustrated in Figure 3.1. The rapid laser deconsolidation experiments prepare and analyze different degrees of deconsolidated CF/PEEK tapes. Subsequently, the tape will be subjected to a compressive test which can be said to either mimic the intimate contact development phase underneath a compaction roller or resemble the concept of the intimate contact models squeeze a tape onto a rigid surface.

Both before and after the intimate contact development experiment, the surface profiles will be measured to quantify roughness and waviness, and cross-sectional microscopy will be used to quantify the void content and visualize the fiber and matrix arrangement. During the intimate contact test in-situ gap length measurements provide valuable information regarding intimate contact development and afterwards the degree of intimate contact will be assessed.

Comparison between the different degrees of deconsolidation will lead to conclusions regarding the effects of the degree of deconsolidation on the characterized properties. The cross-sectional images provide additional qualitative understanding of what physical mechanisms are dominant which might help with evaluating intimate contact development theories based on squeeze flow of surface asperities versus fiber re-impregnation based concepts.

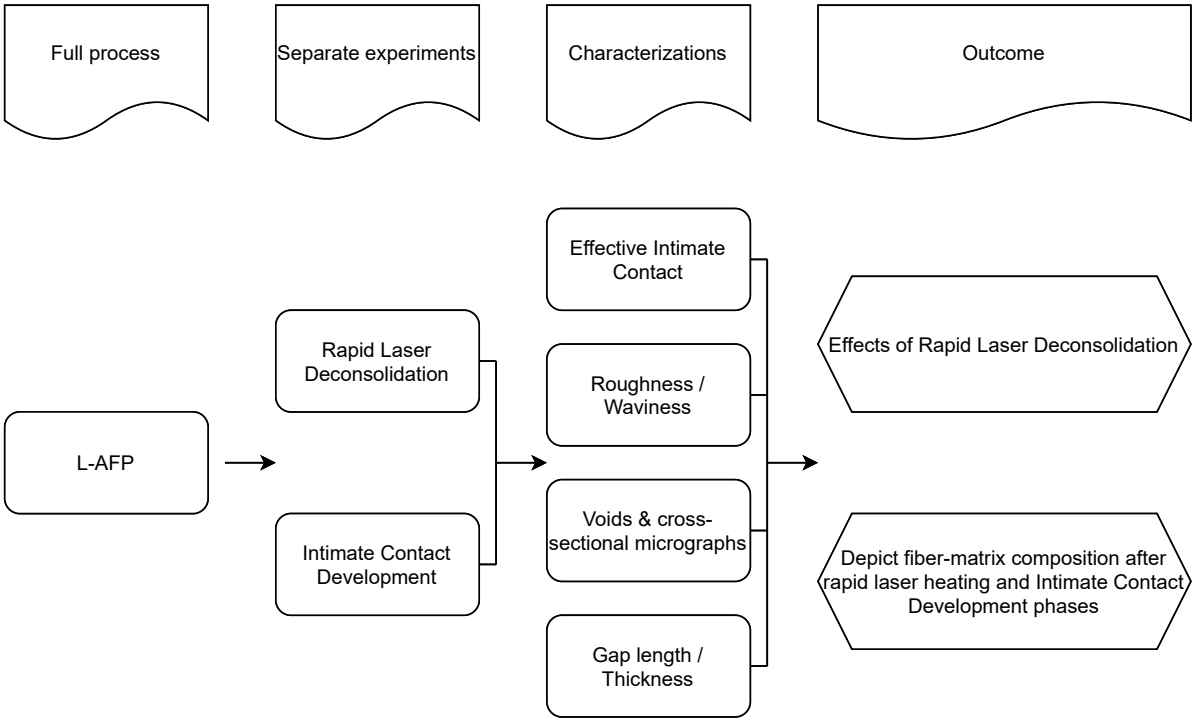


Figure 3.1: Schematic illustration of research framework, showing how L-AFP is separated into two experiment phases, the subsequent characterizations, and the conclusions that can be extracted from that data.

## 3.3 Research Questions

The following research objective is formulated to aid the derivation of the research question:

**Research Objective**

*The research objective is to gain understanding about the effect of rapid laser deconsolidation on intimate contact development by comparing different degrees of deconsolidation with their final effective degree of intimate contact under varying temperature profiles and pressure levels.*

During the Rapid Laser Deconsolidation experiments, the degree of deconsolidation will be varied. The subsequent Intimate Contact Development experiments will employ different maximum intimate contact development temperatures at various pressure levels. The effects of these various configurations will be studied via the characterizations listed in Figure 3.1.

RQ 1 What are the effects of different (a) degrees of laser deconsolidation, (b) pressure levels, and (c) temperature profiles on the (1) in-situ specimen thickness (at glass transition, melting point, and end of experiment), (2) void content, (3) projected area, (4) roughness, (5) waviness, and (6) developed degree of intimate contact?

RQ 2 Can any conclusions or observations be drawn from visual images, such as cross-sectional microscopy and surface pictures, of the specimens pre- and post-intimate contact experiment regarding acting physical mechanisms like squeeze flow of surface asperities or re-impregnation of dry fiber beds?

## 3.4 Hypotheses

The following set of hypotheses will be used to assess the results in order to answer parts of some of the research questions.

HP 1 Higher (a) initial states of deconsolidation, lower (b) applied pressure levels, and lower (c) the temperature profiles, cause (1) more void volume content, (2) increased in-situ thickness, (3) less projected area, (4) increase in roughness, (5) increase in waviness, and a (6) decrease of DEIC.

HP 2 10 kPa pressure is a so called critical pressure at which neither consolidation nor deconsolidation occurs during the intimate contact experiment, hence the roughness, void content, and thickness will remain constant whereas at higher pressure levels a clear decrease in roughness, void content, and thickness will be observed.

HP 3 Between the glass transition and melting region there is no development of intimate contact, only when the melting region is reached a significant amount of intimate contact will develop.

# Chapter 4

# Experimental Set-up

This chapter deals with the materials and experimental set-ups that were deployed. First more information on the material choice and characteristics is provided in Section 4.1. The experiments can be divided into two phases. The laser set-up and the used settings are discussed in Section 4.2 which is the first experimental phase. The second phase is the intimate contact development experiment of which Section 4.3 covers all the details. Many characterization were performed on the specimens between and after these experimental phases, Section 4.4 explains the need for them and how they were carried out.

## 4.1 Material

PEEK is a high performance thermoplastic material that is often found in aerospace applications due to its structural performance and high glass transition and melting temperatures. Additionally, PEEK has been used in intimate contact development and rheological research concerning the L-AFP process. Therefore, there is a lot of reference material available in literature that the results can be compared with.

A spool of quarter inch TenCate Cetex TC1200 PEEK AS-4 is used throughout the research of this thesis. This material has a low initial void content (less than 1%), has been reduced to quarter inch via secondary slitting by the manufacturer and exhibits a glass transition temperature of $T_g = 143\,^{\circ}\text{C}$ and a melting temperature of $T_m$ 343 °C [1].

An overview of a full cross-section is found in Figure 4.1. Many of the cross-sections show a small fiber bundle detached from the rest of the tape at the edge. Specimens were rejected when this was visually observed before the experiments, however there were numerous specimens where an edge fiber bundle only physically detached during the final resin casting stage. It also seems like in some cases the pre-intimate contact tape exhibits a detached fiber bundle, but the bundle is not detached anymore in the post-intimate contact tape material. This poor edge quality is suspected to stem from secondary slitting that is performed to obtain quarter inch tapes. A closer look at detached fiber bundles at the edges is provided in Figures 4.2a and 4.2b. Better edge quality tape edges are shown in Figures 4.2c and 4.2d.

The fiber-volume fraction locally varies throughout the cross-section. For example, Figure 4.3 shows a resin rich area in the middle of the cross-section. The fiber-matrix density distribution has not been quantified and Figure 4.3 is a worst case example of a pristine tape. It is assumed that these local

[1] TenCate Product Data Sheet: CETEX-TC1200_DS_012417

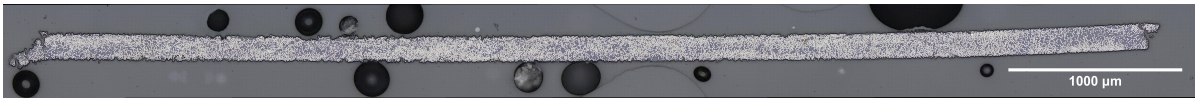


Figure 4.1: Cross-section of pristine quarter inch TenCate Cetec TC1200 PEEK AS-4 tape.

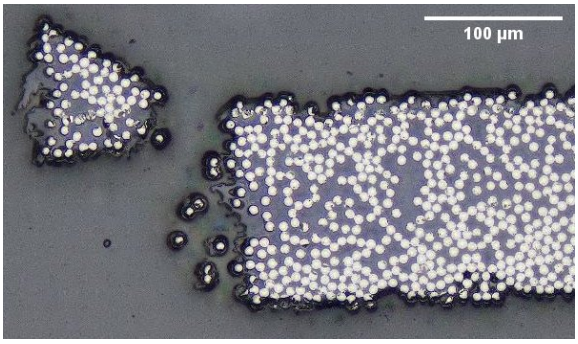


(a) Detached edge fiber bundle.

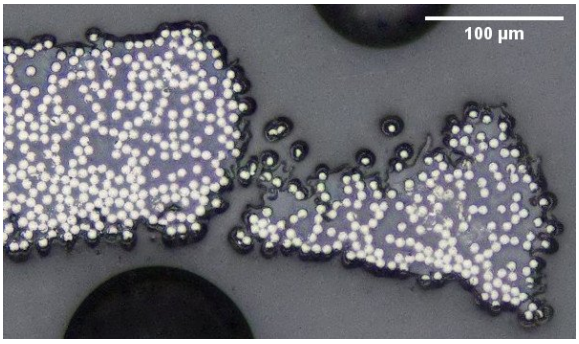


(b) Detached edge fiber bundle.

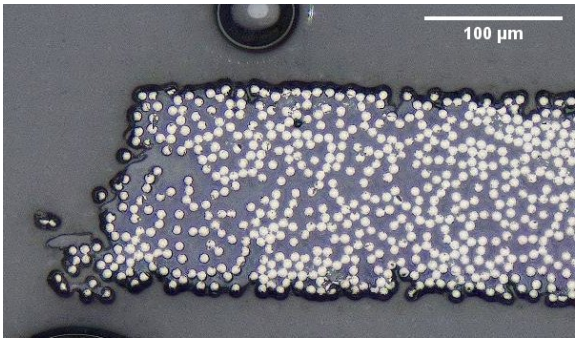


(c) Good edge quality.

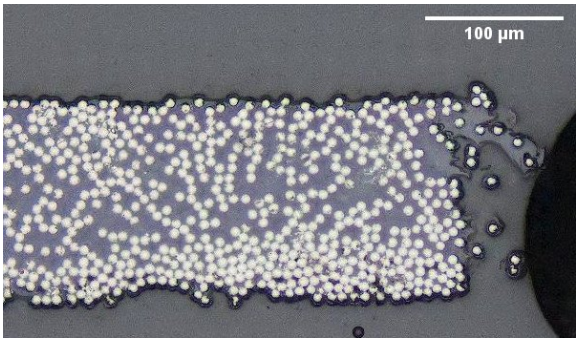


(d) Good edge quality.

Figure 4.2: Close-up of cross-section edges of pristine tape material.

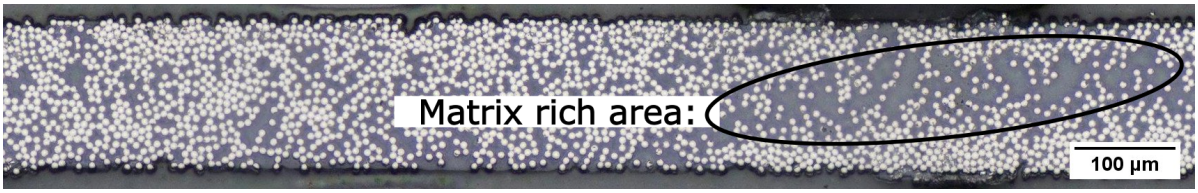


Figure 4.3: Close-up fiber distribution with encircled matrix rich area.

material variations will not significantly affect the experimental results since characterizations will be applied to the whole width of multiple sections of a specimen and three repetitions of each configuration has been carried out. However, it affects the temperature distribution since the matrix is transparent to the laser beam. Additionally, Kok [7] and Choudhary [49] observed fiber rich surfaces due to the rapid leaser heating which could be either positively or negatively impacted locally by these variations. The change of fiber-matrix ratio near the surface affects intimate contact development described by squeeze flow of surface asperities via the viscosity and geometry of the surface asperities and when looking at the fiber re-impregnation description, the fiber volume fraction distribution affects the behavior.

## 4.2 Rapid Laser Deconsolidation Experiment

A VCSEL module is used to perform the rapid laser deconsolidation of a CF/PEEK tape. The set-up is similar to the one employed in configuration 1 by Choudhary [49]. A VCSEL laser consists of many emitters resulting in a uniform light distribution [73]. A PPM412-12-980-24-c VCSEL module is being used throughout the experimental part of this thesis, see Figure 4.4. This module emits IR light at a wavelength of 980 nm and 2.4 kWh maximum power [8]. The VCSEL emitters are placed in a rectangular grid which can be controlled via 12 sections called zones that span the whole width of the laser beam. The power of each zone can be individually controlled by the software that connects with the laser driver. The module requires water cooling, nitrogen atmosphere to prevent condensation and

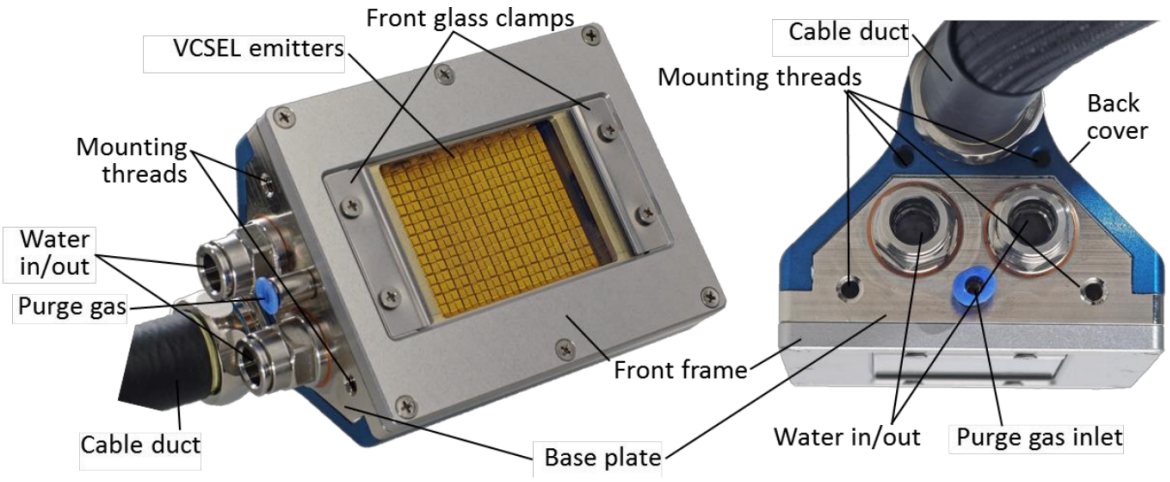


Figure 4.4: Overview of VCSEL module from user manual [8].

is placed in an enclosure to prevent the IR light from damaging its surroundings.

Advantages of this the 980 nm wavelength for L-AFP are that the carbon fibers are highly absorbent to the IR light while the PEEK matrix is transparent to the light [74]. This prevents or lowers the chance of burning and oxidizing of the matrix material [16]. The amount of power and application time can be accurately controlled. For the purpose of this research, the laser intensity distribution is uniform, but for production processes this can be tuned to desire [75].

This section proceeds with a description of the actual set-up employed for the experiments of this work and a detailed sequence of the procedure applied to the specimens.

### 4.2.1 Set-up

The VCSEL module is mounted at 5 cm distance parallel to the specimen. Figure 4.5 shows how the laser module and FLIR thermal camera are mounted inside the laser enclosure.

The specimen is mounted with Kapton tape on a black painted aluminum C-profile, a photo is shown in Figure 4.6. This tool with specimen is then placed underneath the laser module, see Figure 4.7. A total of around 8 cm length of the CF/PEEK tape is exposed and heated by the laser. Two alignment marks are drawn onto the tool to aid in cutting the specimen out after the rapid laser deconsolidation test. A carpenter's square was used to overlay the lines from the tool onto the deconsolidated specimen, then a pair of scissors was used to cut the specimen out of the rest of the deconsolidated material, this resulted in a specimen length along the fiber direction of 6 to 8 mm long. Two clamps with a small metal plate are used to easily align the tool with respect to the laser module. The Kapton tape is used to make sure that the specimen is fixed and laying flat underneath the laser. Additionally, the two long edges of the tool are covered with Kapton tape as well to align the specimen at the middle of the tool. The tool is placed directly on top of the table inside the laser enclosure, physical guides are installed to aid placing the tool at exactly the same location for every deconsolidation experiment.

A FLIR A655c thermal camera with FOL25 lens, also present in Figure 4.5, is mounted at a 55° angle to measure the temperature distribution. The temperature calibration range of the camera is set at 100 to 650 °C. The image size was set to 640 by 120 pixels and a frame rate of 200 Hz. An emissivity value of 0.8 with a thermal camera to object distance of 0.25 m was used based on calibration with thermocouples, see Appendix B for a detailed report on the method.

### 4.2.2 Settings

Three degrees of deconsolidated specimens will be subjected to the intimate contact tests. One of these degrees of deconsolidation is the as-received state of the tape. The other two degrees of deconsolidation will be referred to as highly laser deconsolidated and slightly laser deconsolidated. In some graphs and table the as-received, slightly laser deconsolidated, and highly laser deconsolidated specimens will also be referred to as: ASR, SLD, and HLD, respectively. The laser settings used for the high and

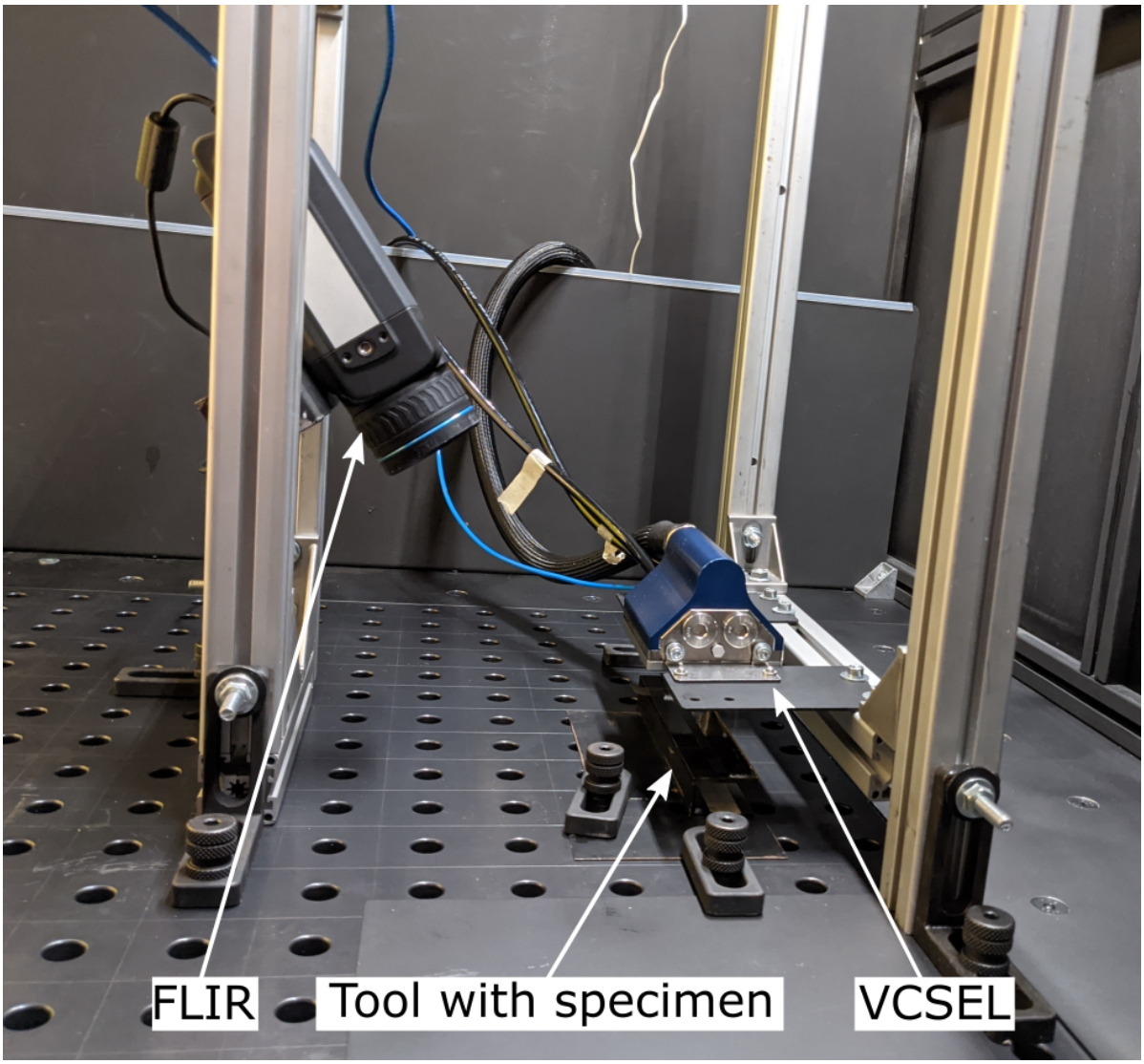


Figure 4.5: VCSEL module mounted perpendicular to the table and FLIR thermal camera mounted at 55 °C inside the laser enclosure.

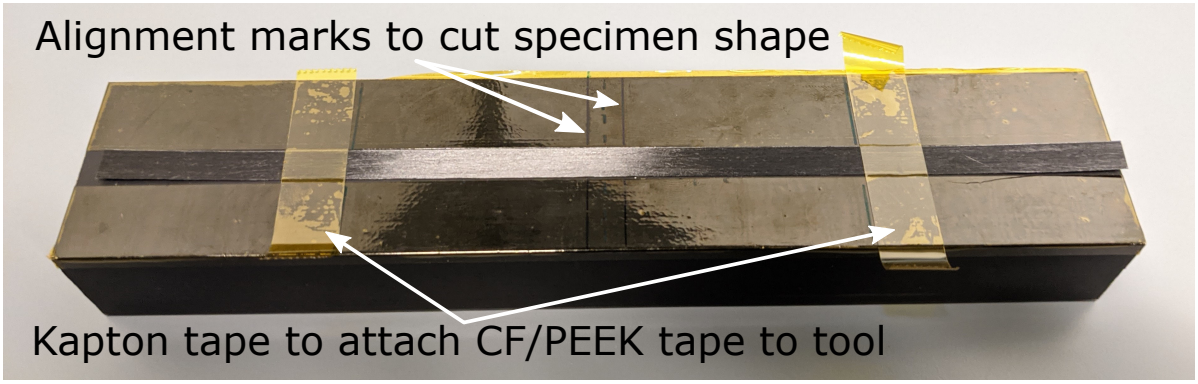


Figure 4.6: Black painted aluminum c-profile to place, align, and laser deconsolidate the specimens.

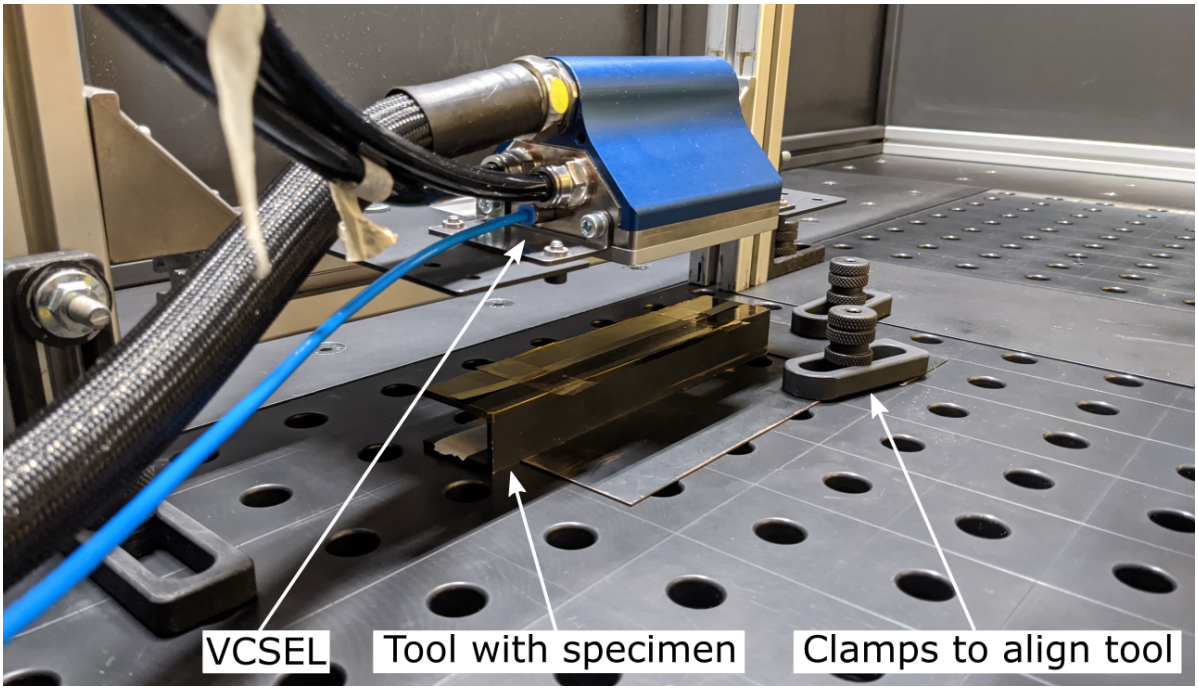


Figure 4.7: Place and alignment of tool underneath laser.

Table 4.1: Laser deconsolidation settings.

| | Zones | Total Power W | Time ms | Mean Temperature °C |
|---|---|---|---|---|
| Highly Laser Deconsolidated | 1–11 | 550 | 800 | 471 |
| Slightly Laser Deconsolidated | 1–11 | 286 | 800 | 270 |

low degrees of deconsolidation are shown in Table 4.1. The reasoning behind choice for the settings is explained in the next two paragraphs.

The main purpose of the settings for the highly laser deconsolidation settings was to increase the roughness, void content, and fibers sticking out of the bed significantly. Heated length and heating time were identified to significantly increase the surface roughness and void content [49]. More specifically, the configuration with an 80 mm heated spot length (which is achieved using zones 1–11 when the laser is mounted at 5 cm distance from the specimen), 800 ms heating time, 121 °C/s cooling rate and a total power input of 660 W exhibited the highest roughness and void content [49]. Based on these results, the heating time was also set at 800 ms with zones 1–11 to obtain a high heated spot length. The power was tuned to 550 W to achieve a peak temperature, averaged over the whole specimen area, of at least around 400 °C which is a common process temperature for CF/PEEK composite materials. The resulting average over all specimens used was 471 °C.

A lower degree of deconsolidation, opting for a roughness in-between the pristine tape material and the high degree of deconsolidation and a low amount of through-thickness voids, was chosen while keeping the amount of zones and heating time constant. Based on several trial runs, the void content was low when the maximum temperature was below the melting temperature. A power of 286 W was found to result in temperatures between the glass transition and melting temperature and produce a laminate that was in-between the state of an as-received and highly laser deconsolidated tape cross-section, void content, and roughness.

More in-depth information about the peak temperatures and thermal profile, measured by the FLIR thermal camera, is found in the next chapter in Section 5.1. A complete list per specimen of the measured 3-by-3 pixel maximum and specimen average peak temperatures during the rapid laser deconsolidation, can be found in the tables of Appendix A.

## 4.3 Intimate Contact Development Experiment

The choice for the apparatus to perform the intimate contact test was largely based on the requirement to have an environment chamber that is able to achieve temperatures over 400 °C, with high heating rates, and the desire for accurate force and gap measurements. The TA Instruments RSA-G2 Solids Analyzer was chosen for its forced convection oven rated for temperature up to 600 °C, enabling high heating and cooling rates of 60 °/min. The machine is also capable of measuring small gap length changes with a displacement resolution of 1 nm[2]. A compression fixture was used with 15 mm diameter steel platens rated up to 500 °C. During the intimate contact development experiment, the carbon fiber tape was sandwiched between two Kapton films to prevent the PEEK matrix from sticking to or contaminating the platens of the machine. The Kapton films were 25 µm thick, rated to withstand temperature up to 400 °C, and supplied by DuPont. In Figure 4.8 a specimen sandwiched between two Kapton films is shown, laying on the steel platens with the environment chamber opened.

This section proceeds by first showing temperature measures at the specimen surface during versus the oven gas temperature in Section 4.3.1. Then, Section 4.3.2 presents the applied pressure level and temperature profile configurations. The method of obtaining the gap length curve from the raw gap length measurement data is explained in Section 4.3.3. An analysis of the flatness of the compression platens is provided in Section 4.3.4. Finally, Section 4.3.5 summarizes the data that was obtained during the experiment and which of these will be used in the results chapters.

### 4.3.1 Temperature Difference Between Oven Gas and CF/PEEK Tape

Figure 4.9a shows the gas temperature of the forced convection oven, reported by the built-in data acquisition of the machine. The gas temperature is able to follow the high 60 °C/ min heating and cooling rates while only slightly overshooting at 400 °C. Measurements with a thermocouple were performed to compare the specimen temperature with the gas of the forced convection oven. A high temperature resistant K-type thermocouple was inserted between the top side of the tape and Kapton film and 20 to 50 measurements were captured per second. Clearly, the temperature on the surfaces lags behind the gas temperature and the peak temperature measured by the thermocouple is reached when the gas is already entering the cooling phase. The time above the melting temperature with the high temperature setting is around 107.7 s as depicted in Figure 4.9b. A closer inspection of the lag between the gas and thermocouple temperatures is provided in Figure 4.9c. During the heating phase, the tape temperature is around 55 °C colder than the gas temperature of the forced convection oven. For the experiments, the temperature of the specimen is more important than the gas temperature. Hence, it is the measurement from the thermocouple of the top surface of the specimen that is referred to when discussing the temperature during the intimate contact experiment. Only the next section will discuss the machine set maximum temperature levels of the oven gas and relate these to the corresponding thermocouple measurements.

### 4.3.2 Settings

The settings can be categorized into three series of settings. A high temperature setting above the melting point, a low temperature configuration between the glass transition and melting point, and a range of temperature profiles near the melting point. Table 4.2 summarizes the settings of the high and low temperature profiles, a full list of the applied settings per specimen is found Appendix A. The temperature profiles consisted of heating and cooling rates of 60 °C/min in order to reached the maximum set temperatures as quickly as possible, staying close to the L-AFP process, and minimizing oxidation effects of the PEEK matrix.

The high temperature setting used a maximum target temperature of 400 °C with a dwell time of 20 s resulting in a maximum temperature at the specimen of 363 °C measured by the thermocouple which is higher than the melting temperature of 343 °C. All three degrees of deconsolidated were subjected to this temperature profile at pressure levels of 10, 50, 100, and 300 kPa. Pressures higher than 300 kPa, sometimes caused problems when trying to find their set value and aborted the test due to overshooting to the maximum force. Each configuration of temperature profile, pressure, and degree of deconsolidation was repeated three times.

[2]From RSA-G2 Solids Analyzer specification sheet online: https://www.tainstruments.com/rsa-g2/

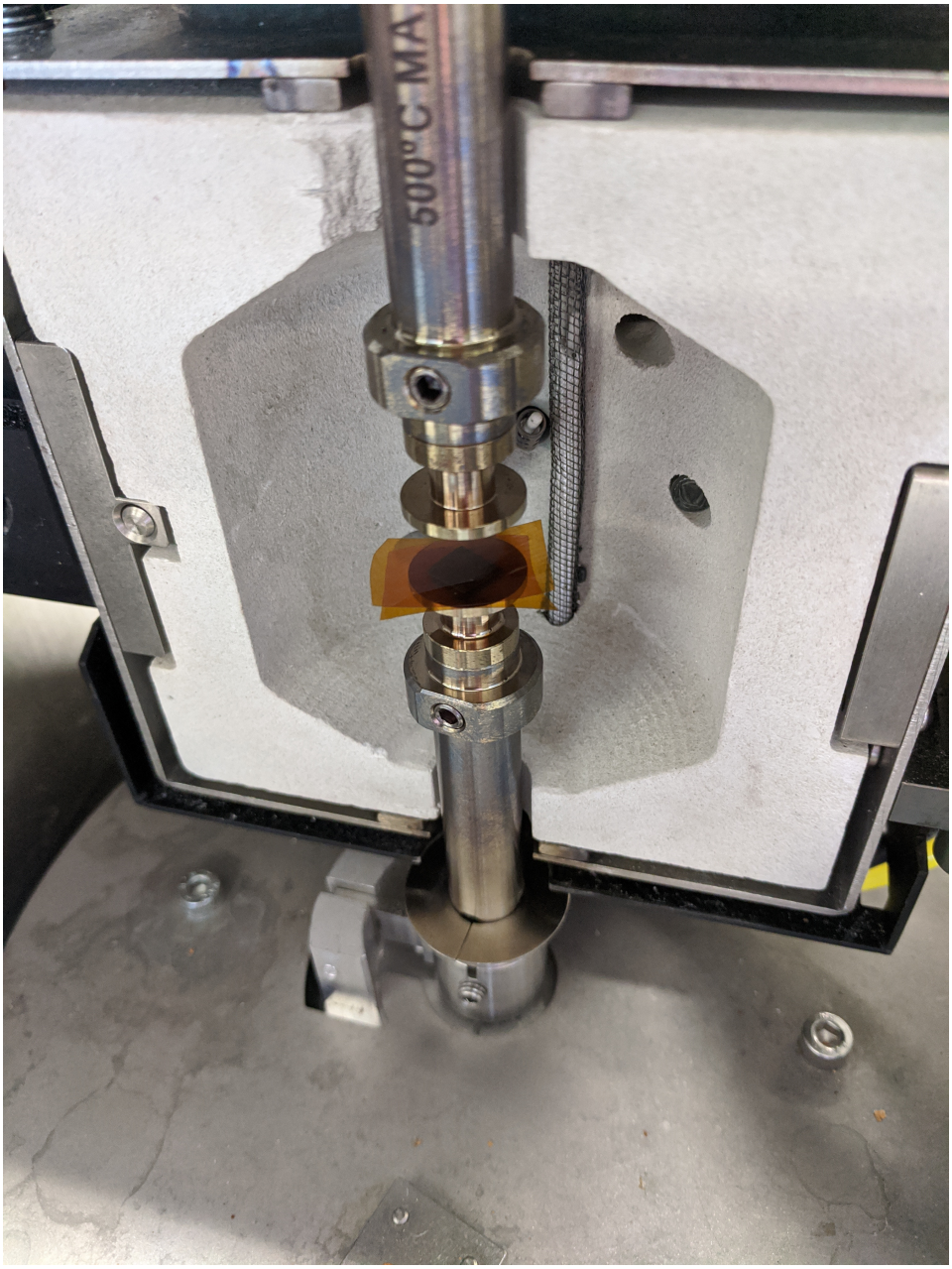


Figure 4.8: Specimen with Kapton tape between platens of RSA-G2 compression fixture.

Table 4.2: Temperature profile settings of RSA-G2 machine for intimate contact experiments with maximum temperature measured by thermocouples.

| | Start ˚C | Heating ˚C/min | Max oven ˚C | Dwell s | Cooling ˚C/min | Max Thermocouple ˚C |
|---|---|---|---|---|---|---|
| High<br>Low | 25 | 60 | **400**<br>**245** | **20** | 60 | **363**<br>**200** |
| Temperature variation | 25 | 60 | **350**<br>**365**<br>**385**<br>**400** | **0** | 60 | **301**<br>**311**<br>**331**<br>**343** |

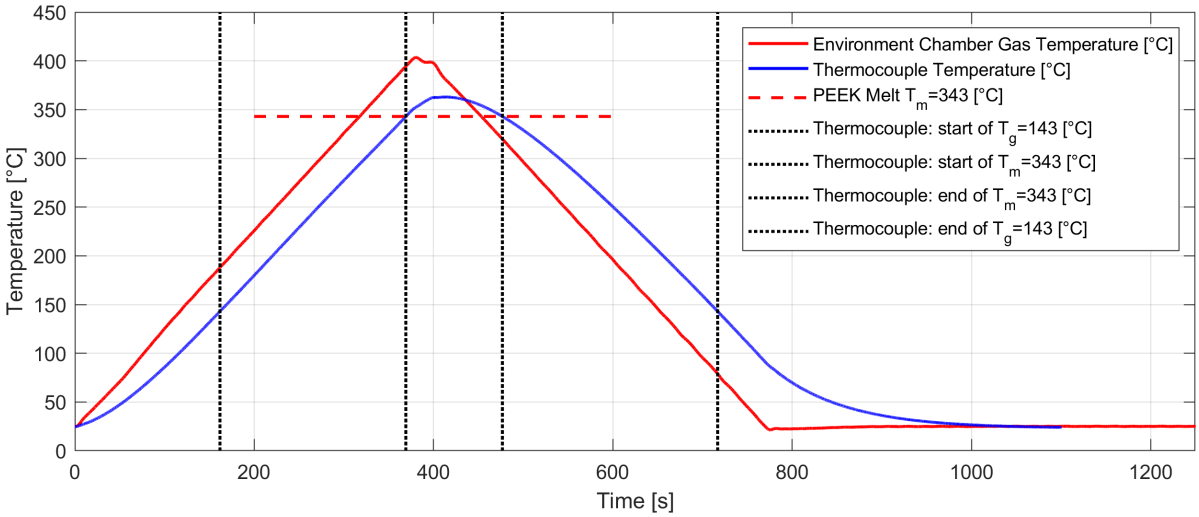


(a) Overview of forced confection oven and thermocouple temperature profiles

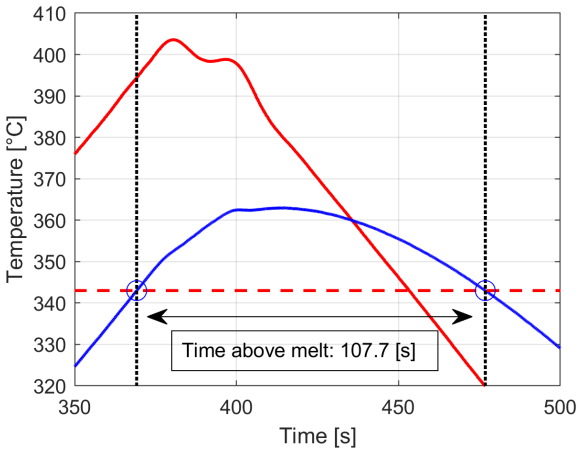


(b) Zoom-in PEEK melt range

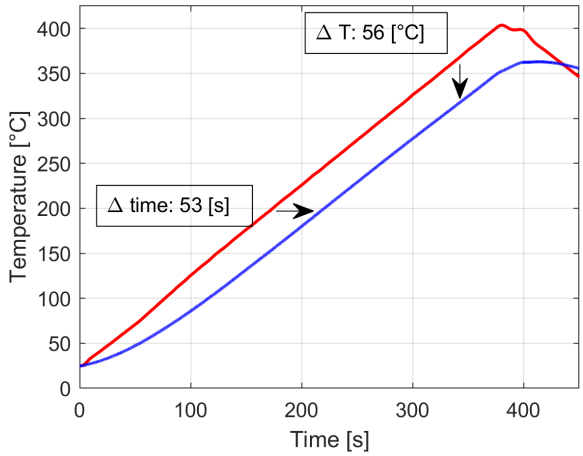


(c) Zoom-in, lag of thermocouples with respect to gas temperature of forced convection oven

Figure 4.9: Overview of high temperature profile during intimate contact test.

The low temperature configuration applied a maximum set temperature of 245 °C and a dwell time of 20 s to have a similar shape around the maximum temperature as the high temperature setting. The maximum temperature measured by the thermocouple was 200 °C which is more than the glass transition temperature of 143 °C, but lower than the melting temperature of 343 °C. This series also tested all three degrees of deconsolidation, but only at 300 kPa pressure in order to see the effect of the highest pressure setting below melting temperature. Omitting the lower pressures reduced the amount of testing time. Still three repetition per specimen configuration was performed.

Finally, a temperature variation series was performed at set temperatures of 350, 365, 385, and 400 °C. This time, 0 s dwell time was used which resulted in a narrower peak near the maximum temperature than the temperature profiles of the other settings. The resulting CF/PEEK tape temperatures measured by the thermocouple are 301, 311, 331, and 343 °C, respectively. Only as-received carbon fiber tapes were tested without repetition of the setting. The pressure was set to 300 kPa so that the results could be compared with the main experiments at higher and lower temperatures. This series served as investigation to see if the specimens were subject to gradual changes between the low temperature setting and the melting point.

### 4.3.3 Correcting Gap Length Curves

Non-linear behavior was found around the start, end, and peak temperatures of the experiment. This is caused by the thermal expansion of the fixture or other components in its connection to the displacement sensor since it was observed during trial tests with only the platens, thus neither CF/PEEK tape nor Kapton film was inserted. Unfortunately, the RSA-G2 operating software only allows to correct for a linear coefficient of thermal expansion which might be acceptable for much lower heating and cooling rates. This ruled out the possibility to perform gap controlled tests since due to the thermal expansion of the fixture, the gap length is actually decreasing which also caused the clamping force to quickly rise to the machine limit of 35 N. Therefore, all tests were performed under force control. Figure 4.10a shows the measurement curve of the gap length with a CF/PEEK tape sandwiched between two Kapton films inserted between the platens. The total amount of gap length change is over 0.5 mm which is much more than the thickness of the sandwiched sample. In order to capture the behavior of the 150 µm thick CF/PEEK tape, a reference curve was captured first, shown in Figure 4.10b, containing only two Kapton films in-between the platens. Subsequent data processing was used to subtract the gap length data of the reference curve, consisting of platens with Kapton film, from the measurements of the specimen, the carbon fiber tape sandwiched between two Kapton films, resulting in the curve of thickness of the specimen throughout the experiment, see Figure 4.10c. The resulting curves repeatedly show the same characteristic behavior and points at a set time or temperature.

Most of the specimen configurations (that is the combination of: degree of deconsolidation, intimate contact pressure level, and temperature profile) were repeated three times, including the corresponding intimate contact test reference run with only two Kapton films. To further improve accuracy, the gap length arrays of the three reference curves for each configuration were averaged by overlaying the time axis. Now, all three raw carbon fiber tape specimens within one configuration used the same reference curve. Based on these curves, the characteristic thickness values (shown in Figure 6.3) were extracted that form the basis for the bar charts in Chapter 6. Besides, for the purpose of presenting the in-situ gap length measurements, it was chosen to also average the CF/PEEK specimen gap length curves. This prevented presenting an overflow of data since three gap length curves are now shown as one average curve. The gap length curves now represent all the measurement data together, while the characteristic points and behavior of the curves is preserved which shows that the overlay, in terms of the gap length behavior induced by the temperature profile, between the repeated tests matches closely.

### 4.3.4 Platens

To assess the effect of the platens on the developed intimate contact and surface roughness of the specimens, their surface roughness was characterized to compare it with the surface roughness of the specimens after the intimate contact test. The height map, shown in Figure 4.11a, shows the flatness of the platens. The root-mean-square roughness values, using a 0.8 mm cut-off length and 7 sampling lengths, were between $0.32 \leq R_q \leq 0.61$ µm. There were also roughness features at a smaller scale as can be seen in Figure 4.11b.

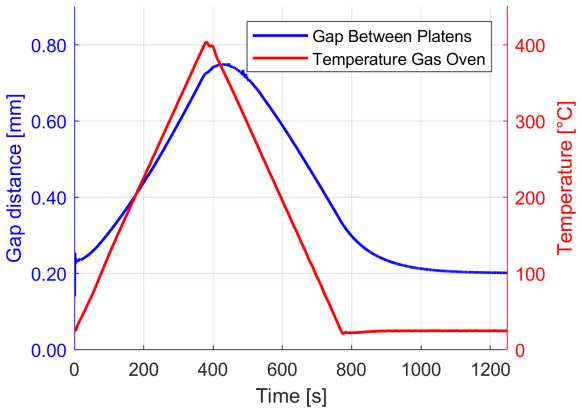


(a) CF/PEEK tape with two Kapton films

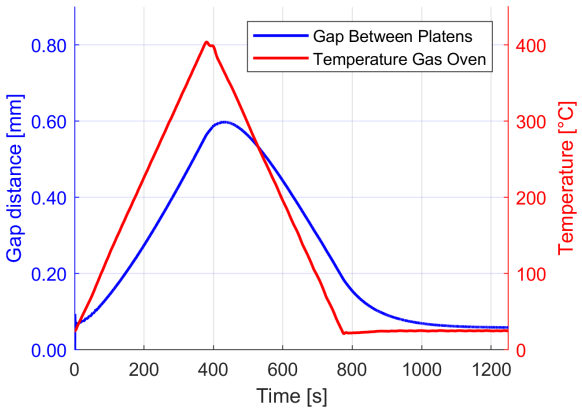


(b) Reference of two Kapton films

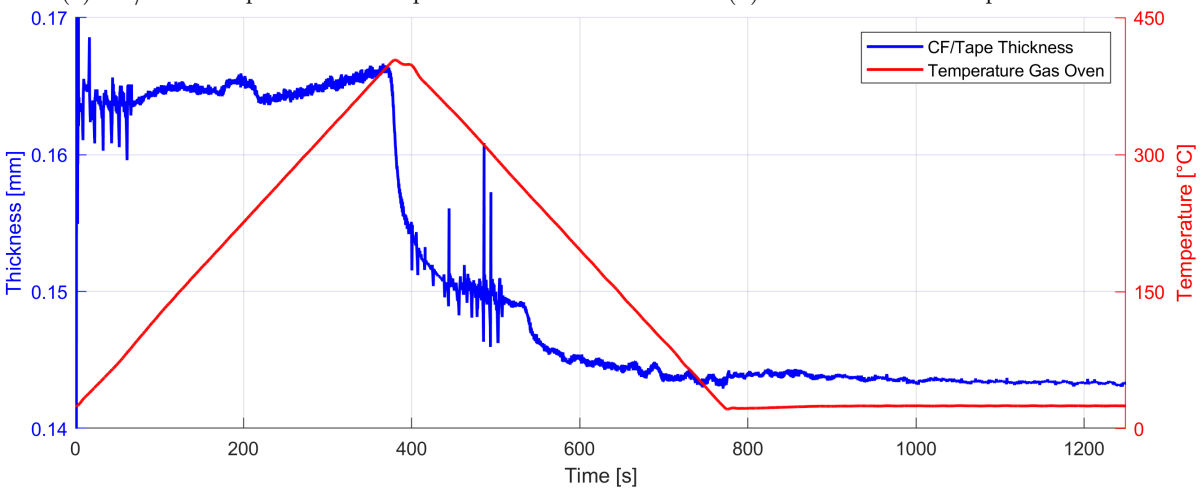


(c) Resulting CF/Tape thickness curve

Figure 4.10: Illustration of subtracting reference curve containing only Kapton film (b) from full experiment data of CF/Tape sandwiched in Kapton film (a) resulting in the thickness curve of CF/Tape (c).

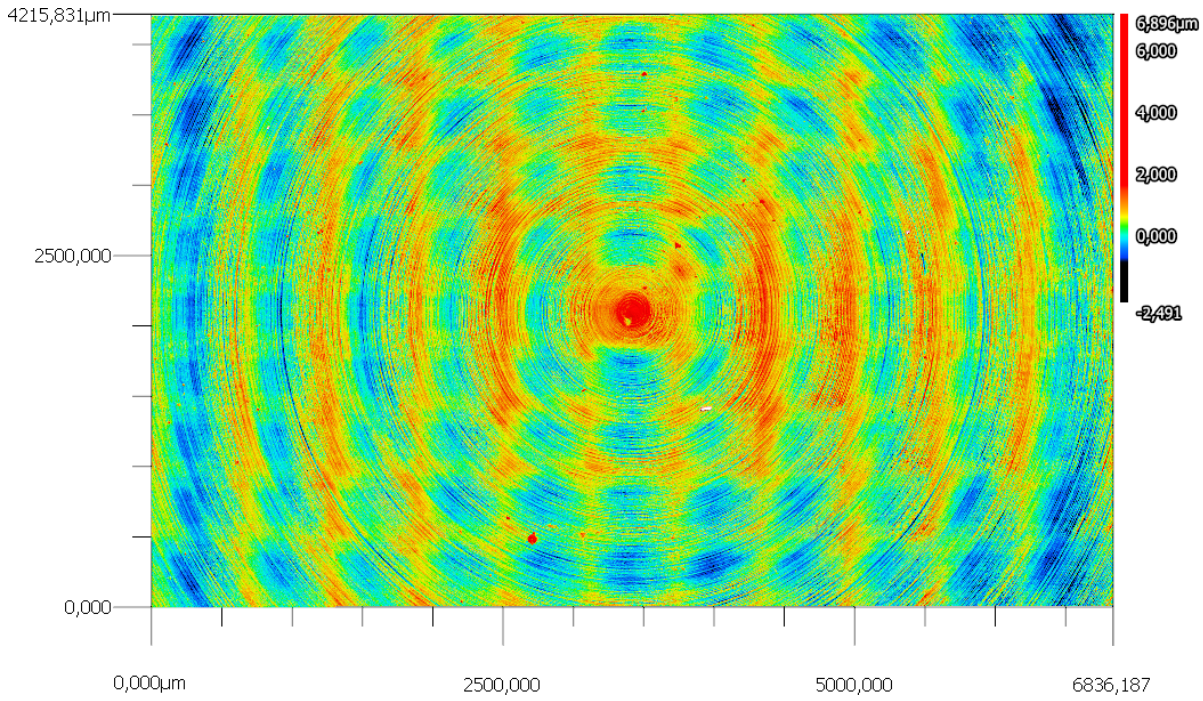


(a) Height map of surface

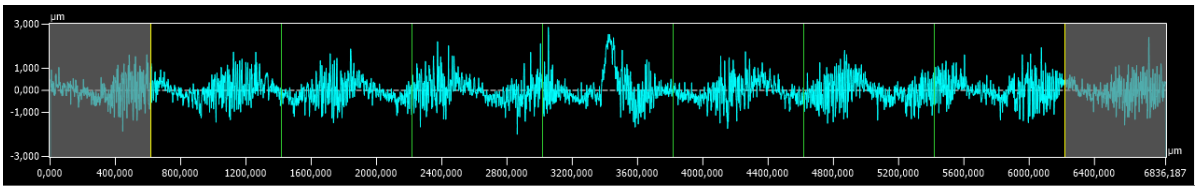


(b) Roughness profile using 0.8 mm cut-off length and 7 sampling lengths

Figure 4.11: RSA G2 compressions platens LSCM analysis using laser confocal settings with 20x lens.

### 4.3.5 Measurement Data

During the experiments the gap length, force, and gas temperature of the forced convection oven were measured at a rate of 25 Hz. The gap length data of the CF/PEEK tape and reference tests, were used to obtain the in-situ thickness curve of the CF/PEEK as was explained in Section 4.3.3 and form the basis of the behavior during the intimate contact test. The force data was analyzed for discrepancies, but is not presented in the results chapter since the force fluctuations were considered to be negligible and the resulting force corresponded with the set value which corresponds to the chosen pressure level. The exact force and resulting pressure values for each specimen can be found in Appendix A. The gas temperature measurements are also omitted from the presented results since the thermocouple measurement are more appropriate to describe the thermal profile experienced by the specimens. After the intimate contact test, the specimen was subjected to various characterizations, discussed in the next section, of which the developed degree of effective intimate contact, in Section 4.4.3, is essential for the purpose of this research as a pre-requisite of bonding in L-AFP.

## 4.4 Material Characterization

On top of the data obtained during the intimate contact development experiments, several tests were conducted to characterize the tapes both prior to and after the consolidation during intimate contact development experiment. These characterizations allowed to study the main phenomena induced by consolidation of different degrees of laser deconsolidated tapes.

Surface characterization, which will be discussed in Sections 4.4.1 and 4.4.2, was performed with LSCM both before and after the intimate contact phase. The area of the whole specimen was also captured before and after the intimate contact experiment, see Section 4.4.2. After the intimate contact test, the DEIC was characterized which involved optical microscopy and a post-processing procedure presented in Section 4.4.3. After all the non-destructive characterizations were performed, cross-sectional analysis was used for more information of the fiber-matrix deformations that took place. The set-up to make resin-casted specimens and the microscopy thereof is described in Section 4.4.4. The cross-sectional micrographs were used to quantify the void content which is explained in Section 4.4.5.

### 4.4.1 Roughness and Waviness

Rapid laser deconsolidation increases the CF/PEEK tapes surface roughness whereas intimate contact development is associated with a decrease in surface roughness. Root-mean-square surface roughness can be used to quantify the surface quality of the tape and assess its development, how much it is affected by rapid laser deconsolidation, and whether the surface can be changed back to its pristine condition with the intimate contact development experiment. Besides the surface roughness, the waviness profile is obtained as difference between the primary and roughness profiles. The waviness profile provides more information about the geometrical out-of-plane shape of the global specimen. A Keyence VK-X1000 LSCM was used to characterize the surface of the specimens before and after the intimate contact test. The LSCM employs a 404 nm laser and was used with a 20x lens and the 'laser confocal' settings.

Profiles spanning the whole width of the specimen were captured at three sections. The sections were chosen at the top, middle and bottom with respect to the fiber direction of the specimen on both top and bottom side surfaces of the specimen. This allows to obtain an average value for the surface roughness at both the laser heated (top) and tool (bottom) sides. Also, with three sections per side provide an indication of the variance over the specimen. For the roughness values, most results address the laser exposed (top) side measurements only, unless specifically stated otherwise. The waviness results, on the other hand, are averaged over both laser exposed (top) and tool (bottom) sides of the specimens since the waviness represents much more the whole cross-section behavior than the roughness metric does.

ISO–4287 guidelines state to use a roughness sampling length of 0.8 mm for roughness values of $0.1 < R_a << 2$ µm. Post-intimate contact specimens that were subjected to higher pressure and temperature range are within this roughness region, however the pristine tape material is slightly higher in roughness, 2.5–3.5 µm, and highly deconsolidated material exhibits $R_a$ roughness values of 8–11 µm. A problematic result of using higher sampling lengths is that with a 2.5 mm sampling length only 2 sampling lengths will fit in the width of the 6.35 mm cross-section whereas ISO–4287 recommends an

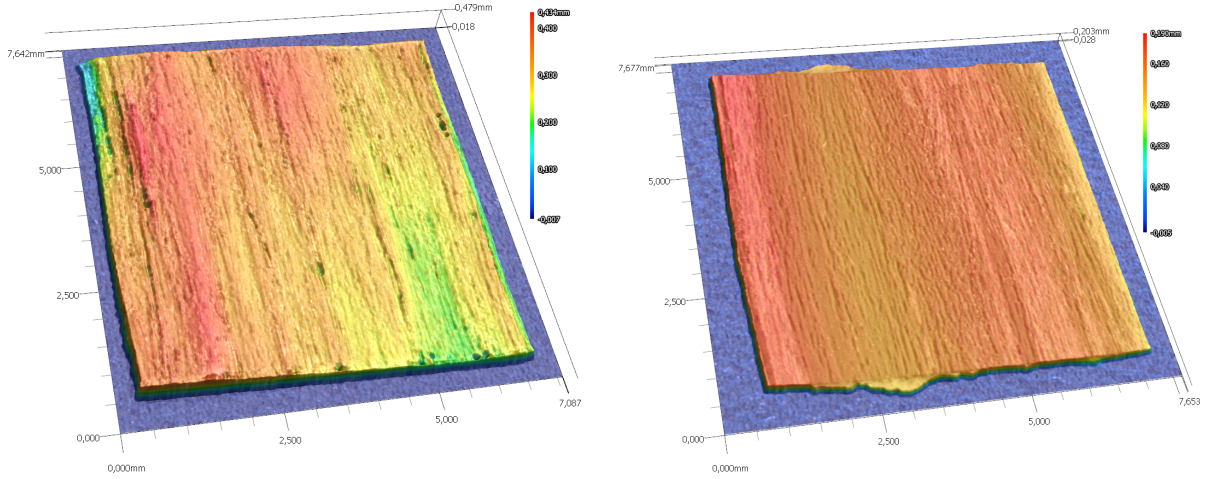

(a) Pre-intimate contact

(b) Post-intimate contact experiment subjected to a maximum temperature of 363 °C at 300 kPa.

Figure 4.12: Area map of highly laser deconsolidated specimen before and after intimate contact experiment.

evaluation length containing at least 5 sampling lengths. Hence, a sampling length of 0.8 mm was chosen with 7 evaluation lengths captured along the width of the tape.

Each section was first corrected for tilt using the automatic mode in the Keyence Multi-File Analyzer software suite. Then a multi-line grid was projected along the width to extract 11 profiles with the aforementioned 0.8 mm sampling length and a total evaluation length spanning 7 times the sampling length. Then the average, minimum, and maximum $R_a$ and $R_q$ roughness values of the 11 profiles were exported for each section to be further averaged with the other sections of that specimen. In the end, $R_a$ was only used for reference with the ISO–4287 standard and the root-mean-square roughness and waviness, $R_q$ and $W_q$, parameters are presented in the results. Additionally, the waviness parameters with a highbandwidth filter of 2.5 mm were also extracted. The highbandwidth parameter allows to eliminate some of the global tape shape from the primary profile. Section 5.2 provides more information about the effects with examples of applying this filter.

### 4.4.2 Specimen Area

The area was measured to calculate the required force value to reach the desired pressure level for the intimate contact development experiment. Additionally, an area ratio of the specimen after and before the intimate contact experiment was used to investigate squeeze flow of the whole specimen area. A Keyence VR-5000 was used to map the sample with a low magnification factor of 12x in conjunction with the automatic high resolution capturing settings. Mapping the whole specimen with this microscope provided a good overview of the whole specimen and its out-of-plane shape, Figure 4.12 shows a specimen before and after the intimate contact experiment.

To calculate the area of the specimen, the projected area was used which is the 2D area from a perspective perpendicular to the specimen. The area is automatically extracted with the software that comes with the microscope. The measurement was first leveled with respect to the table that the specimen was placed on, then only the area was considered that is more than 25 µm high and contains more than 10,000 enclosed pixels (to eliminate noise and other particle peaks). This procedure was applied to both the laser exposed (top) and tool (bottom) surfaces of each specimen. Unless otherwise specified, the average (projected) area of the specimen is reported. Due to a small change in the threshold of considering only area higher than 25 µm, some of the pressures applied to the specimens, see the tables in Appendix A, are not exactly at the chosen 10, 50, 100, or 300 kPa. These deviations are, however, small with respect to the difference between these aforementioned pressure level configurations. Hence, these differences between set pressure levels and actual pressure value due to the area calculation are ignored.

Table 4.3: DEIC values of two pristine tape samples.

| Sample Name | DEIC | | Unit |
|---|---|---|---|
| | Top | Bottom | |
| Pristine Sample 1 | 6.5 | 5.3 | % |
| Pristine Sample 2 | 5.4 | 6.9 | % |
| Averaged | 6.0 | | % |

### 4.4.3 Degree of Effective Intimate Contact

This is one of the key characterizations of the report as the difference of developed intimate contact between the as-received tapes and rapid laser deconsolidated tapes can increase the knowledge about the applicability of current intimate contact simulation models. A Keyence VHX-2000 microscope with VH-Z100UR lens at 200x magnification was used to capture and stitch an image of the whole surface of the post intimate contact specimens. Both top and bottom surfaces of each specimen were captured.

Based on Çelik et al. [39], the concept of Degree of Effective Intimate Contact (DEIC) is used to quantify the developed intimate contact of the specimens. When the surface is resin rich and flat it will reflect light of the microscope and result in very bright areas which is considered as 'Effective Intimate Contact'. The top of the fibers come up very bright, since the top of a circle is perfectly perpendicular at its highest point from a top view, but shall be excluded in the definition of 'Effective Intimate Contact' since the absence of resin impedes subsequent bonding via autohesion [39].

A rectangular area, within the edges of the tape, was manually cropped from the image captured by the microscope. This cropped image, therefore, only contains the specimen itself, no surrounding elements or area. A close-up of such an image is provided in Figure 4.13a. A MatLab script was written that imports the cropped image, converts the image to grayscale, then uses the Otsu method to automatically select a threshold value. Figure 4.13c shows the grayscale histogram with the Otsu threshold. All values brighter than the threshold are regarded as Effective Intimate Contact. Visual inspection was performed, by highlighting Effective Intimate Contact area in blue, like in Figure 4.13b, for each specimen to assess if the Otsu threshold was appropriate and the threshold would be manually tuned based on qualitative judgment if deemed necessary. The top surface of the fibers showed up very bright and these areas are, to a large extend, excluded by removing all enclosed areas that are smaller than 500 $\mu m^2$. Figure 4.13b shows these removed areas in red. The DEIC can now be calculated via the ratio of blue highlighted area over the total surface area of the image.

The DEIC of the as-received state of the tape was characterized as reference for the DEIC values after the intimate contact test. Both top (side that corresponds with laser exposed side during rapid laser deconsolidation) and bottom (corresponds with tool side during rapid laser deconsolidation) sides of two pristine tape samples are presented in Table 4.3.

### 4.4.4 Cross-sectional Microscopy

Resin-casting was used to analyze the cross-section of the tape for void content. Also, the cross-sectional images were used for qualitative assessment of the state of the tape. After the tape is embedded in the resin, it cannot be analyzed for other purposes anymore, hence it was applied as the very last step during the characterization of post-intimate contact test specimens. Figure 4.14 shows a CF/PEEK tape after rapid laser deconsolidation and indicated the cross-sectional cut post-intimate contact test. Besides these post-intimate contact test specimens, the tape material near where the specimen has been cut from the rest of the tape is used to resemble the state of the specimen prior to the intimate contact test and represent the (cooled down) nip-point state of the material. These pre-intimate contact experiment cross-sections, also shown in Figure 4.14, were tried to obtain as close as possible to the specimen material. Hence, for each specimen, two cross-sectional images of pre-intimate contact (but after rapid laser deconsolidation) material near the specimen area were obtained and one cross-sectional image post-intimate contact test at the middle of the specimen.

The tape material was mounted per 5 in a plastic Struers clip, see Figure 4.15. Some additional weights were added to prevent the specimens from floating around while filling the holder with resin. The grinding and polishing routine was tuned to remove 3 mm of material which is the same length as

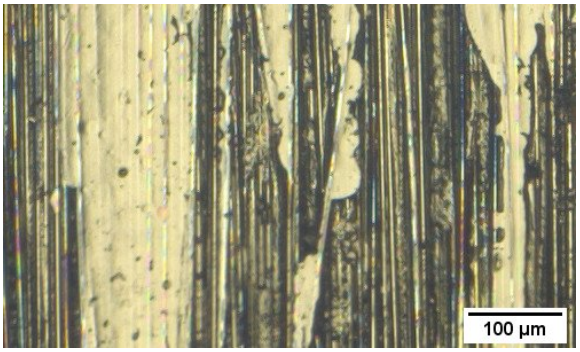


(a) Zoomed-in view of specimen surface

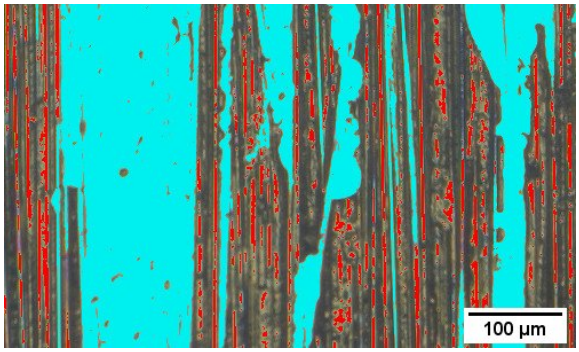


(b) Highlighted Effective Intimate Contacte area in blue, removed smaller than 500px areas in red

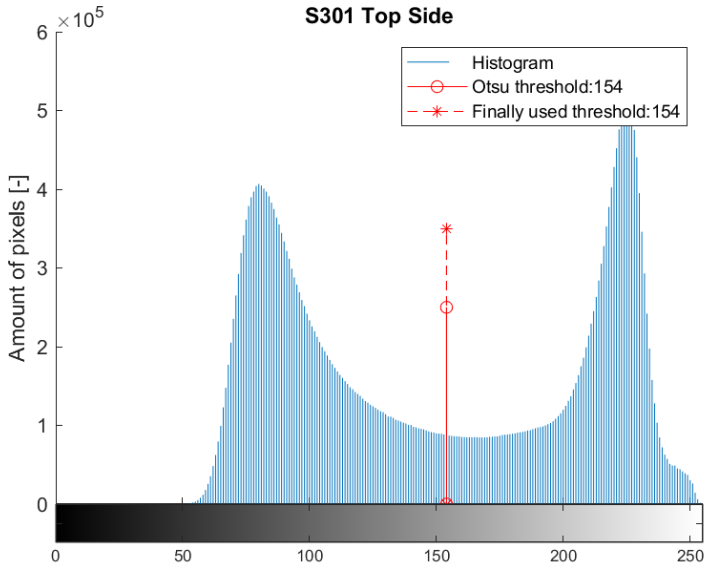


(c) Histogram of grayscale image with Otsu threshold by MatLabs default function

Figure 4.13: DEIC quantification illustrations.

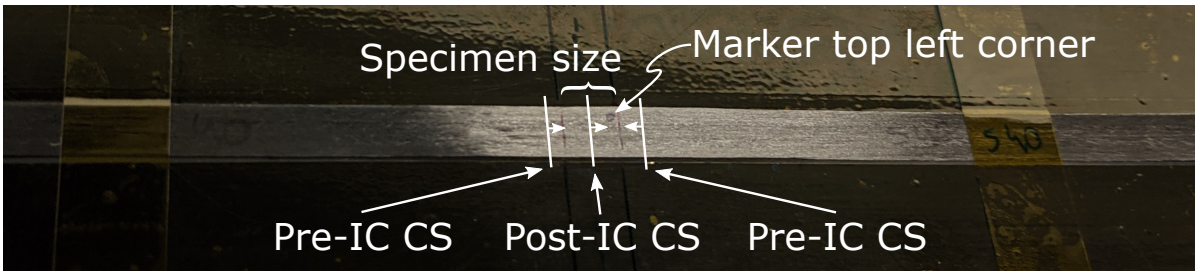


Figure 4.14: CF/PEEK tape still mounted on the tool after rapid laser deconsolidation: annotated specimen length, lines at which cross-sections will be obtained, and arrow direction of cross-section points to the material that will be ground and polished away in the final cross-sectional micrographs.

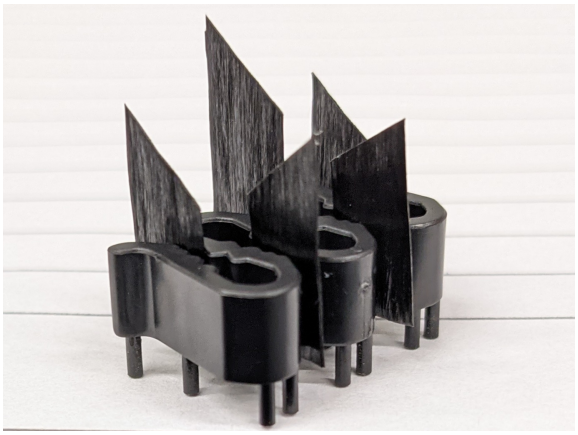

(a) Grinding and polishing occurs at bottom side in picture, the angled cut tape ends are for convenience to indicate the tape end that is of no interest.

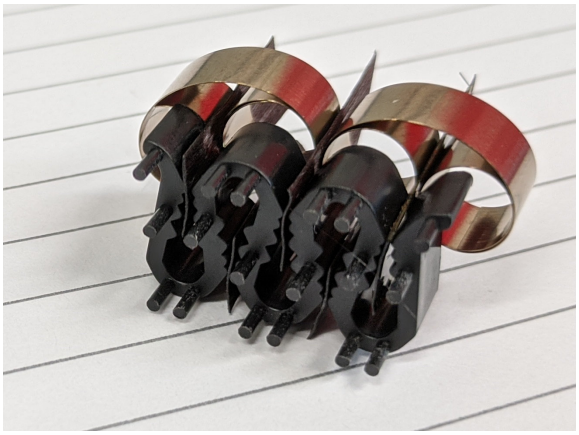

(b) Tape material aligned with respect to the legs of clip to reduce the amount of material ground away, also with weights to prevent the object to float in the resin.

Figure 4.15: Pre-intimate contact experiment CF/PEEK tape material mounted in Struers clips before resin casting.

the legs from the plastic clips, visible on the bottom side of Figure 4.15a and facing towards the camera in Figure 4.15b. This knowledge was used for positioning the tape material with respect to the legs of the clip. For the pre-intimate contact material around 1 mm of CF/PEEK tape length was in the length of these legs to ensure the cross-section was reached in the grinding steps while still minimizing the amount of length of the tape that would be ground away. The post-intimate contact specimens themselves were placed with around 1 mm accuracy with the middle of the tape at the end of the legs of the clip.

The resin casting was performed with Struers Epofix kit and was cured in a Struers CitoVac at a low atmospheric pressure of 0.50 bar to reduce voids. Grinding was performed in a Struers Tegramin-20. A customized was used that is listed in Table 4.4, different from the standard routine is that it skips the diamond polishing steps and goes straight from the finest grinding step to the chemical step. After the chemical step, the same cloth disk was used with water only as a cleaning step to remove the chemical OPS non-dry solution. Finally, the sample was cleaned in a sink with some cotton and consumer dish soap, then dried with pressurized air, flushed with ethanol and dried again with pressurized air.

Table 4.4: Grinding / polishing routine on Struers Tegramin-20.

| Plate | Solution | Time [min:sec] |
|---|---|---|
| SiC Foil #180 | Water | 00:10 |
| SiC Foil #320 | Water | 00:25 |
| SiC Foil #1000 | Water | 00:30 |
| SiC Foil #2000 | Water | 00:40 |
| SiC Foil #4000 | Water | 00:40 |
| Chem | OP-S NonDry | 03:00 |
| Chem | Water | 01:00 |

The cross-sectional images were shot and stitched with the Keyence VK-X1000 LSCM using the 20x lens with 'Focus Variation' method. Figures 4.3 – 4.4 and 4.16a were all obtained via this method. The microscope automatically saves the image with best focused focal depth and stitches it together. The height data can be used to distinguish voids from contamination laying on top of the cross-section.

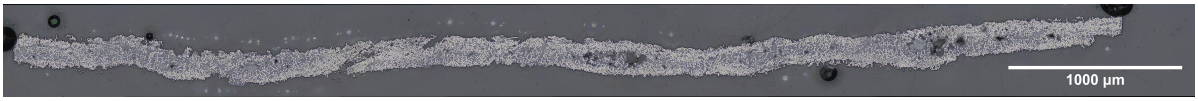


(a) Resulting image from cross-sectional microscopy.


(b) Manually removed background using ImageJ.

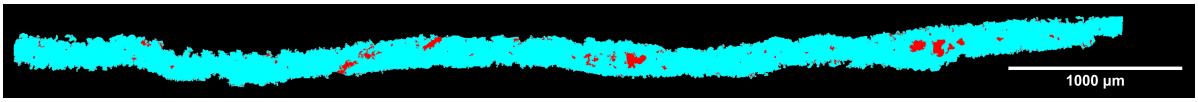


(c) Processed imaged from MatLab routine, black area is not considered, blue area is carbon fiber and PEEK matrix, and the red area is the void content area.

Figure 4.16: Processing cross-sectional microscopy images to extract void content. The used cross-sectional is a highly laser deconsolidated specimen pre-intimate contact development experiment.

### 4.4.5 Void Content

Void content formation has a significant role in thermal deconsolidation, as was explained in Section 2.4. Therefore, the void content is quantified before and after the intimate contact development experiment. This allow to first get a grasp on how the rapid laser deconsolidation phase affects the pristine tape material. The second key interest is too see how much the voids will be reduced by the subsequent intimate contact development experiment. The void content characterization is performed by processing the cross-sectional microscopy images.

The first processing steps consists of manually removing the area surrounding the cross-section, so that Figure 4.16a becomes Figure 4.16b, which was done using the publicly available ImageJ software tool, version ImageJ 1.53e. Using the 'wand (tracing) tool' with either the 'legacy' or '4-connected' mode, a white-ish pixel in a carbon fiber was picked and then the threshold was increased until 1 or 2 values before the selection area encompassed outside of the CF/PEEK tape area. This method proved to effectively select nearly all of the tape area while not including the darker shade around the edge that stems from the different material effects during the grinding/polishing steps effect. The area was then inverted so that it selected the whole figure except for the tape cross-section, this selection was then removed resulting in writing zeros, black pixels, to this selected area.

The approach of post- and pre-intimate contact specimens was different. For the post-intimate contact specimens, ImageJ was again used to select the voids via its threshold function where the threshold value was manually tweaked so that the selected area corresponded to the visually observed voids. The selected area was than summed while subjecting to a minimum area of 20 pixel$^2$ and a circularity of $>0.1$ to ignore the area of some shadows around fiber edges. For the pre-intimate contact specimens another method was employed. Firstly, the pre-intimate contact as-received void content was set at 0.7 % based on the work of Choudhary [49]. The pre-intimate contact rapid laser deconsolidated tapes exhibit a rough surface and cavities at the surface, using manual assessment and the 'wand' tool, the void areas were selected and set as black pixels. Then a MatLab routine further processed these images with a second step dividing the void content from the fibers and matrix, highlighted in Figure 4.16c. A further breakdown of the steps of a zoomed-in section is provided in Figure 4.17. The code works by employing an edge algorithm to extract area where fibers are present, transforming the grayscale image, Figure 4.17a, to Figure 4.17b. This image is then dilated, in Figure 4.17c, and the holes are filled, resulting in an area that is slightly larger than the cross-section, shown in Figure 4.17d. After a final erode step, shown in Figure 4.17e which looks nearly identical to the previous step since there is only 4 pixels difference, the obtained area is the size of the cross-section.

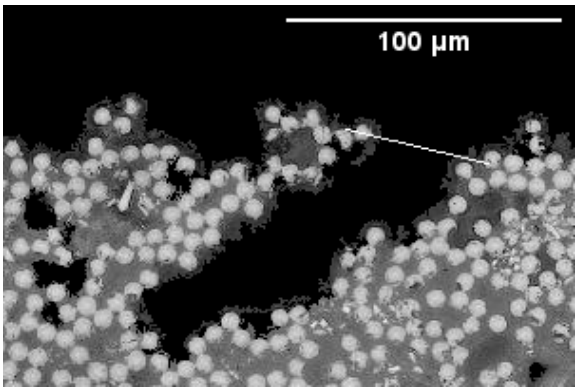


(a) Grayscale with removed (black) background

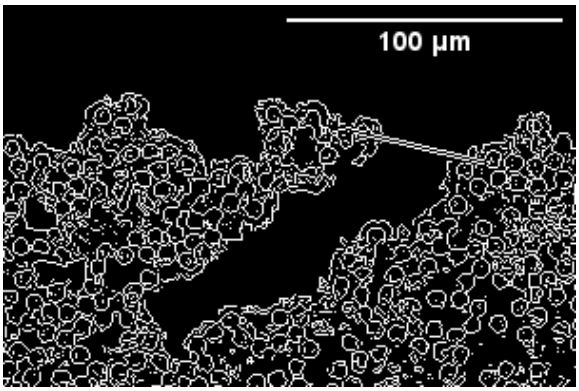


(b) MatLab edge detection function

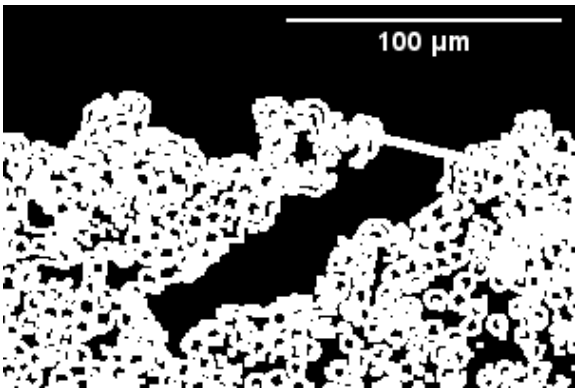


(c) Dilated by 3 pixels


(d) Filled holes


(e) Eroded by 4 pixels

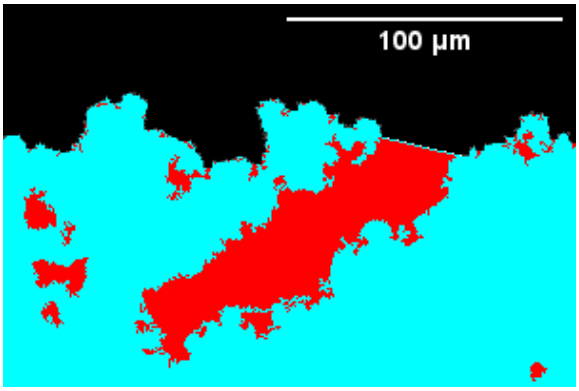


(f) Non-tape area black, void content red, and rest of tape blue

Figure 4.17: Zoom-in at cross-section of MatLab routine process steps from imported grayscale image to image highlighting fiber+matrix area, void content, and surrounding area.

# Chapter 5

# Rapid Laser Deconsolidation

This chapter looks at the state of the specimens after the rapid laser deconsolidation experiments. Both quantitative results and qualitative images of the tapes will be presented. Firstly, Section 5.1, shows the temperature measurements during laser heating and the cooling down phase. The subsequent sections analyze the cooled-down state of the specimens. In Section 5.2, the roughness results between the as-received and deconsolidated state are discussed. Section 5.3 analyses the tape material in the vicinity of the specimen to present the void content and a further qualitative perspective on the cross-sections.

## 5.1 Thermal Camera Data

Table 5.1 shows the peak temperatures that were reached with the laser settings from Table 4.1. The peak temperature is the highest temperature during the laser heating time. Two temperatures are reported which are annotated in Figure 5.1: a 3-by-3 pixel average at the location of the maximum temperature picked at the time of the peak temperature (hence representing the maximum temperature of the specimen) and the average of the whole specimen area. These two temperature definitions give an idea of the thermal history of the samples in Figure 5.2.

The slightly deconsolidated samples achieved local maximum temperatures close to the melting point (343 °C) of the PEEK matrix. The average temperature, 270 °C, of the tape was more in-between the glass- and melt transition temperatures. The specimens clearly reached temperature well above the glass transition (143 °C) point with the the lowest average temperature of 232 °C. The lowest average temperature experienced by a highly laser deconsolidated tape was 395 °C. This assures that the temperatures experienced by the highly laser deconsolidated tapes is at least in the normal processing range, but often reached higher temperatures with an average mean temperature of 471 °C. Therefore, this degree of deconsolidation represents a very severe state of deconsolidation. With these differences of reported temperatures between the two degrees of deconsolidation, it is clear that the highly laser deconsolidated tapes represent a significantly different thermal history than the slightly deconsolidated samples.

Table 5.1: Peak temperatures recorded by the FLIR A655c thermal camera, a 3-by-3 pixel averaged maximum, and an average of the whole specimen are reported, the columns provide information about the mean, extreme, and standard deviation values of the specimens.

| | | Mean | Max | Min | Std | |
|---|---|---|---|---|---|---|
| Slightly Laser Deconsolidated (286 W) | Max 3x3 px | 309 | 341 | 268 | 21 | °C |
| | Average | 270 | 296 | 232 | 20 | °C |
| Highly Laser Deconsolidated (550 W) | Max 3x3 px | 527 | 566 | 448 | 34 | °C |
| | Average | 471 | 511 | 395 | 33 | °C |

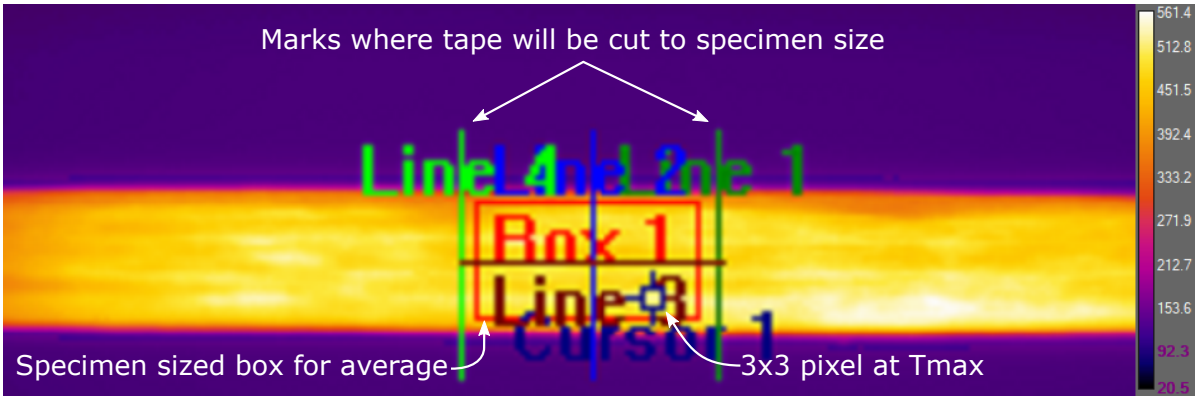


Figure 5.1: Highly laser deconsolidated tape, showing the moment at peak temperature. Three thermal line profiles (vertical) are measured of which the outer lines correspond with where the specimen was later cut from the rest of the tape, the red box is used to obtain the average specimen temperatures, and the 3x3 pixel marker was used to extract the maximum temperature inside the specimen area.

Figure 5.2 provides a closer look at the thermal history. The peak temperature corresponds with the temperatures reported in Table 5.1 and is reached at the end of the laser pulse of 800 ms. The average temperature of the whole specimen and the 3-by-3 pixel grid difference is quite consistent. At around 300 °C, the 3-by-3 average curve of the highly laser deconsolidated specimens increases in slope. This might be linked to changes of the locations of the local temperature distributions. Choudhary [49] showed a relation between out-of-plane deformation and local temperature of a deconsolidating CF/PEEK tape. When a local area develops out-of-plane waviness, it comes closer to the laser and is not touching the tool which acts as heatsink, these mechanisms then promote an increase in temperature even further. This also explains the local heating variations in Figure 5.1. These local temperature variations changed from measurement to measurement, three temperature profiles along the width of the tape, indicated in Figure 5.1, are shown for a specimen with a very uniform temperature distribution in Figure 5.3a, but many specimens had larger temperatures differences along the width as shown in Figure 5.3b which has a 50 °C difference.

## 5.2 Surface Characterization

After rapid laser deconsolidation, the surface roughness significantly increased, shown in Figure 5.4 which contains the roughness ranges of each degrees of deconsolidation. The as-received (ASR) specimens, representing the pristine tape, were not exposed to the laser and the top and bottom sides have nearly the same average root-mean-square roughness. Looking at the rapid laser deconsolidated specimens, the laser exposed (top) surface is rougher than the tool (bottom) surface. Due to this observation, the laser exposed and bottom sides will be investigated separately when characterizing the state after the intimate contact development experiment. The roughest as-received and smoothest slightly deconsolidated samples have a small overlap in roughness. There is no overlap of the roughness of highly deconsolidated samples and the other degrees of deconsolidation.

Regarding the waviness, the rapid laser deconsolidated specimens exhibit a significantly higher waviness than the as-received state of the tape material in Figure 5.5a. However, the slightly laser deconsolidated specimens have significantly more waviness than the highly laser deconsolidated specimens which is counter intuitive. This is caused by warpage of the tape: the slightly laser deconsolidated tapes often have one or two points where the cross-section bends causing a higher out-of-plane deformation than the highly laser deconsolidated tapes which exhibit more bending points, resulting in less total out-of-plane deformation. The slightly laser deconsolidated tape in Figure 5.6a has a bending point at around 2400 µm along the width while the sections to its right and left are fairly straight. It is hypothesized that the thermal stress or change in the residual stresses causes the only very few bending points along the cross-section while the rest of the cross-section stays relatively stiff. The highly laser deconsolidated tape, shown in Figure 5.6b, contains many more of these bending points due to the higher temperature it was exposed to, but due to the temperatures above the melting point does not have the

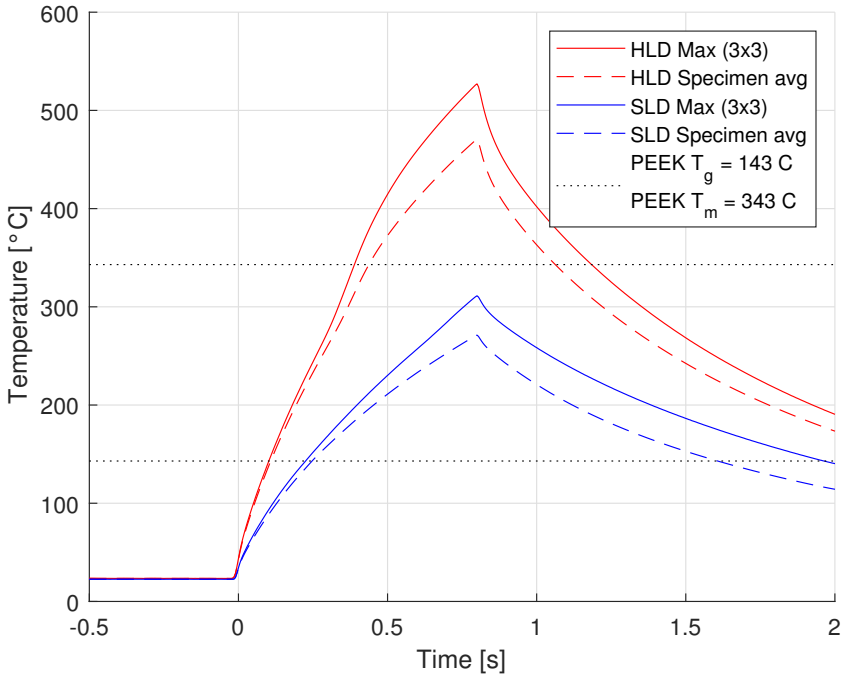


Figure 5.2: Temporal plot of specimens during rapid laser deconsolidation, the maximum and specimen average temperature curves are shown for both slightly laser deconsolidated (SLD) and highly laser deconsolidated (HLD) specimens.

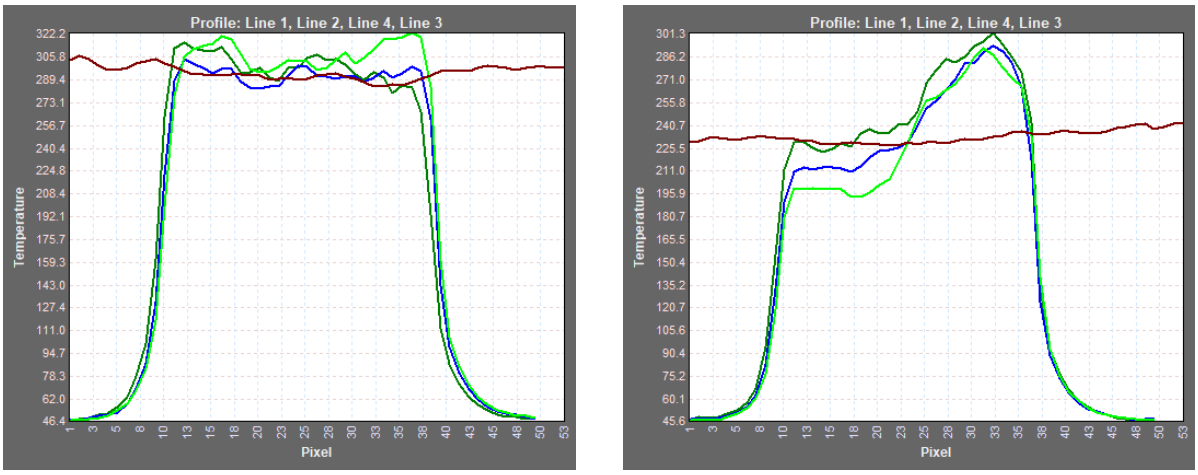


(a) (b)

Figure 5.3: Temperature profile at peak temperature time for two slightly laser deconsolidated tapes. Line colors correspond to the indicators in Figure 5.1.

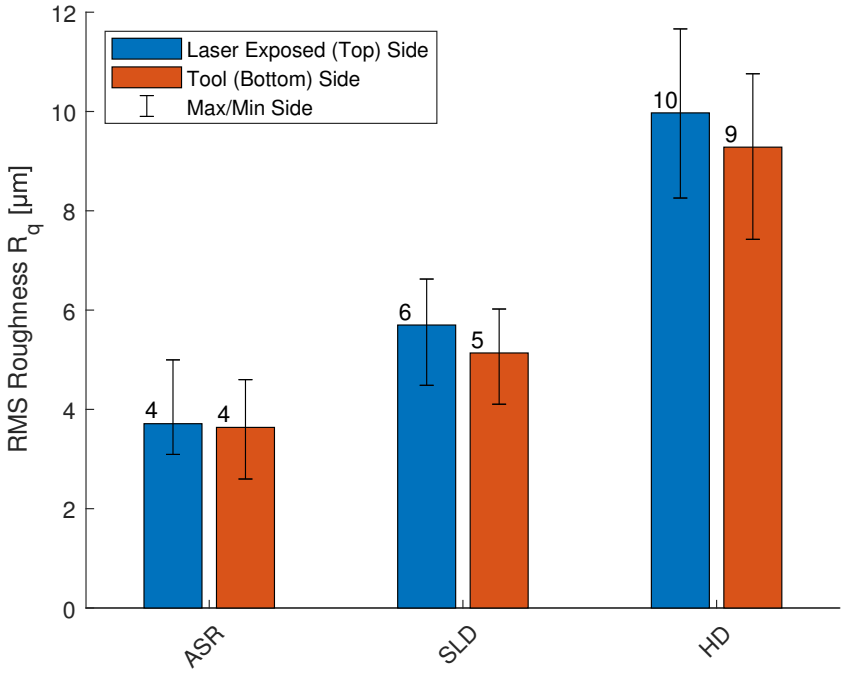


Figure 5.4: Root-mean-square roughness of each degree of deconsolidation.

structural support to develop any out-of-plane deformation. In order to remove the global shape of the profile that affects the waviness value, a high bandwidth filter of 2.5 mm was applied. The resulting waviness curves of the same primary profiles of Figure 5.6 are shown in Figure 5.7. Now the waviness of the highly laser deconsolidated specimen is clearly larger than the slightly laser deconsolidated which is also the case when looking at the average values in Figure 5.5b where the 2.5 mm high bandwidth filter has been applied. These results also agree better with the visual difference in waviness between the two cross-sections shown in Figure 5.6.

## 5.3 Void Content and Cross-sections

The void content of the as-received and rapid laser deconsolidated samples is shown in Figure 5.8. The slightly laser deconsolidated specimens is with a void content of 2.8 a significantly higher than the as-received tapes even though the specimens did not experience temperatures above the melting point. The void content of the highly laser deconsolidated specimens is 4.6. Mostly the amount of voids and locations with voids increases from the slightly to the highly laser deconsolidated tapes which is also clearly the case in the cross-sections in Figure 5.6.

Figure 5.9 shows a representative cross-section for each degree of deconsolidation. The laser deconsolidation induces waviness and warpage in the tape. The slightly deconsolidated specimens contain a few big voids around the middle of the tape whereas the highly deconsolidated tapes contain many voids. The overall cross-section quality clearly decreases when increasing the amount of deconsolidation which manifests in an increase of void content, increase of local thickness, and higher roughness. Interestingly, there are some local sections of the cross-section that do not seem to be affected much or at all by the laser. This might be because these local area are touching the tool which acts as heatsink or due to weak spots in the laser distribution which can be seen in Figures 5.1 and 5.3.

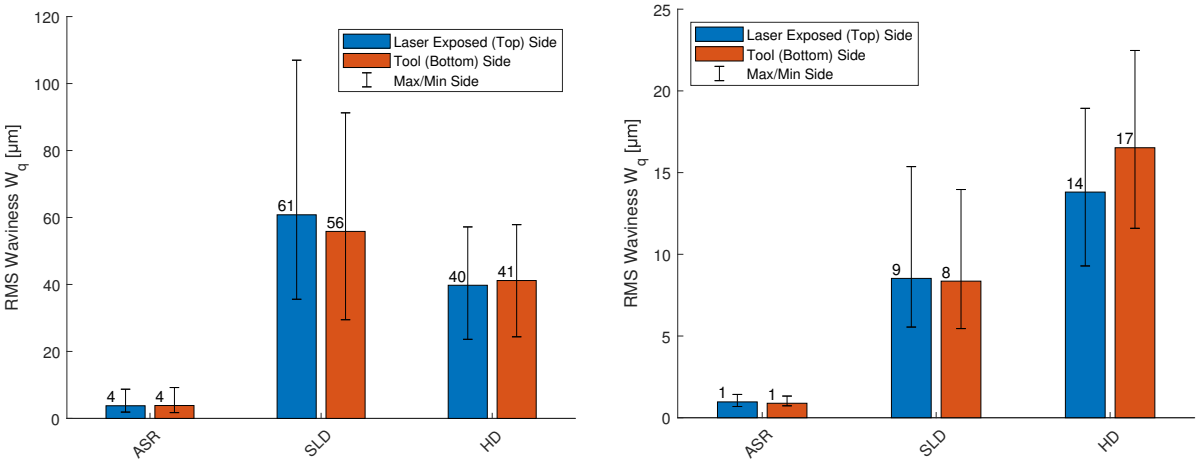


(a) No additional high bandwidth filter.

(b) 2.5 mm high bandwidth filter.

Figure 5.5: Root-mean-square waviness of each degree of deconsolidation.

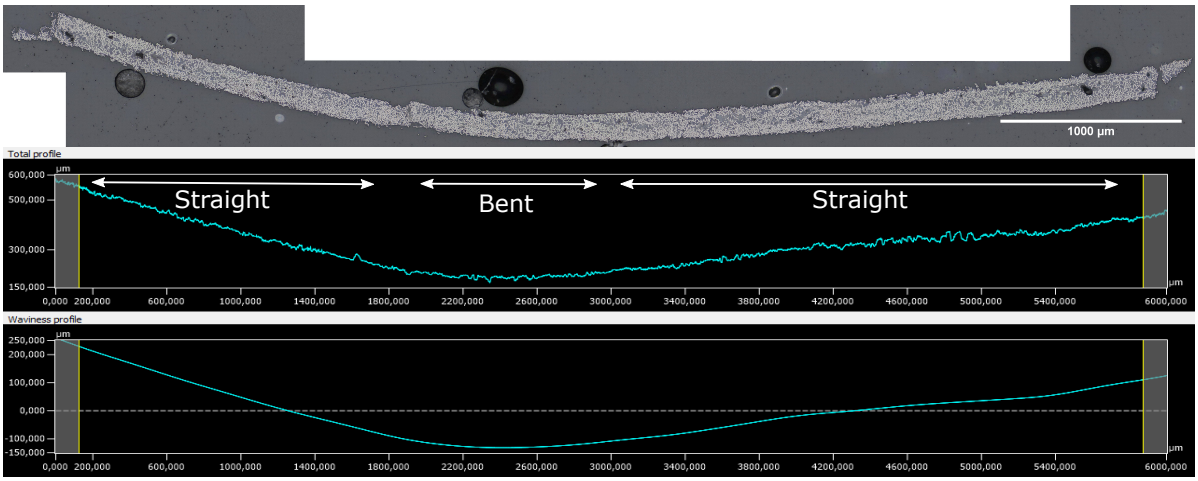


(a) Slightly laser deconsolidated profile, root-mean-square waviness of 91 µm.

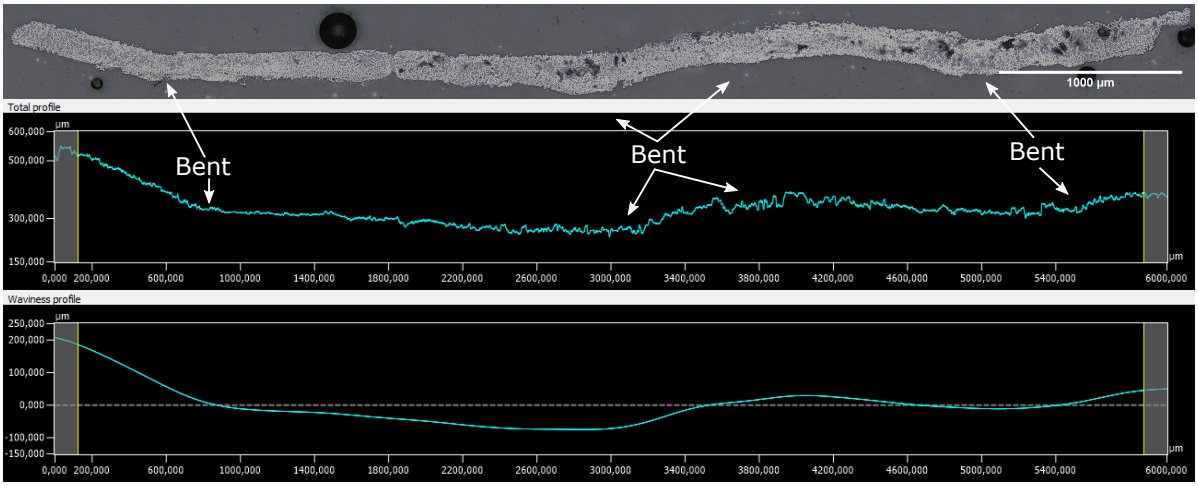


(b) Highly laser deconsolidated profile, root-mean-square waviness of 52 µm.

Figure 5.6: Example of slightly and highly laser deconsolidated tapes to depict the reason for the difference in waviness values.

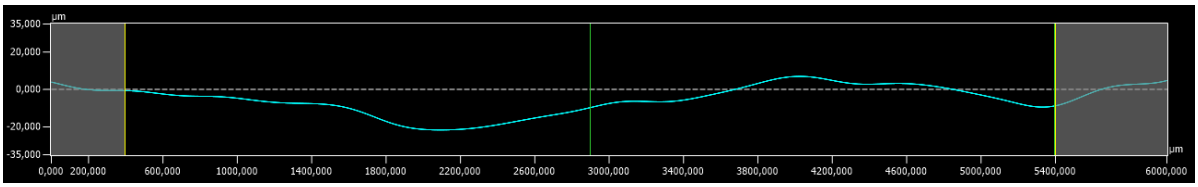


(a) Slightly laser deconsolidated profile, root-mean-square waviness of 9 µm.

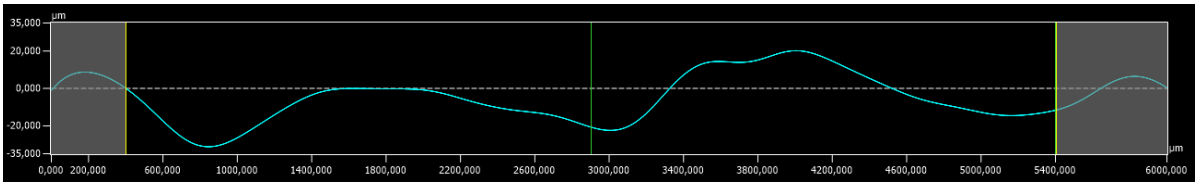


(b) Highly laser deconsolidated profile, root-mean-square waviness of 14 µm.

Figure 5.7: Slightly and highly laser deconsolidated tape waviness profiles with 2.5 mm high bandwidth filter.

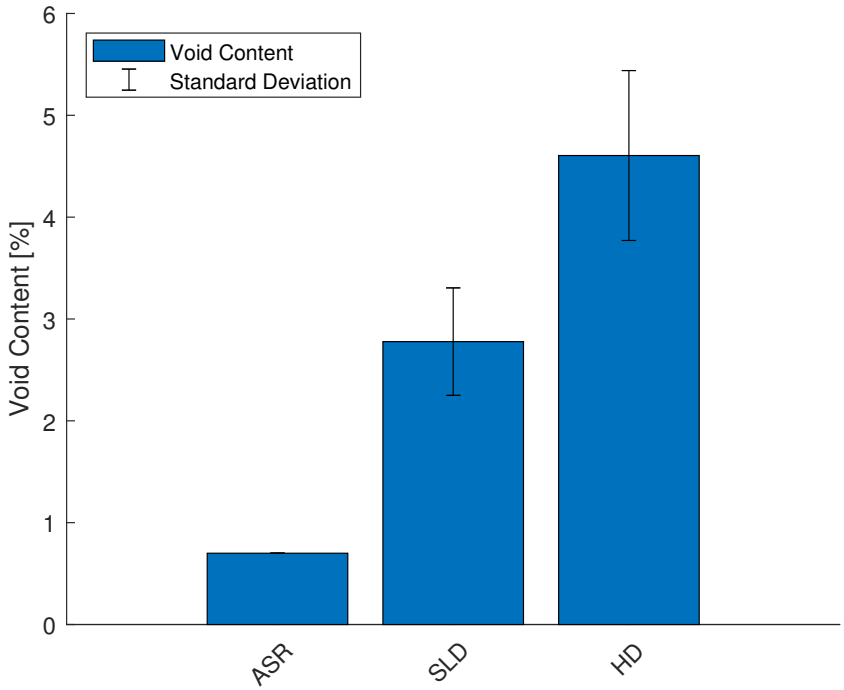


Figure 5.8: Void content of all specimens grouped per degree of deconsolidation pre-intimate contact experiment.

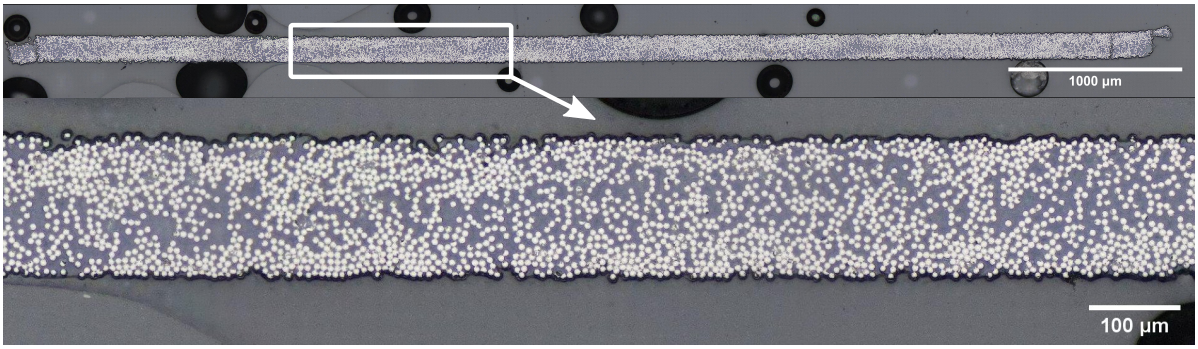


(a) As-received

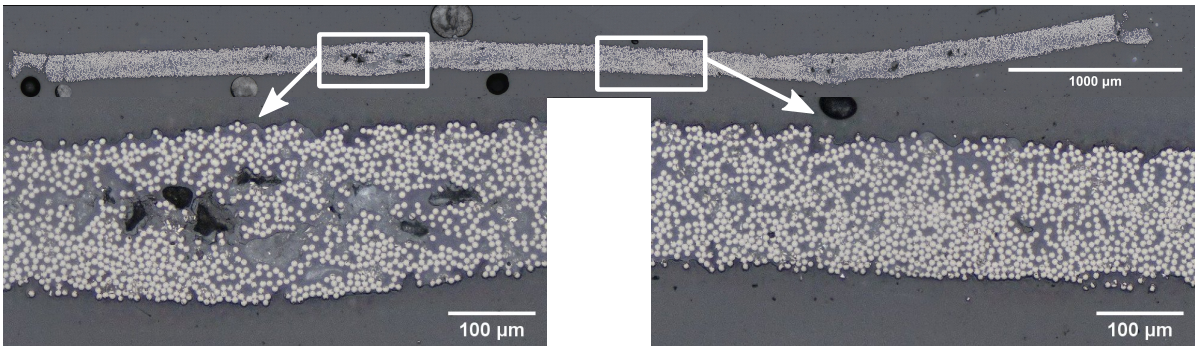


(b) Slightly deconsolidated

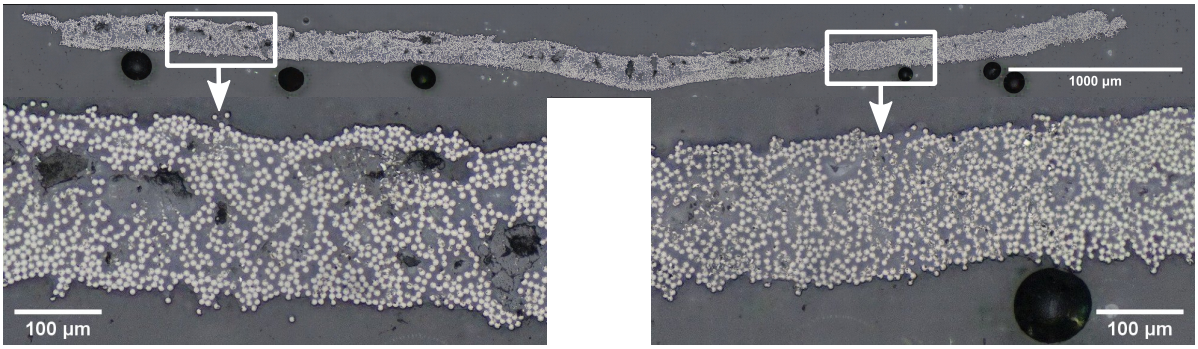


(c) Highly deconsolidated

Figure 5.9: Example of cross-section of each degree of deconsolidation.

## 5.4 Conclusion

Three degrees of deconsolidation were prepared: the as-received samples which have not been exposed to the laser, a slightly deconsolidated setting which reached temperatures between glass and melt transition points of the PEEK matrix, and a set of highly deconsolidated samples that reached temperatures above PEEK melt.

The root-mean-square roughness of the specimens showed significantly increased with each increasing step of the state of deconsolidation. There is a small overlay in roughness values of the as-received and slightly deconsolidated specimens, but the highly deconsolidated samples do not have any roughness overlap. For the laser deconsolidated samples, the laser exposed side is rougher than the bottom side.

Through cross-sectional microscopy, the effect of rapid laser deconsolidation onto the tape microstructure was shown. Void content significantly increased with laser deconsolidation. Also the geometrical shape changes: the laser deconsolidated samples have bending points at many locations along the cross-section which was also quantified by waviness which is a factor 10 higher for the highly laser deconsolidated specimen than the as-received specimens.

The next chapter will shed more light on whether and how these differences affect intimate contact development.

# Chapter 6

# Intimate Contact Development

This chapter shows and discusses the effects of degree of deconsolidation, pressure, and temperature on the in-situ gap length measurements, final thickness, void content, projected surface area, roughness, waviness, and DEIC. Section 6.1 presents the results from varying the pressure above the melting temperature also referred to as 'high' temperature setting. Results of the 'low' temperature setting are found in Section 6.2 which zooms-in to the mechanisms that take place around the glass transition region. Finally, a set of experiments was carried out to see the evolution of as-received tapes between the glass transition and melt regions in Section 6.3.

## 6.1 Pressure Variation Above Melting Temperature

All data presented in this section was obtained with the intimate contact experiment settings corresponding to the 'high' temperature configuration in Table 4.2.

### 6.1.1 In-situ Gap Length

Gap length data was measured during the intimate contact experiment by the RSA-G2 machine. The gap length data processing procedure as explained in Chapter 4 and Figure 4.10 was used. For the purpose of comparing different degrees of deconsolidation and pressures with each other, the gap length measurements have been averaged into a single curve for each set of three repetitions of each configuration (degree of deconsolidation, maximum temperature setting, and pressure level). These averaged curves still exhibit the same characteristic features as the individual measurements. Together with the gap length, the temperature measured by a thermocouple is shown so that characteristic behavior can be traced to the temperature of the tape.

#### Effect of Pressure

Three charts, one for each degree of deconsolidation (as-received, slightly laser deconsolidated, and highly laser deconsolidated), are shown in Figure 6.1. Each chart shows the average gap length curves for all the pressure levels that were tested at the 'high' temperature profile setting.

**As-received** For the 10, 50, and 100 kPa pressure settings, a clear trend is observed in Figure 6.1a: increasing the pressure decreases the gap length over the whole experiment. The 300 kPa curve, however, is increasing in gap length while warming up towards the glass transition temperature. This results in a higher thickness with respect to the 50 and 100 kPa pressure curves until the temperature during the cooling phase is back to the glass transition temperature. At 10 kPa, the initial gap length is much higher than at the other pressure levels. The gap length drastically reduces, from 190 µm to almost 150 µm, during the heating phase as the temperature approaches glass transition. The 50 and 100 kPa curves are decreasing less drastically during the heating phase below the glass transition temperature, the reduction in gap length is around 7 µm which is equal to the diameter of a carbon fiber.

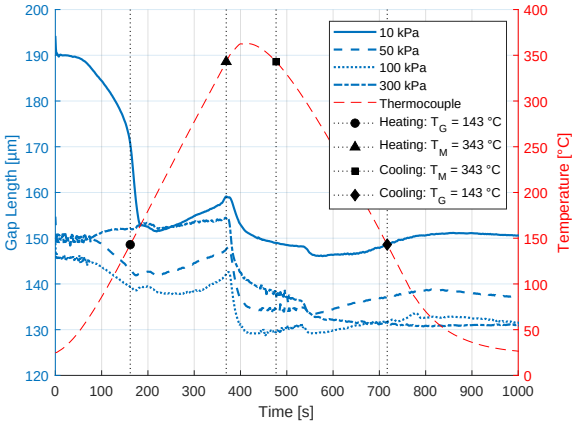


(a) As-received.

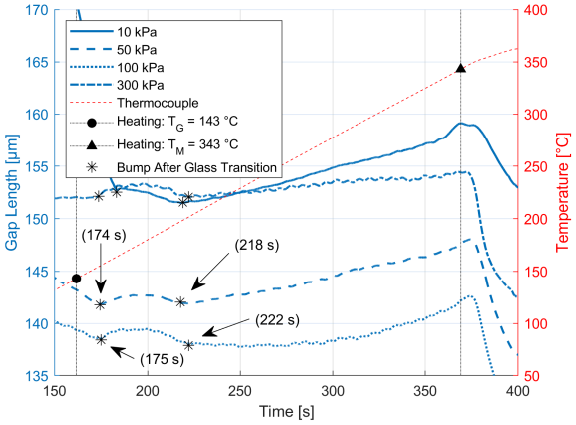


(b) As-received zoom-in.

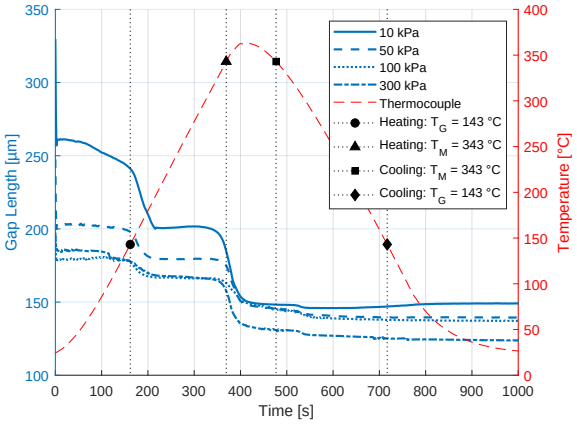


(c) Slightly laser deconsolidated.

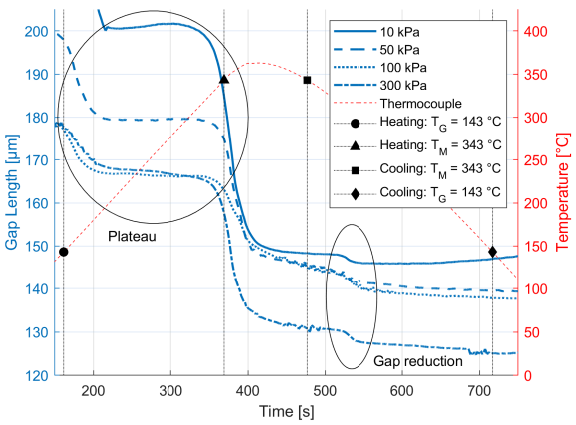


(d) Slightly laser deconsolidated zoom-in.

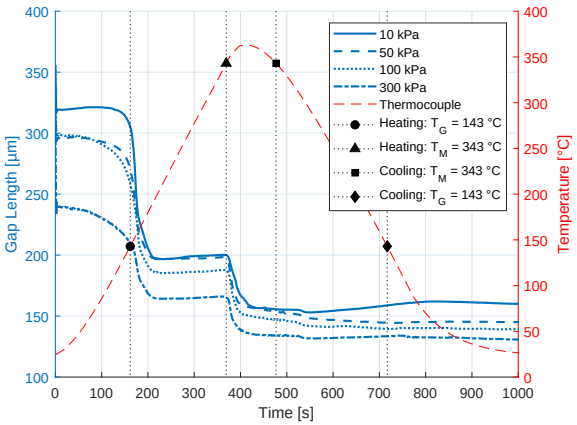


(e) Highly laser deconsolidated.

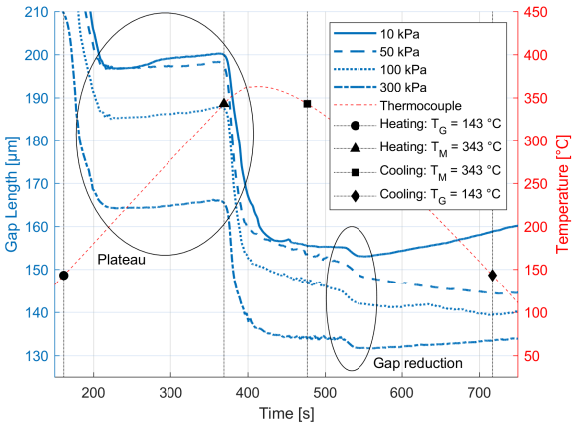


(f) Highly laser deconsolidated zoom-in.

Figure 6.1: Gap length measurements showing all pressure levels, grouped per degree of deconsolidation, subjected to a maximum temperature of 363 °C.

Right after the glass transition temperature, the decrease in gap length of the 10, 50 and 100 kPa configurations stopped and a 'bump' can be identified. Figure 6.1b provides a close-up and marks the start and end points of the bump. It starts around 175 s and first increases and then decreases in gap length which is done at around 220 s. After this bump, at 220 s, the gap length of all the pressure level configurations is increasing up to a local peak in gap length that corresponds with the thermocouple reading crossing the melting temperature at which a drastic collapse in gap length starts. During the cooling phase, between the melting and glass transition temperatures, another small thickness compaction bump is visible near 550 s.

**Slightly Laser Deconsolidated** The slightly laser deconsolidated specimens all start with an initial thickness that is larger than the nominal 150 µm of a pristine tape, see Figure 6.1c. During the initial heating below (the glass transition temperature), the gap length slowly decreases for all pressure levels. When the glass transition temperature is reached, the gap length reduces more quickly until around the 220 s. Between glass transition and melt regions there is a plateau from around 220 to 350 s where the gap length remains fairly constant, Figure 6.1d zooms-in at this plateau. Then, instead of the rapid collapse in gap length that was observed for the as-received specimens (Figure 6.1b), the slightly laser deconsolidated specimens start to decrease earlier on and initially more gradually in gap length. Similar to the as-received samples, a small reduction bump is present during the cooling phase near 550 s while the temperature is between the melting and glass transition region.

**Highly Laser Deconsolidated** The highly laser deconsolidated samples, see Figure 6.1e, exhibit similar trends as the slightly laser deconsolidated samples. The higher degree of deconsolidation specimens have a higher initial thickness at room temperature than a pristine tape. Initially, the 50 kPa curve overlaps with the 100 kPa curve until the glass transition temperature is reached. Between the glass transition and melting temperatures the 50 kPa curve overlaps with the 10 kPa measurement. Besides these overlaps, higher pressure levels clearly result in lower gap length curves. The gap length after the glass transition region up to the melting temperature, between 220 and 350 s, shown as the plateau in the encircled area in Figure 6.1f, increases only a few microns with a maximum increase of 5 µm for the 10 kPa pressure configuration. The gap length reduction bump during cooling near 550 s which has been observed for the as-received and slightly laser deconsolidated samples is also present in Figure 6.1f.

### Effect of Degree of Deconsolidation

The curves from the previous section are regrouped and this section compares the three degrees of deconsolidation for each pressure level. Figure 6.2 contains the graphs for all pressure levels. The following paragraphs describe the observations per pressure level.

**10 kPa** Figure 6.2a shows all samples have a significantly higher initial thickness at room temperature than the nominal 150 µm thickness of a pristine tape. The initial thicknesses are clearly different for all configurations, increasing with the degree of deconsolidation, ranging from 190 µm for as-received to 320 µm for highly laser deconsolidated. The gap length of the as-received and slightly laser deconsolidated samples start to decrease earlier than the highly laser deconsolidated specimens while approaching the glass transition region. During the heating phase between the glass transition and melting temperature, the two laser deconsolidated gap length curves overlap with each other. Subsequently, the slightly laser deconsolidated curves overlaps with the as-received gap length all the way until the end of the experiment. When cooled down below the glass transition temperature, the as-received and slightly laser deconsolidated specimens have decreased in gap length to the nominal thickness of a pristine tape. The highly laser deconsolidated specimens' gap length at the end of the test is 160 µm.

**50 kPa** Increasing the pressure to 50 kPa, see Figure 6.2b, reduces the initial gap length at room temperature to 150 µm for the as-received specimens. The laser deconsolidated samples also reduced in initial gap length to around 200 µm for the slightly laser deconsolidated and 300 µm for the highly laser deconsolidated specimens. The gap length reduction during heating is the lowest for the as-received tape which decreased with 10 µm, the slightly laser deconsolidated tape reduces more thickness during the glass transition temperature, and the highly laser deconsolidated tape reduced almost 100 µm in

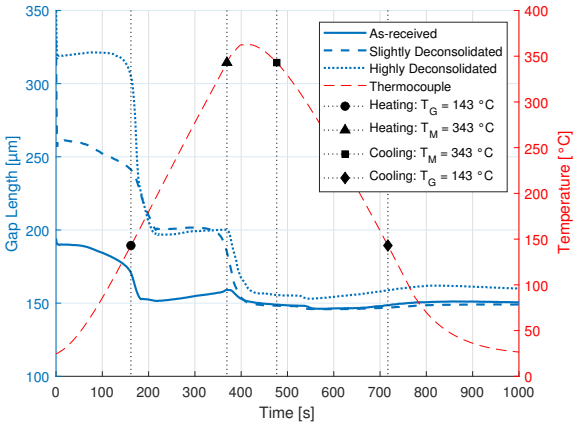


(a) 10 kPa pressure.

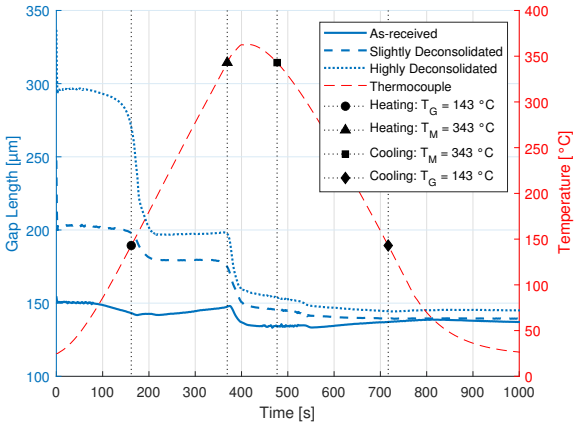


(b) 50 kPa pressure.

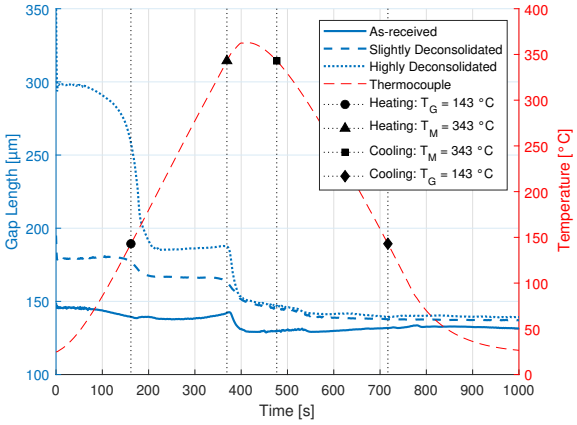


(c) 100 kPa pressure.

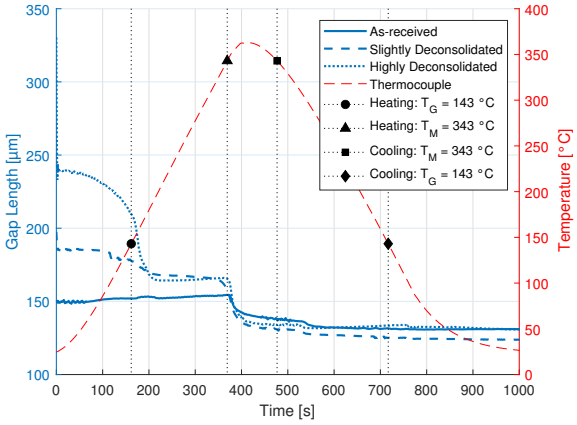


(d) 300 kPa pressure.

Figure 6.2: Gap length measurements of different rapid laser deconsolidated states, grouped per pressure level, subjected to a maximum temperature of 363 °C.

gap length. When crossing the melting temperature during the cooling phase, the slightly laser deconsolidated specimens decrease in gap length to just below the 150 µm. The highly laser deconsolidated specimens are reaching values below 150 µm after the reduction bump near 550 s. Similar to the 10 kPa case, the final gap length values are the same for the as-received and slightly laser deconsolidated samples. Additionally, all samples are below 150 µm gap length.

**100 kPa** The initial gap length values at 100 kPa and its behavior, see Figure 6.2c, are very similar to the 50 kPa case. Only the initial thickness of the slightly laser deconsolidated specimens decreased from 200 to 180 µm while the as-received and highly laser deconsolidated tapes remained their initial gap length. From the melting temperature onwards, the laser deconsolidated curves overlap. The laser deconsolidated gap length curves compact to sub 150 µm gap length values while the temperature is above the melting point. The final gap length measurements are all below 150 µm nominal tape thickness. The laser deconsolidated specimens are almost equal and slightly higher than the gap length of the as-received tapes.

**300 kPa** The gap length curves at 300 kPa pressure are displayed in Figure 6.2d. The initial gap length of the highly deconsolidated specimens is lower at 300 kPa than at 50 and 100 kPa, the other degrees of deconsolidation start at similar gap lengths as the 100 kPa configuration. During the heating phase, the slightly and highly laser deconsolidated specimens overlap from slightly above the glass transition temperature until the melting temperature. After the peak temperature, during cooling all the way until the end of the experiment, the slightly laser deconsolidated specimens have the lowest gap length. The highly deconsolidated gap length curve overlaps with the as-received measurements from the bump near 550 s to the end of the experiment.

### Characteristic Points

During the observation of the gap length curves, a number of characteristic points were discussed. Figure 6.3 shows four characteristic points that are extracted from each gap length curve of every specimen:

**Initial Gap** Average of 15 s (between 5 s and 20 s measurement time to wait for force actuator equilibrium of the machine) at the start of the experiment at room temperature.

**Gap After Glass Transition** Gap length value around 220 s when the gap length has stabilized after the rapid collapse of gap length that corresponds with the glass transition temperature. For the as-received tape this point corresponds with the gap length after the 'bump' that is also marked in Figure 6.1b. For the laser deconsolidated specimens, the first derivative of the gap length curve was used in order to pick the point where the gap length change became (near) zero.

**Gap at Melt** Gap length right before the collapse of gap length that corresponds with the melting temperature. The point is picked at the moment that the gap length is reducing with 20 µm/s as this procedure is consistent for all degrees of deconsolidation. For the as-received specimens, this point occurs right after the peak that which is present near the melting temperature, see Figure 6.1b. The slightly deconsolidated gap length curves start decreasing slowly while being far away from the melting temperature without crossing the 20 µm/s gap length change, therefore, the point might be less representative for this degree of deconsolidation. The highly laser deconsolidated specimens change more abruptly, see Figure 6.1f, and the chosen point is near the local gap length peak corresponding with the melting temperature.

**End Gap** Average gap length of the last 15 s of the measurement which includes a significant cool-down period to ensure all thermal expansion effects between the measurement with tape and reference test have reached equilibrium.

The gap length values at these points and ratios between points allows to present charts where all degrees of deconsolidation and all pressure levels can be compared with each other.

The initial gap length when the sample was loaded at room temperature is provided in Figure 6.4a. When the clamping pressure is increased, the specimen is flattened more, only from 50 to 100 kPa pressure the highly laser deconsolidated specimen remains at more or less equal gap length. The figure also shows a clear increase in gap length when the degree of laser deconsolidation is increased. Only

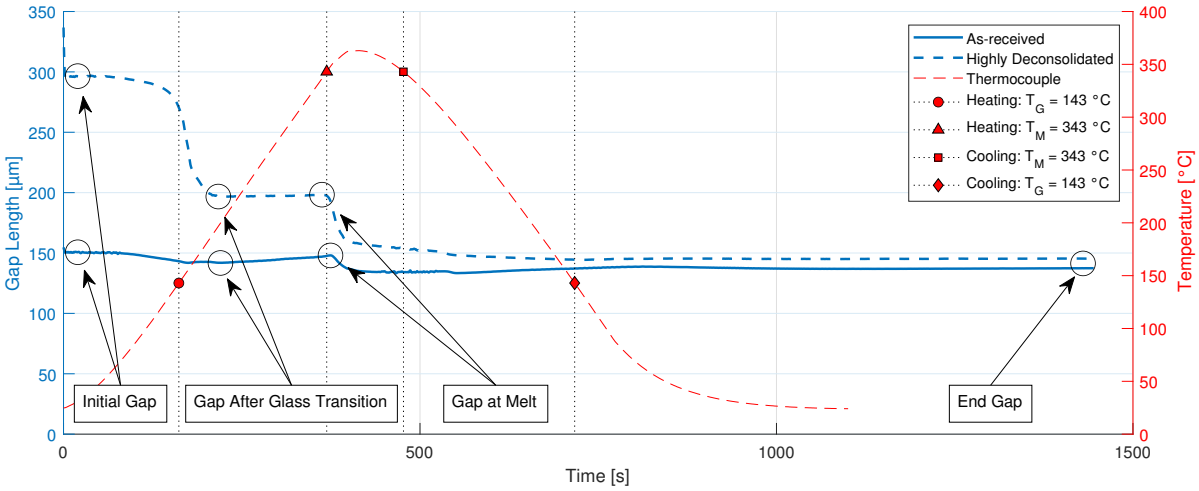


Figure 6.3: Characteristic points identified in gap length measurements of 360 °C maximum temperature setting intimate contact experiment.

the as-received specimens are compressed to a gap length that is near the nominal pristine thickness of 150 µm, thus the cooled down deconsolidated states cannot be reverted back to pristine tape thickness at room temperature.

Figure 6.4b depicts the gap length after the glass transition temperature, shows that only the as-received samples were compacted to and below the nominal pristine thickness of 150 µm at the pressure levels of 10, 50 and 100 kPa while the laser deconsolidated samples are significantly thicker. At 300 kPa, the gap lengths at different degrees of deconsolidation are much closer to each other, the rapid laser deconsolidated specimen are still above the nominal thickness. Strangely, the as-received samples resulted in a thickness slightly higher (around 2 µm) than the nominal thickness at 300 kPa whereas it was compressed to smaller sizes at lower pressures. Significant difference between the slightly and highly laser deconsolidated tapes is only observed at 50 and 100 kPa, at the two pressure levels the higher degree of deconsolidation also has a higher gap length after the glass transition region.

The gap length values of the points after the glass transition and at the melting point are very close to each other which was highlighted as the plateau in Figures 6.1d and 6.1f. Therefore, the data is presented as difference between the melting point and glass transition as a percentage in Figure 6.5a. The as-received tapes show a significant 9 µm increase in gap length at 10 kPa to gradually decrease to a gap length difference of less than 3 µm at 300 kPa. The highly laser deconsolidated increase less than 3 µm for all pressure configurations. The values for the slightly laser deconsolidated specimens does not represent the same as for the as-received and highly laser deconsolidated specimens since the gap length starts to decrease much more gradually before the melting temperature (see Figure 6.1d), therefore the chosen melting point has a much lower value.

Figure 6.5b shows the difference between the gap length after the glass transition region and at the end of the experiment. The scatter between the repetitions is quite large. There is a clear distinction between the as-received and laser deconsolidated specimens. At 10 kPa, the as-received tapes do not change in thickness on average, but with increasing pressure, the tapes are more compacted more, resulting to around 20 µm compaction at 300 kPa. Both laser deconsolidated specimens compact between 30 and 50 µm varying over all pressure levels.

The final thickness of the specimens is presented in Figure 6.6 which contains the gap length at the end of the intimate contact test and the thickness measured from the microscopy images of the cross-sections. The data from both methods match with each other except for the magnitude with respect to a pristine tape at 10 kPa. At 10 kPa, the as-received and slightly laser deconsolidated specimens are around the nominal pristine tape thickness based on the gap length data whereas the cross-sectional microscopy data shows lower than pristine tape thickness values for these specimens. The highly laser deconsolidated specimens are clearly thicker than a pristine tape after the intimate contact test. With increasing pressure, the final thickness is reducing for all degrees of deconsolidation. At 50 kPa pressure,

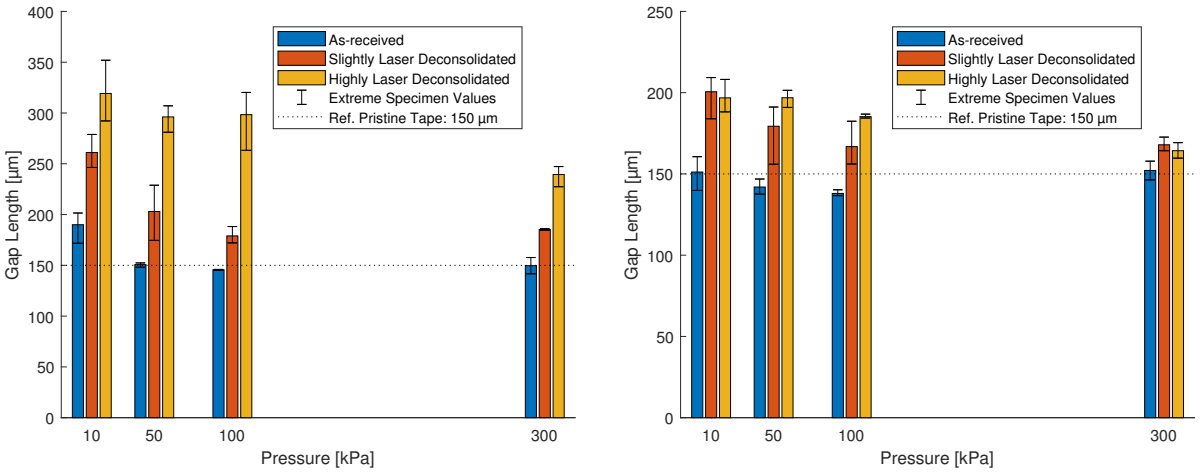


(a) Initial gap length at room temperature.

(b) Gap length after glass transition.

Figure 6.4: Initial gap length (a) and gap length after the glass transition (b) of different laser deconsolidated specimens and pressure levels at a maximum temperature of 363 °C.

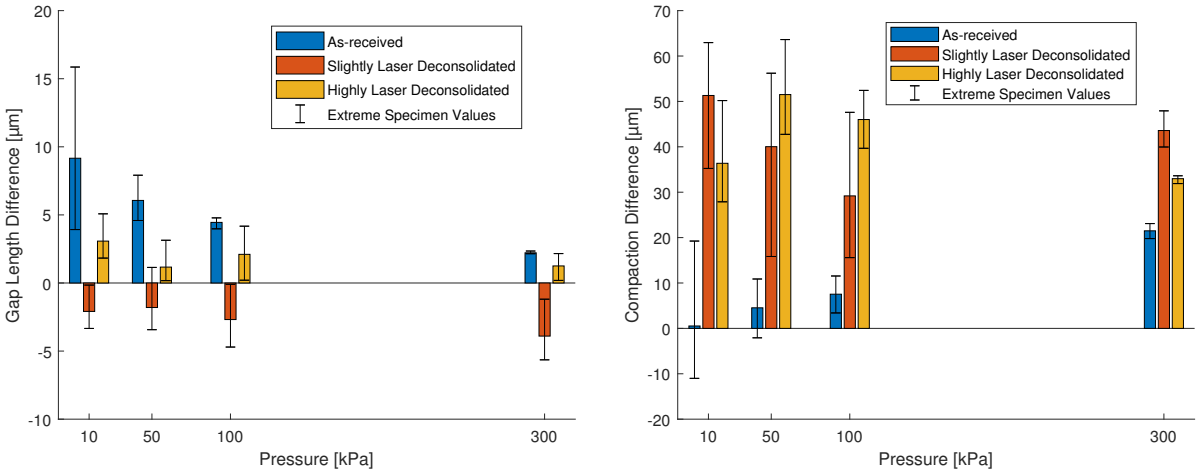


(a) The difference between the gap lengths after glass transition and at the melting point.

(b) The difference between the gap lengths after glass transition and the end of the experiment.

Figure 6.5: Gap length difference at melt (a) and at the end of test (b) with respect to the gap length after the glass transition for different laser deconsolidated specimens and pressure levels subjected to a maximum temperature of 363 °C.

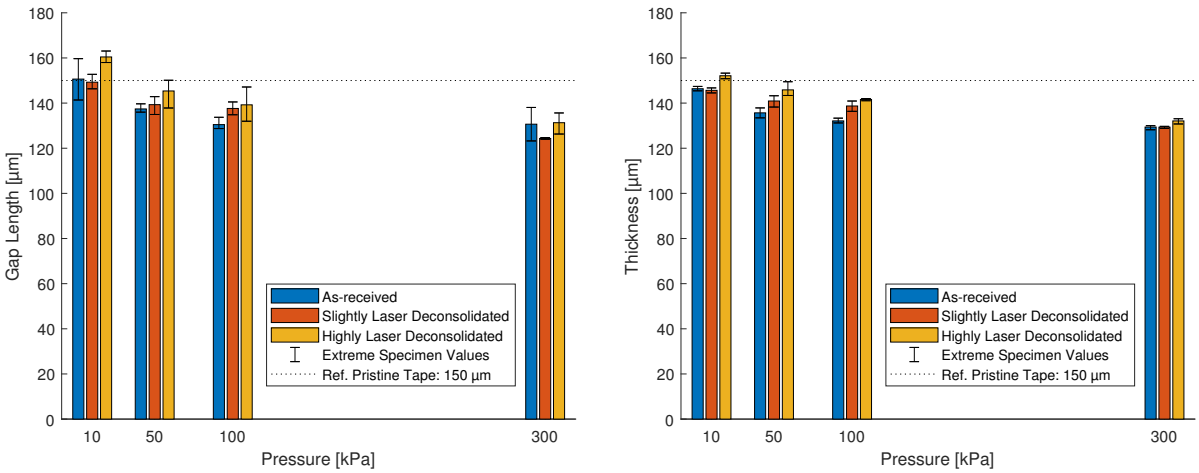


(a) Gap length at end of test at 25 °C.

(b) Thickness from cross-sectional microscopy images.

Figure 6.6: Tape gap length (a) and thickness (b) after intimate contact experiment of different laser deconsolidated specimens and pressure levels subjected to a maximum temperature of 363 °C.

all degrees of deconsolidation are below the 150 µm nominal tape thickness. At 300 kPa pressure, all degrees of deconsolidation results in a similar thickness.

### 6.1.2 Void Content

The void content of the tapes after the intimate contact test is presented in Figure 6.7. Since the intimate contact experiment consists of a single tape, the reported void content is the intralaminar void content. The worst case measurement was a single highly laser deconsolidated specimen subjected to 10 kPa pressure, resulting to 1 % which is still within the manufacturer specifications[1] of <1 %.

The void content results of the as-received tapes are consistently around 0.2 to 0.3 % over all pressure levels. Both slightly and highly laser deconsolidated specimens show a downward trend in the observed void content with increasing pressure. Especially at 10 kPa there seems to be a significant difference between the as-received and both laser deconsolidated specimens. A close-up of the cross-section of a slightly laser deconsolidated specimen is provided in Figure 6.8 showing the size of the voids. At 50 and 100 kPa, there error bars of all degrees of deconsolidation overlap. Interestingly, at 300 kPa the higher the degree of deconsolidation the lower the final void content, however, with such low void volume content the difference is highly sensitive for local features.

A selected set of zoomed-in cross-sectional images is provided in Figure 6.9. The overview shows how the cross-section evolves for each degree of deconsolidation with the applied pressure. For void content, Figures 6.9g and 6.9l depict how void that were present pre-intimate contact have been compressed or even fully disappeared. The highly laser deconsolidated specimens at 10 kPa pressure were found to have more voids, but also often slightly bigger voids, than the slightly laser deconsolidated specimens. For the higher pressures, the void size is often in the order of one to a few carbon fiber cross-sectional areas.

### 6.1.3 Surface Area

The projected surface area of the samples was measured before and after the intimate contact experiment. The specimen areas vary since the specimens were cut manually from a longer piece of tape material, therefore, the ratio of the projected surface area after the intimate contact experiment over the value before the experiment is presented in Figure 6.10.

At a pressure of 10 kPa, most the of measurements shrunk in projected area. Going to 50 and 100 kPa, there is quite some variation for the as-received and slightly laser deconsolidated specimens. The highly laser deconsolidated specimens follow a more stable trend of increasing area ratio with increasing

[1] TenCate Product Data Sheet: CETEX-TC1200_DS_012417

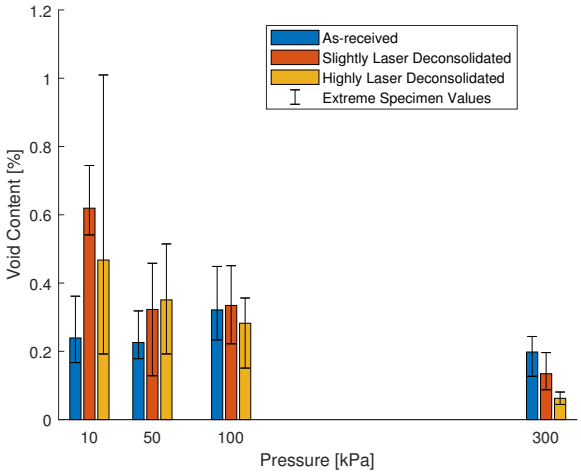


Figure 6.7: Post intimate contact experiment void content of different laser deconsolidated specimens and pressure levels subjected to a maximum temperature of 363 °C.

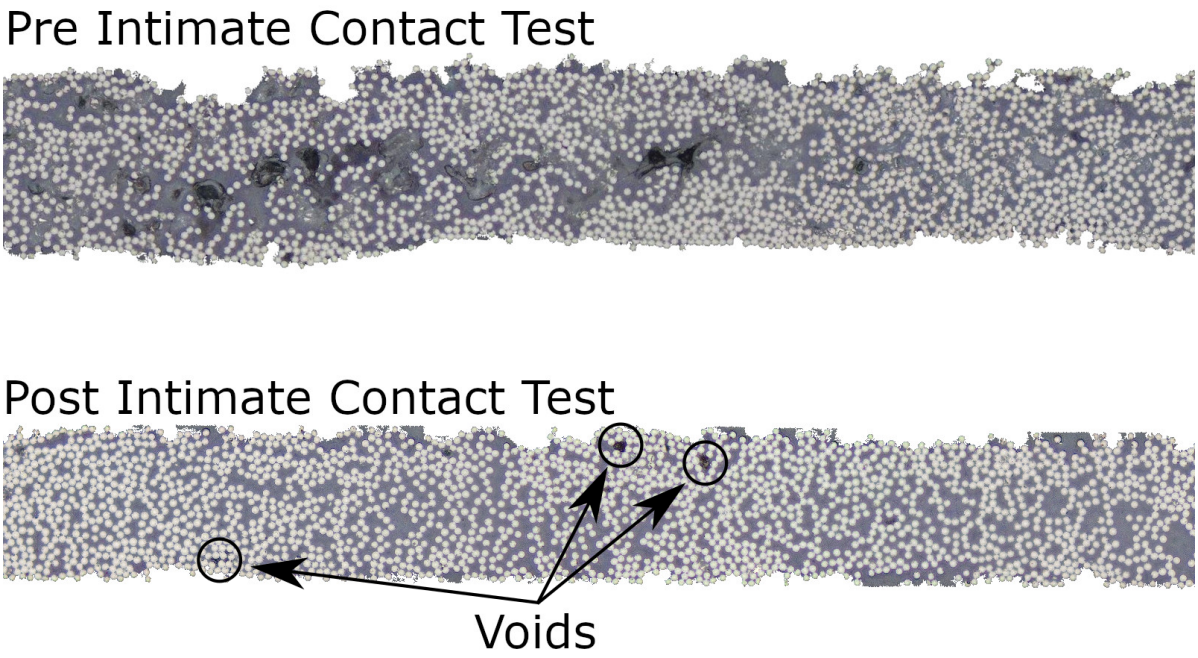


Figure 6.8: Representative void content close-up of slightly laser deconsolidated specimen, before and after intimate contact experiment, subjected to 10 kPa and a maximum temperature of 363 °C.

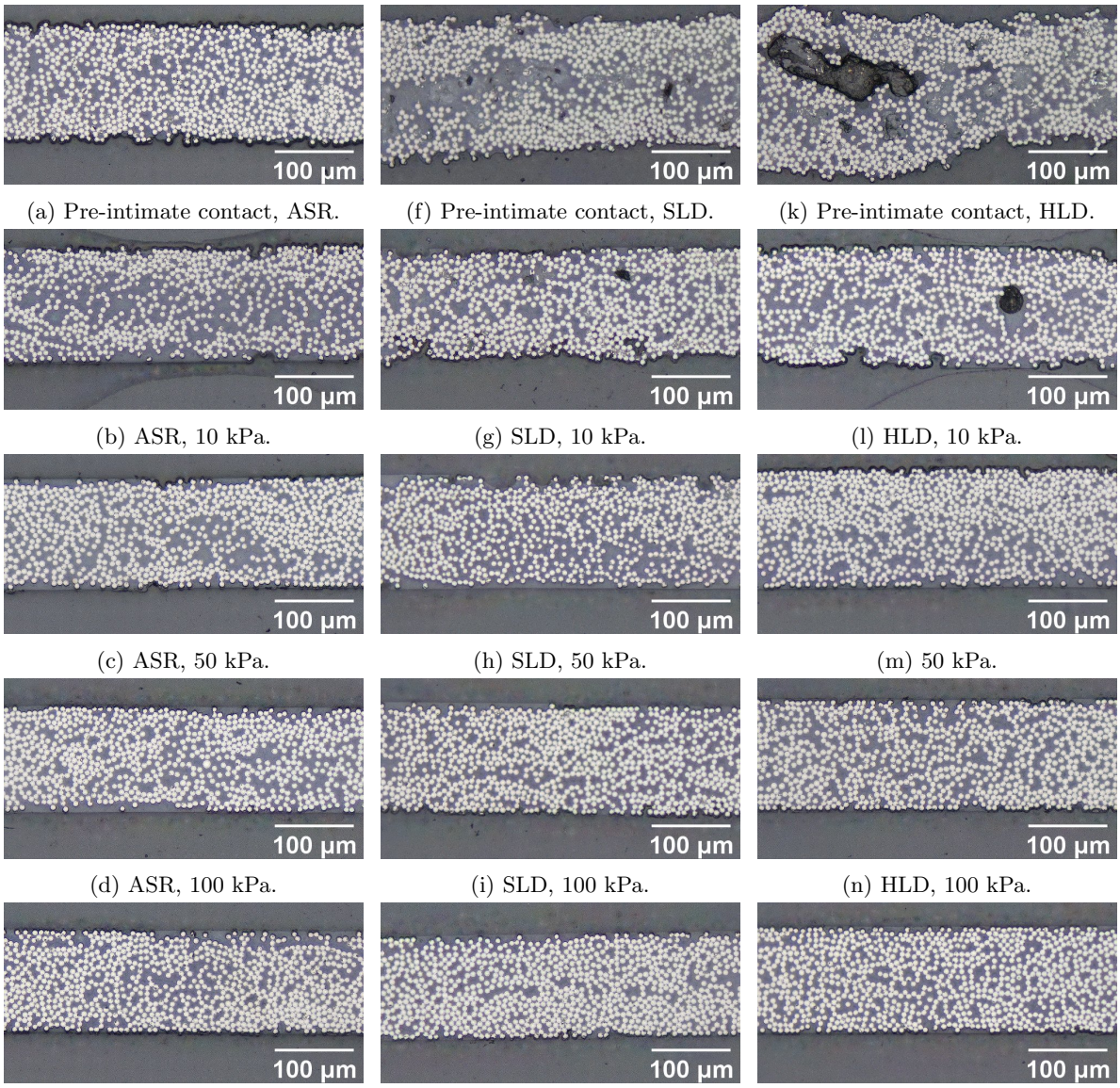


(a) Pre-intimate contact, ASR. (f) Pre-intimate contact, SLD. (k) Pre-intimate contact, HLD.

(b) ASR, 10 kPa. (g) SLD, 10 kPa. (l) HLD, 10 kPa.

(c) ASR, 50 kPa. (h) SLD, 50 kPa. (m) 50 kPa.

(d) ASR, 100 kPa. (i) SLD, 100 kPa. (n) HLD, 100 kPa.

(e) ASR, 300 kPa. (j) SLD, 300 kPa. (o) HLD, 300 kPa.

Figure 6.9: Overview of cross-section evolution with respect to applied pressure for as-received (a, b, c, d, and e), slightly laser deconsolidated (f, g, h, i, and j), and highly laser deconsolidated (k, l, m, n, and o) specimens subjected to a maximum temperature of 363 °C.

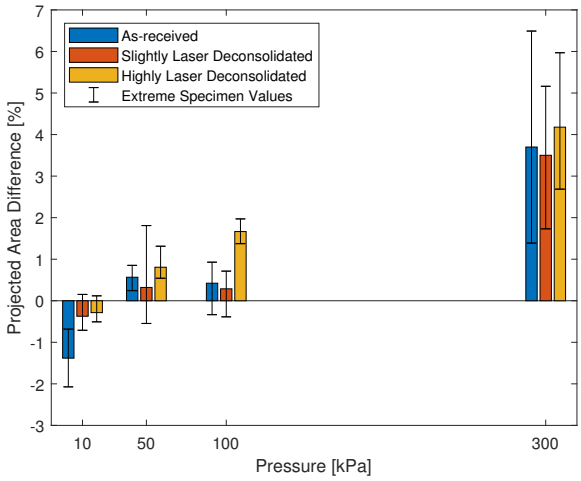


Figure 6.10: Projected area percentage difference post-intimate contact over pre-intimate contact experiment of different laser deconsolidated specimens and pressure levels subjected to a maximum temperature of 363 °C.

pressure, however, when omitting either the 50 or 100 kPa pressure, the as-received and slightly laser deconsolidated specimens also show a clear increasing trend in area ratio with pressure.

At 300 kPa pressure, a clear increase in area is present for all degrees of deconsolidation and the magnitude is similar for all states of deconsolidation. Observation of the microscopy surface images reveals that resin percolation occurs which contributes to the area increase. Figure 6.11 shows that resin percolation is more substantial at 300 kPa than at 100 kPa pressure for the highly laser deconsolidated specimens. Additionally, the higher pressure specimens did not deform uniformly in width: the width at the middle of the specimen increased and is slightly more than at the upper and lower parts of the specimen.

### 6.1.4 Surface Characterization

The surface profile measurements provided a primary profile which was post-processed to a roughness and waviness curve as was explained in more detail in Section 4.4.1. The roughness results are presented first and then the waviness data.

#### Roughness

Root-mean-square roughness values of the laser exposed sides of the specimens are presented in Figure 6.12a. For all pressure levels, a higher degree of deconsolidation led to a rougher surface after the test although at 10 and 100 kPa pressures there is so much overlap between the measurements of the slightly and highly deconsolidated specimens the difference is not significant. Additionally, increasing the pressure resulted in lower roughness of the tape.

The roughness ratio of each specimen post-intimate contact test (Figure 6.12a) over pre-intimate contact test (Figure 5.4) is found in Figure 6.12b. The as-received specimens at 10 kPa are around 20 % rougher after the intimate contact experiment than before, whereas the initially much rougher laser deconsolidated specimens are decreasing in roughness at 10 kPa. The roughness values of the rapid laser deconsolidated tapes at 10 kPa pressure after intimate contact test are, however, still higher than that of a pristine tape.

Interestingly, when looking at the bottom side, opposite of the laser exposed side, of the specimens in Figure 6.13, the trend of roughness values between the degrees of deconsolidation has changed. The slightly laser deconsolidated specimens are consistently rougher than the highly laser deconsolidated specimens. This difference cannot be explained by the roughness of the specimens before the intimate contact test. Figure 5.4 showed a small difference between the laser exposed and tool sides of the specimens, but the highly laser deconsolidated specimens exhibit significantly higher roughness values for both sides than the slightly laser deconsolidated specimens.

(a) 100 kPa pressure.

(b) 300 kPa pressure.

(c) Zoom-in at resin percolation of 100 kPa pressure specimen.

(d) Zoom-in at resin percolation of 300 kPa pressure specimen.

Figure 6.11: Projected area pictures of highly laser deconsolidated tapes after intimate contact experiment at 100 kPa and 300 kPa pressure subjected to a maximum temperature of 363 °C, with zoom-in to longitudinal resin percolation at the end of the tape.

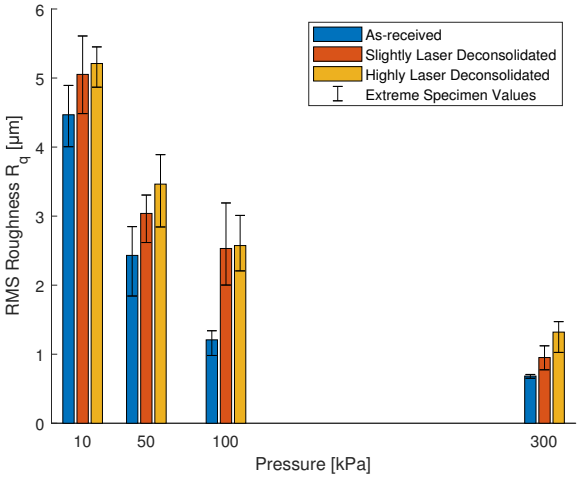


(a) Post-intimate contact experiment.

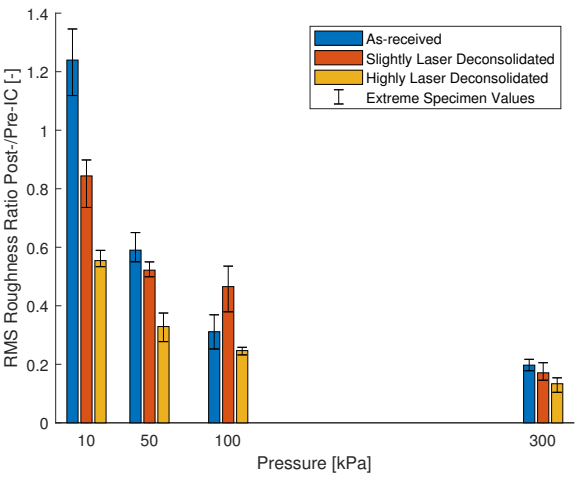


(b) Ratio of values post- over pre-intimate contact experiment.

Figure 6.12: Root-mean-square roughness results of laser exposed (top) side of different laser deconsolidated specimens and pressure levels subjected to a maximum temperature of 363 °C.

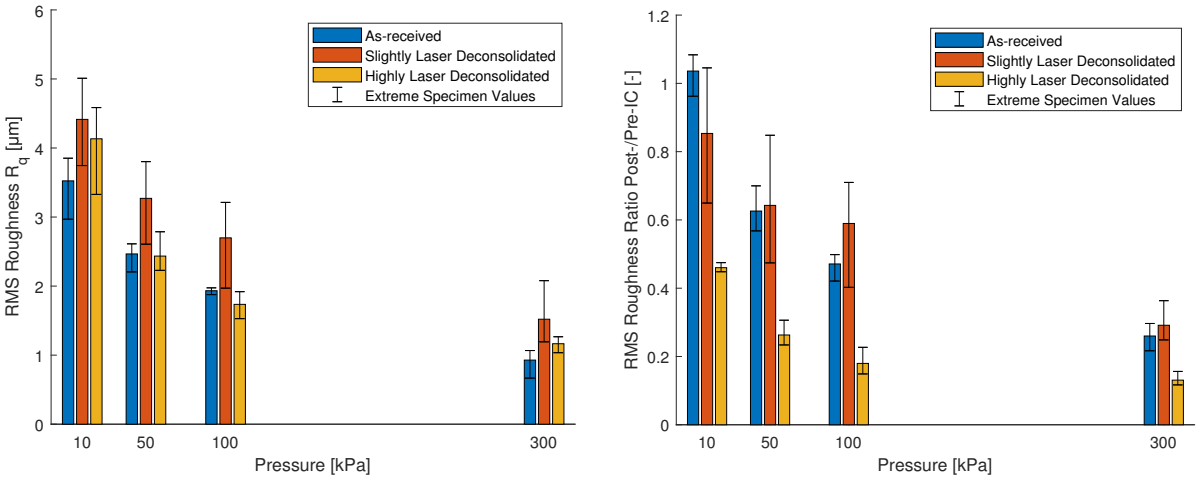


(a) Post-intimate contact experiment.

(b) Ratio of values post- over pre-intimate contact experiment.

Figure 6.13: Root-mean-square roughness results of tool (bottom) side of different laser deconsolidated specimens and pressure levels subjected to a maximum temperature of 363 °C.

#### Waviness

The waviness measurements of the post-intimate contact test are shown in Figure 6.15a. The waviness was averaged over both laser exposed (top) and tool (bottom) sides since there is values are nearly identical. The waviness of the as-received specimens seem to be slightly decreasing with increasing pressure, but for the other degrees of deconsolidation there does not seem to be a clear trend. The rapid laser deconsolidated specimens actually increase in waviness at the higher pressures. At 100 and 300 kPa pressure, both slightly and higher laser deconsolidated specimens exhibit higher a waviness than the as-received samples. However, with only three repetitions per setting and these scatter ranges it is hard to conclude from the data.

A more useful representation is the ratio of the waviness post-intimate contact test (Figure 6.15a) over its value pre-intimate contact test (Figure 5.5a) in Figure 6.15b which shows that the rapid laser deconsolidated specimens' waviness is highly reduced by the intimate contact experiment. The as-received tapes, however, increased in waviness after the intimate contact experiment.

A reason for the large scatter in the measurements is the influence of the overall shape or warpage of the tape. A closer look at the primary and waviness profiles of the laser deconsolidated tapes, two representative profiles are provided in Figure 6.14, shows that the slightly laser deconsolidated sample has a more pronounced shape affecting the waviness value. A recommendation is to apply a shape correction to eliminate the overall shape of the profile and one could investigate more local waviness behavior.

With the 2.5 mm high bandwidth filter applied, the scatter between the measurements was reduced. At 100 kPa the results are more distinct from each other and it seems like the more deconsolidated specimens result in more waviness, but this cannot be confirmed at the other pressure levels where the measurement data range overlaps between the different degrees of deconsolidation. Compared with the pre-intimate contact waviness of 8 to 17 µm in Figure 5.5b, the specimens have become much flatter with a waviness of 1.5 to 2 µm.

### 6.1.5 Developed Degree of Effective Intimate Contact

The DEIC results are, similar to the roughness results, also separately shown for the laser exposed (top) side and bottom side in Figure 6.16. For the 10, 50, and 100 kPa pressure levels, the laser exposed (top) side performs as expected (see Figure 6.16a): the higher the degree of deconsolidation the lower the amount of developed DEIC. At the tool (bottom) side (see Figure 6.16b), however, for the same pressure levels, the highly laser deconsolidated tapes developed more effective intimate contact than the slightly laser deconsolidated tapes. Additionally, the highly laser deconsolidated specimens developed

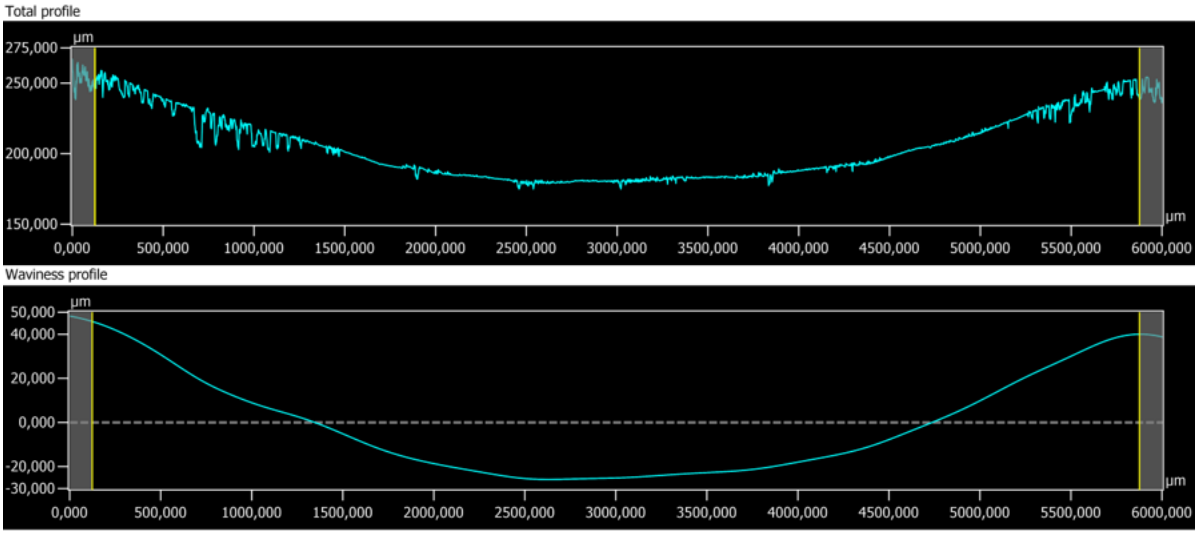


(a) Slightly laser deconsolidated with a root-mean-square waviness of 22.0 µm.

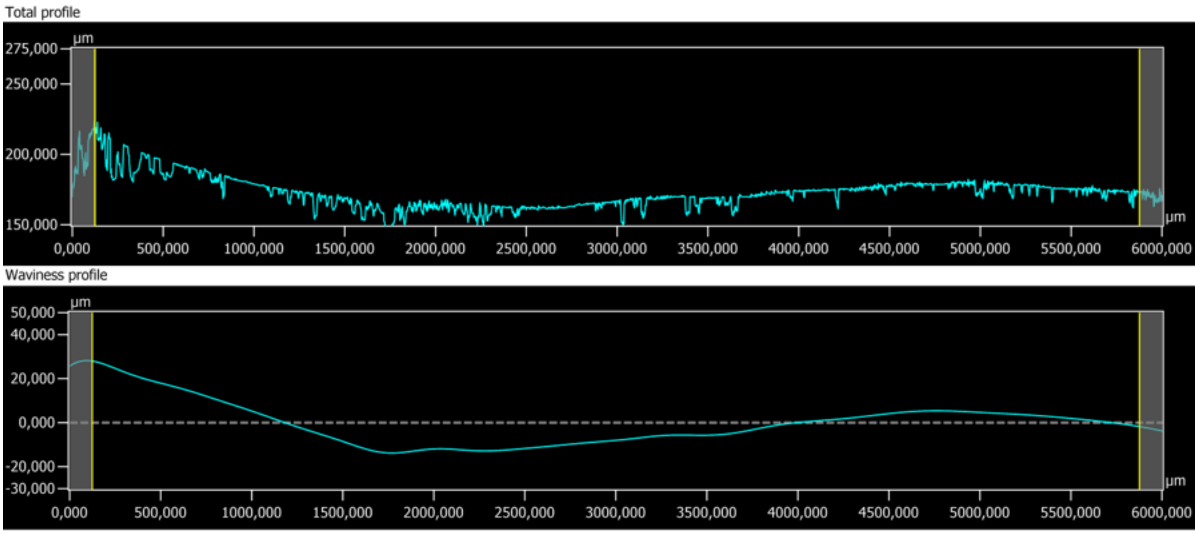


(b) Highly laser deconsolidated with a root-mean-square waviness of 9.7 µm.

Figure 6.14: Primary and waviness profiles of a slightly and highly rapid laser deconsolidated specimen subjected to 50 kPa pressure and a maximum temperature of 363 °C. The profiles were measured at the laser exposed (top) side in the middle of the specimens.

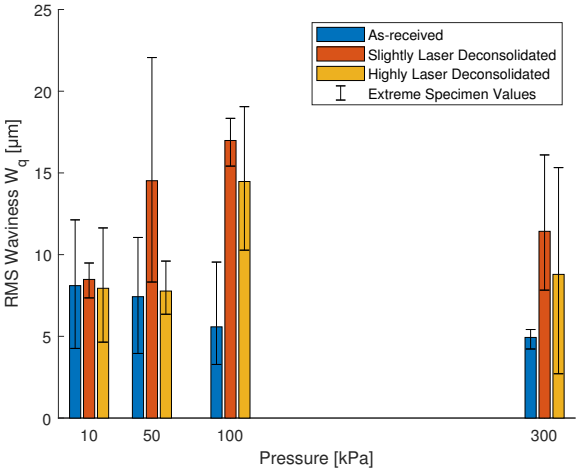


(a) Post-intimate contact experiment.

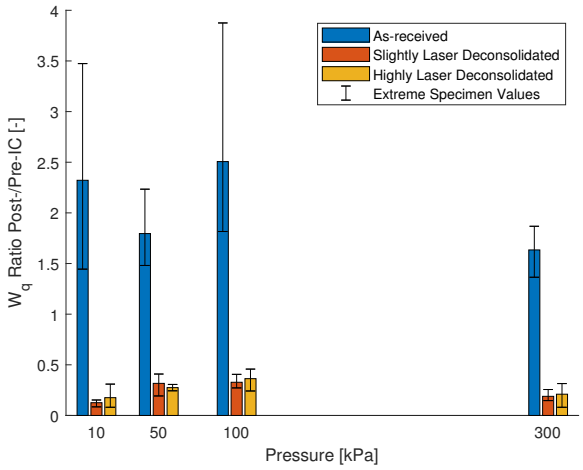


(b) Ratio post-intimate contact over pre-intimate contact.

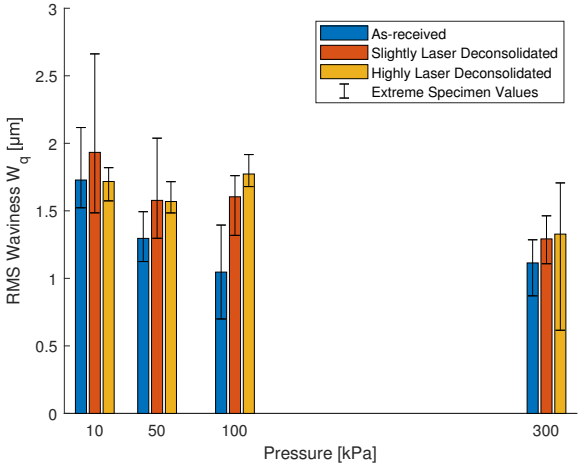


(c) Post-intimate contact with 2.5 mm high bandwidth filter.

Figure 6.15: Root-mean-square waviness results after intimate contact experiment of different laser deconsolidated specimens and pressure levels subjected to a maximum temperature of 363 °C.

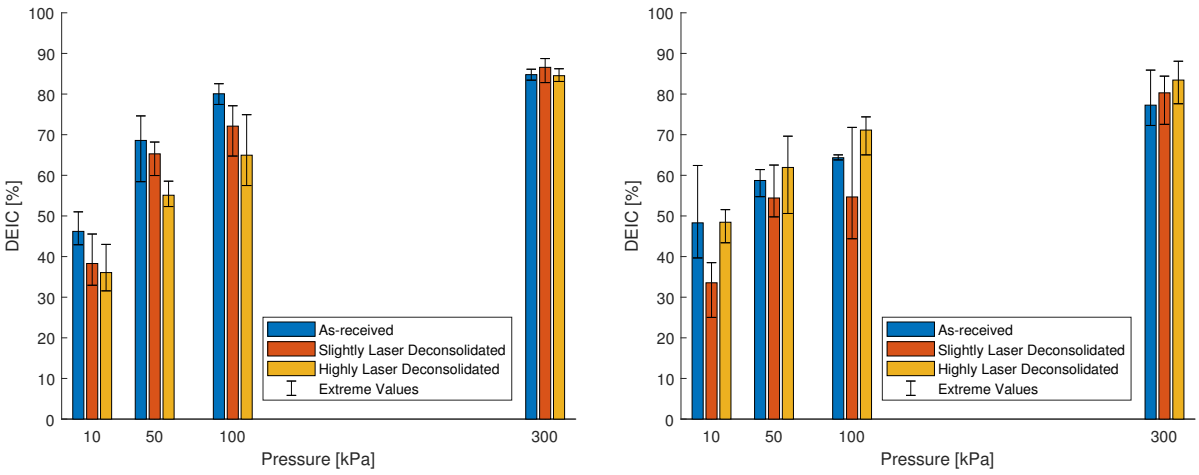


(a) Laser exposed (top) side.

(b) Tool (bottom) side.

Figure 6.16: DEIC results of different deconsolidated specimens and pressure levels subjected to a maximum temperature of 363 °C.

the same amount or more effective intimate than the as-received tapes.

A significant amount of intimate contact is already developed at 10 kPa which is interesting considering that for example the roughness results showed an equal or worse roughness of the as-received tapes after the test with respect to before the intimate contact experiment at this pressure. At 300 kPa pressure, the different degrees of deconsolidation perform comparable and differences are assumed to be within the experimental and chosen grayscale threshold accuracy.

An overview of one surface per configuration (degree of deconsolidation and pressure level) is shown in Figure 6.17. A clear trend is observed: DEIC (bright) and fiber rich (dark) areas mostly orientated along the fiber direction (vertically). Also it is visually clear that the DEIC area increased with pressure, but the difference between the degrees of deconsolidation for a set pressure level is not significant enough to distinguish by eye. The DEIC area seems to develop in a similar manner between the degrees of deconsolidation.

### 6.1.6 Discussion

The presented results evaluated Hypothesis HP 1 for a maximum temperature that was above the melting temperature. For the pressure range between 10 and 100 kPa, increasing the degree of deconsolidation led to higher final tape thickness, higher roughness of the laser exposed side, and a decrease in DEIC of the laser exposed side. This was as expected due to their pre-intimate contact state that was analyzed in in Chapter 5: the rapid laser deconsolidated specimens exhibited higher initial roughness and waviness which affects the same properties as well as the DEIC at the post-intimate contact experiment state at these pressure levels. In order for the rapid laser deconsolidated specimens to be reverted back to pristine tape properties, the global cross-section needs to flattened requiring both deformation of the composite fiber-matrix medium as well as flow of the matrix to wet dry fibers or locally fiber dense areas.

Void content was hypothesized to increase when increasing the degree of deconsolidation or decreasing the applied pressure. However, only at 10 kPa pressure, the void content of the laser deconsolidated specimens was more than the as-received state of deconsolidation, at the other pressure levels the results of the different degrees of deconsolidation within each others range. The reduction of the void content is significant when compared to the cross-section before the intimate contact test in Figure 5.9. One of the reasons for the low void volumes, is that the void migration distance is very small, if voids can escape through the thickness being maximum 75 µm to either top or bottom side from the middle of the tape. Additionally, the time above the melting temperature provides ample time for the voids to migrate, significant void reduction can be established in a matter of seconds especially at small distances [76]. This might be different when two tapes are placed on top of each other and voids are trapped, especially for processing conditions with much smaller time-frames. Two major thickness reductions

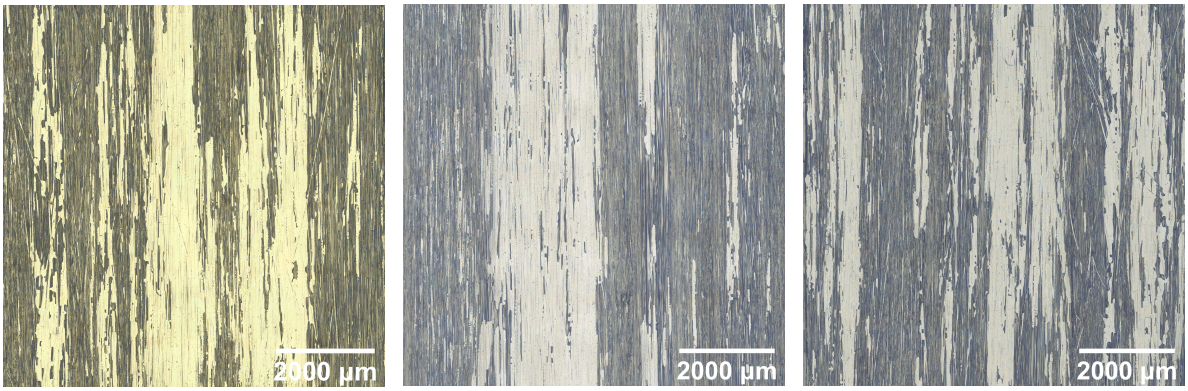


(a) ASR 10 kPa (e) SLD 10 kPa (i) HLD 10 kPa

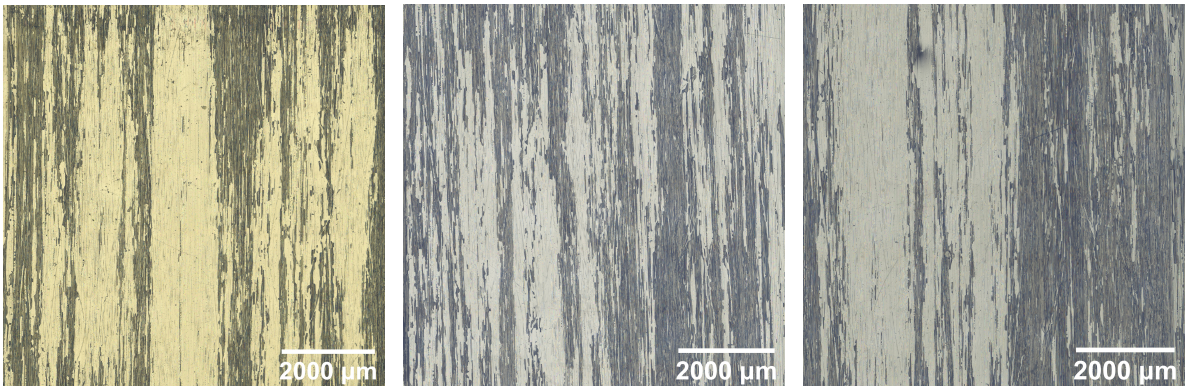


(b) ASR 50 kPa (f) SLD 50 kPa (j) HLD 50 kPa

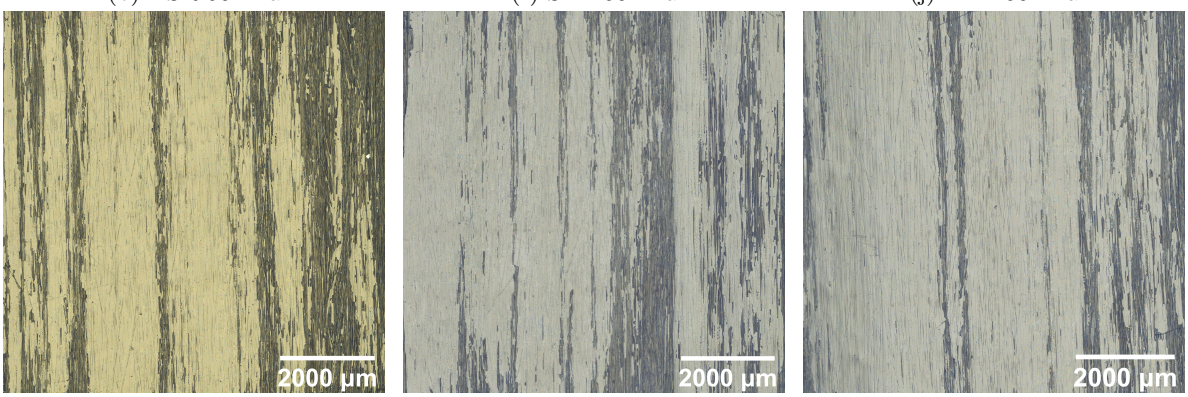


(c) ASR 100 kPa (g) SLD 100 kPa (k) HLD 100 kPa

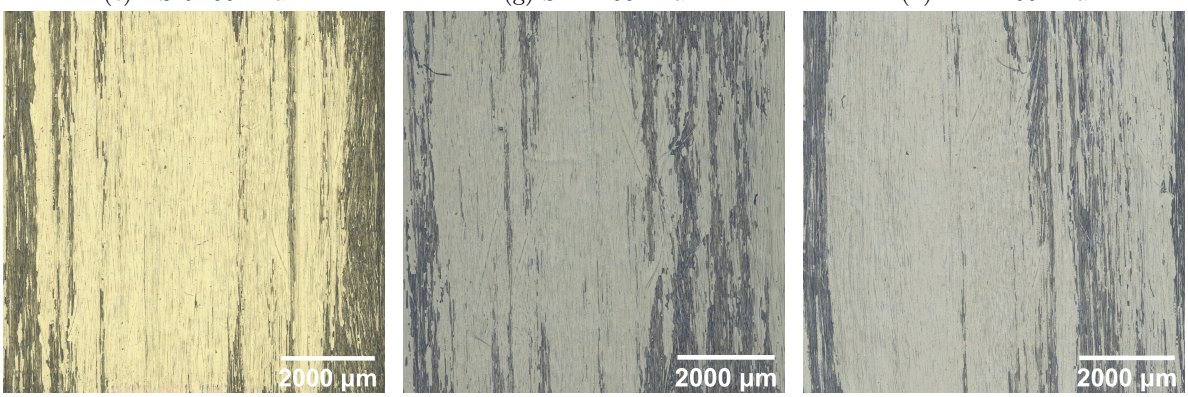


(d) ASR 300 kPa (h) SLD 300 kPa (l) HLD 300 kPa

Figure 6.17: Overview of DEIC surface characterization of as-received (a, b, c, and d), slightly laser deconsolidated (e, f, g, and h), and highly laser deconsolidated (i, j, k, and l) specimens subjected to a maximum temperature of 363 °C.

occurred during the intimate contact experiment: around the glass transition temperature and around the melting temperature. Considering the size of the void before the intimate contact experiment, it can be hypothesized that the majority of void content, together with the waviness (out-of-plane deformations) are eliminated during the first gap length reduction at the glass transition temperature. Then, the second gap length reduction, when the specimen reaches its melting points, should relate with a global squeeze flow deformation in the direction perpendicular to the fibers of the whole tape and matrix flow percolating in the directions along the fibers through-the-thickness. At 300 kPa, the persin percolation along the fibers had increased significantly in Figure 6.11 and areas developed DEIC more significantly in the direction along the fibers. This might indicate that resin percolation along the fiber direction is more dominant than through-the-thickness resin flow. Finally, squeeze flow was expected to contribute to the thickness decrease of the samples, but the projected area results indicate only a more significant increase in area of around 3 % at the highest pressure level setting. This suggests that either the specimens do increase in width because of squeeze flow or they warp, causing the projected area to under-represent its actual surface area.

In HP 2 it was hypothesized that a critical pressure exists at which neither deconsolidation nor consolidation takes place. At 10 kPa, the as-received little to no thickness decrease in Figure 6.6, but both rapid laser deconsolidated configurations did compact significantly with respect to their pre-intimate contact experiment thickness. The projected area difference results from Figure 6.10, suggests the as-received tapes deconsolidated since they shrunk in projected area, and the slightly and highly deconsolidated tapes remained almost identical in their projected area ratio. The roughness results at 10 kPa after the intimate contact test, Figure 6.12a, are slightly higher than that of a pristine tape, shown in Figure 5.4, whereas at 50 kPa the roughness of all degrees of deconsolidation are below the pristine state. It seems that 10 kPa pressure is, therefore, an adequate estimation for a so called critical pressure [55] which compacts the fiber bed to a state similar to the pristine tape state. This result is one order of magnitude lower than the 100 kPa minimum pressure based on overall thickness change found in welding experiments for carbon fiber Polyetherimide (PEI) by Ageorges et al. [77]. More resemblance, however, is found when comparing with the CF/PEEK results of Barnes and Cogswell [40], showing that 20 kPa pressure is minimum pressure to achieve consolidation in a 5 minute windows with a small width increase of the material.

A ‘bump’ was identified in Figure 6.1b which corresponds with the glass transition point of PEEK at 143 °C. Interestingly, the as-received tapes reach a first local minimum after compacting due to stiffness loss related to the glass transition temperature. The glass transition, however, must still be going on as an apparent energy release the of polymer chains result in a temporary thickness increase and subsequent decrease that was identified as a ‘bump’. It is unclear if during this phenomenon also fiber rearrangement occurs or that that whole thickness change can be attributed to the PEEK properties itself. The point at which the rapid laser deconsolidated specimens reached their gap length after glass transition correspond to the end of the ‘bump’, at 218 to 222 s. Thus the behavior occurs only for a densely arranged fiber bed like as-received specimens which are for all pressures at or below the pristine tape thickness of 150 µm whereas the rapid laser deconsolidated specimens do still exhibit significant difference with respect to the pristine tape state, all shown in Figure 6.4b.

## 6.2 Glass Transition Behavior Investigation

An additional setting was carried out with 300 kPa pressure and a maximum temperature measured by the thermocouple of 200 °C, which will also be referred to as ‘low’ temperature setting, see Table 4.2. This low temperature setting was applied to all degrees of deconsolidation and this section presents these results and relates them with the 300 kPa pressure setting subjected to a maximum temperature of 363 °C from the previous section also referred to as ‘high’ temperature setting. The comparison will then be able to find which of the observations of the high temperature configurations happen during the glass transition and which of the deformations occur when the specimens reach their melting point.

### 6.2.1 In-situ Gap Length

The gap length measurements during the intimate contact experiment are shown in Figure 6.18a. The as-received specimens start at the nominal tape thickness of 150 µm at room temperature and do not change significantly in gap length compared to the laser deconsolidated specimens. The laser

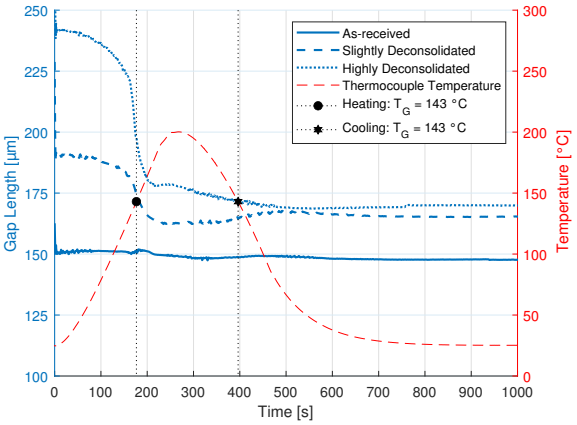


(a) Configurations subjected to a maximum temperature of 200 °C.

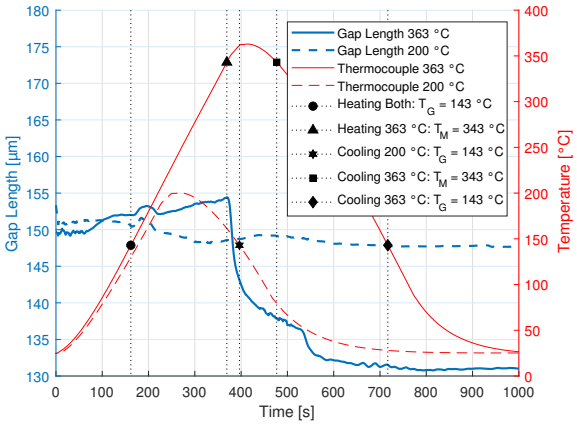


(b) As-received, maximum temperature 200 °C versus 363 °C.

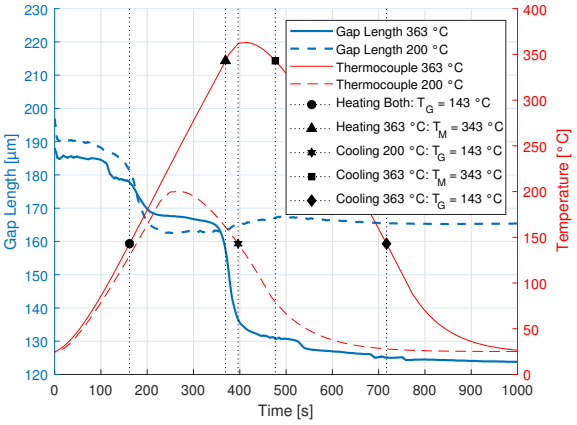


(c) Slightly laser deconsolidated, maximum temperature 200 °C versus 363 °C.

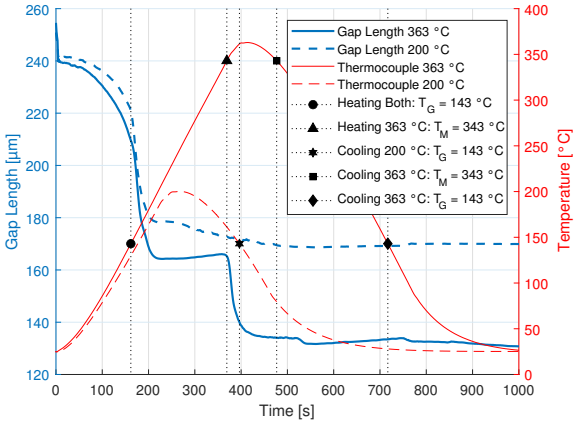


(d) Highly laser deconsolidated, maximum temperature 200 °C versus 363 °C.

Figure 6.18: Gap length measurements of different rapid laser deconsolidated states subjected to maximum temperatures of 200 and 363 °C at 300 kPa pressure

deconsolidated specimens start at a higher initial gap length and also after the glass transition region they remain at a higher gap length than the as-received tapes. The difference in gap length between the slightly and highly laser deconsolidated specimens starts at around 50 µm, significantly reduces to 15 µm right after the glass transition region during the heating phase, to then gradually converge to a difference of less than 5 µm when the temperature during the cooling phase decreased to slightly below the glass transition temperature.

A comparison between the as-received tapes of both temperatures is provided in Figure 6.18b. The 200 °C data should follow the same behavior up to around 200 °C as the higher temperature curve. The bump after the glass transition temperature in also present at the 200 °C curve. At the end of this bump, the gap length difference between both temperature settings is less than 3 µm and increases to 6 µm difference at the moment that the high temperature setting starts to melt. The gap length of the low temperature setting remains constant while the high temperature setting experiences a significant thickness reduction during melting.

The slightly and highly laser deconsolidated low temperature gap length curves are also very similar to their high temperature counterparts up till the glass transition, see Figures 6.18c and 6.18d respectively. The maximum difference in gap length between the two temperatures during heating before the melting temperature is reached is less than 5 µm for the slightly laser deconsolidated and less than 14 µm for the highly laser deconsolidated specimens.

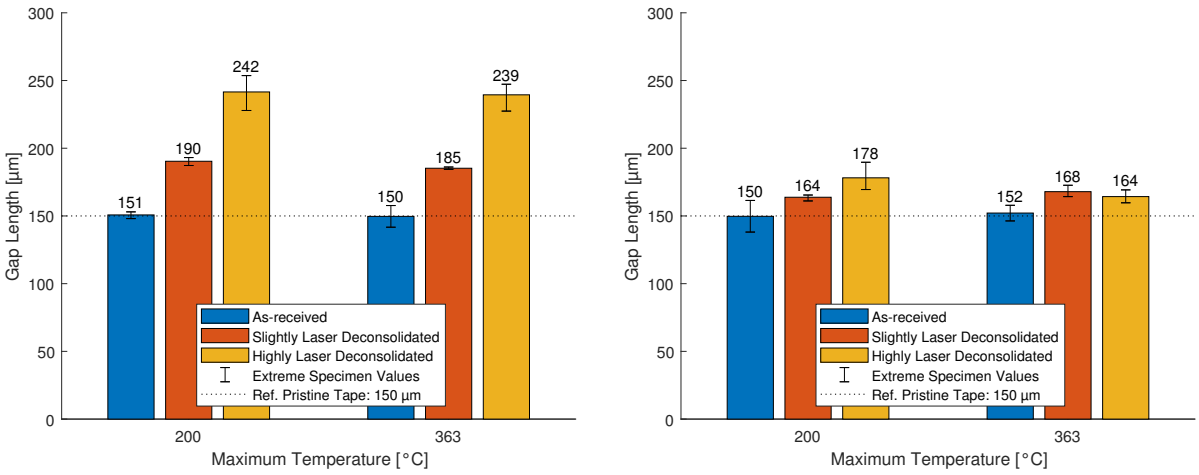


(a) Initial gap length at room temperature.

(b) Gap length after glass transition

Figure 6.19: Initial gap (a) and gap length after glass transition (b) of different laser deconsolidated specimens subjected to maximum temperatures of 200 and 363 °C at 300 kPa pressure.

### Characteristic Points

The initial gap, the gap after glass transition, and the gap at the end of the test were extracted from the individual measurements as is shown for the high temperature curve in Figure 6.3 and explained in more detail back in Section 6.1.1.

The initial gap length of a degree of deconsolidation, see Figure 6.19a, is nearly identical between the low and high temperature setting. Thus, the two sets of specimens have initially the same thickness within each state of deconsolidation which is as expected and shows that there is no large variance in the initial states between the two temperature settings. Increasing the temperature to above the glass transition, shown in Figure 6.19b, the as-received samples remained at the nominal thickness of 150 µm whereas the slightly laser deconsolidated tapes are at least around 10 % thicker after the glass transition. Both temperature profile settings perform similar for these two states of deconsolidation since the applied temperature profiles do not deviate yet. The highly laser deconsolidated specimens of for the 200 °C maximum temperature setting perform as expected: exhibiting a higher thickness at glass transitions temperature than the slightly laser deconsolidated category. The high temperature setting, however, has a lower gap length value than expected, even lower than the slightly laser deconsolidated configuration.

Figure 6.20 shows both the gap length at the end of the intimate contact experimental as well as the thickness after the experiment obtained via cross-sectional microscopy. Both measurement methods result in almost identical values for the 200 °C maximum temperature data. The as-received tape at low temperature setting remains at the pristine tape thickness. The laser deconsolidated tapes are about 10 to 15 % thicker than a pristine tape. Only the high temperature specimens, that experienced temperatures above melt, have significantly decreased in thickness and result all in nearly identical thickness values of about 130 µm based on the cross-sectional microscopy data in Figure 6.20b.

Figure 6.21 shows the difference between the gap length after glass transition and at the end of the experiment. The low temperature setting shows that after the specimens have reached the glass transition temperature, the gap length remains practically constant for the as-received and slightly deconsolidated specimens. The highly deconsolidated data at the low temperature setting might show a bit of gap length decrease or its value is within the accuracy of the test setup.

Another way to analyze the effect of the melting region is by comparing the thicknesses from cross-sectional microscopy after the low temperature and after the high temperature test. The difference between the thicknesses is shown in Figure 6.22, the as-received tapes decrease with 20 µm and the laser deconsolidated tapes with around twice that amount.

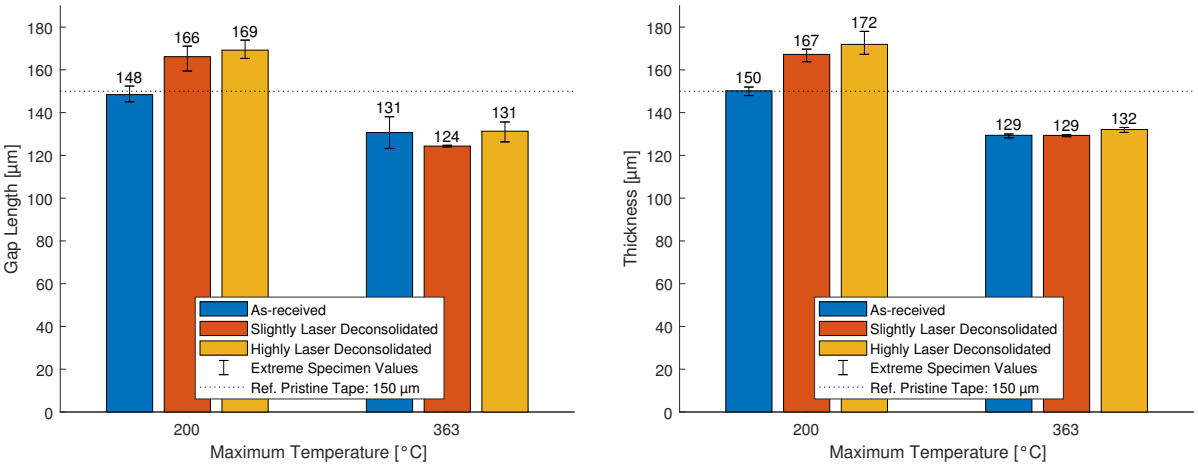


(a) Gap length at end of test at 25 °C.

(b) Thickness from cross-sectional microscopy images.

Figure 6.20: Tape gap length and thickness after intimate contact experiment of different laser deconsolidated specimens subjected to maximum temperatures of 200 and 363 °C at 300 kPa pressure.

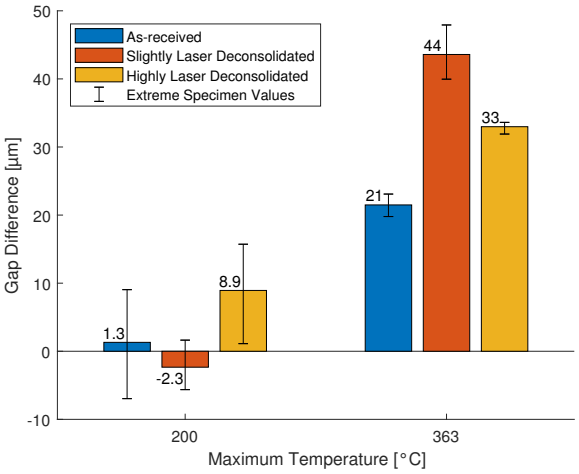


Figure 6.21: The difference between the gap lengths at glass transition and the end of the test, for different laser deconsolidated specimens subjected to maximum temperatures of 200 and 363 °C at 300 kPa.

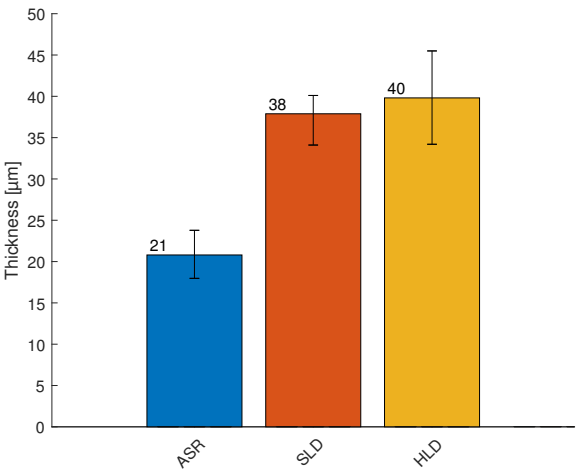


Figure 6.22: Difference between thickness after the intimate contact experiment of 200 and 363 °C maximum temperature configurations at 300 kPa, based on cross-sectional microscopy extracted thickness.

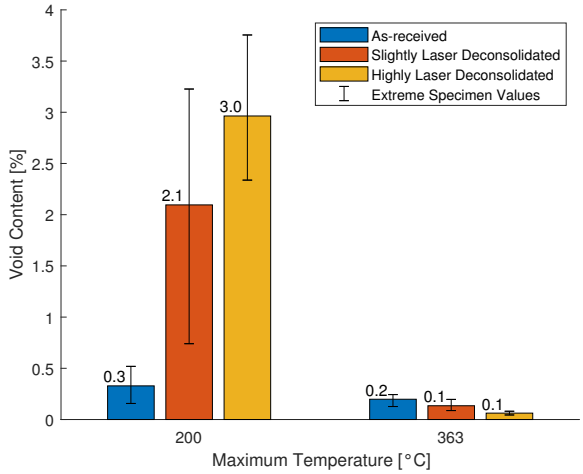


Figure 6.23: Post intimate contact experiment void volume of different laser deconsolidated specimens subjected to maximum temperatures of 200 and 363 °C at 300 kPa pressure.

### 6.2.2 Void Content

The void content data in Figure 6.23 shows that the as-received specimens at the low temperature setting have a very low void content of 0.3 % similar to that of the high temperature specimens which is lower than the pre-intimate contact void content of 0.7 % shown in Figure 5.8. The slightly and highly laser deconsolidated specimens, however, do show a significantly higher amount of void volume content of 2.1 and 3 %, respectively.

A qualitative view of representative cross-sections of as-received and laser deconsolidated specimens pre-intimate contact test and post-intimate contact test subjected to both the 200 and 363 °C maximum temperatures is shown in Figure 6.24. The close-up sections were chosen to represent the overall state of a specimen subjected to 300 kPa pressure. There is no visible difference between the as-received cross-section before, in Figure 6.24a, and after, in Figure 6.24b, the experiment when subjected to a maximum temperature of 200 °C. When the temperature is increased to above the melting point, the top and bottom surfaces are noticeably smoother as shown in Figure 6.24c.

The highly laser deconsolidated tape however, shows a significant reduction in roughness and waviness of the tape when subjected to a temperature of 200 °C, see the Figure 6.25. Not all the voids are compressed, however, the void content post-intimate contact test is roughly half of its size pre-intimate contact test. When subjected to a maximum temperature of 363 °C, there is no visual difference between the as-received and laser deconsolidated tape anymore, see Figures 6.24c and 6.24f, and the void content values, <0.2 %, are basically within the measurements accuracy.

### 6.2.3 Surface Area

Figure 6.26 presents the surface area difference between post-intimate contact and pre-intimate contact experiment of both low and high temperature levels. The as-received and slightly laser deconsolidated specimens have a negligible amount of deformation. The highly laser deconsolidated specimens show a small amount of increase in the projected area. An image, used to measure the projected area is shown in Figure 6.27. No sign of resin percolation appear, unlike the 'high' temperature setting that was shown in Figure 6.11.

### 6.2.4 Surface Profile Characterization

This section shows and discusses the roughness and waviness values that were extracted from three sections along the full width of the tapes, see Section 4.4.1 for more details regarding the procedure.

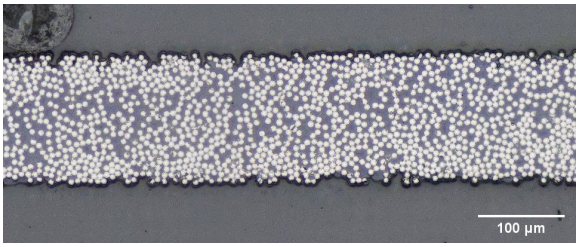


(a) Pre-intimate contact: as-received tape (pristine state).

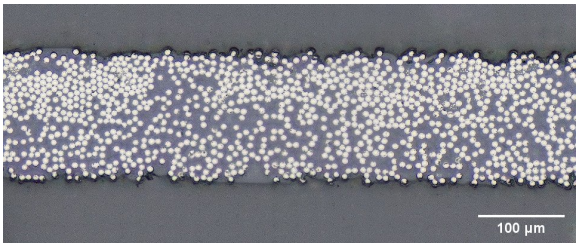


(b) Post-intimate contact: as-received tape subjected to 200 °C.

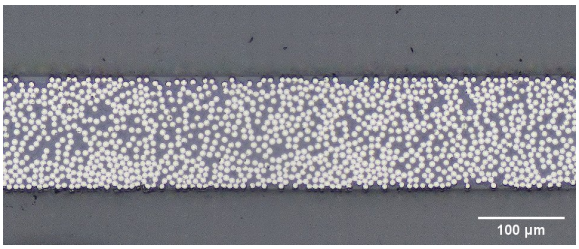


(c) Post-intimate contact: as-received tape subjected to 363 °C.

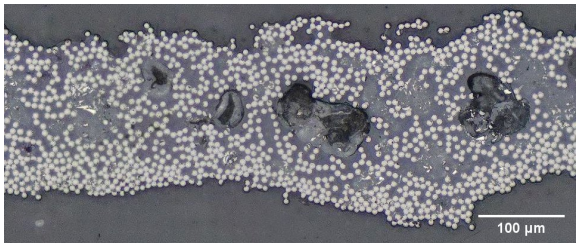


(d) Pre-intimate contact: highly laser deconsolidated tape.

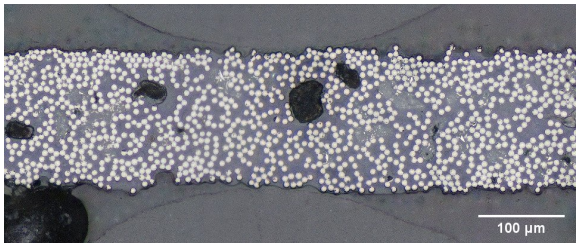


(e) Post-intimate contact: highly laser deconsolidated tape subjected to 200 °C.

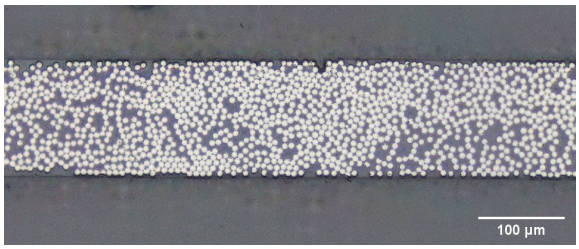


(f) Post-intimate contact: highly laser deconsolidated tape subjected to 363 °C.

Figure 6.24: As-received (a, b, and c) and highly laser deconsolidated (d, e, and f) cross-sections at states before intimate contact experiment (a and d), after intimate contact experiment subjected to a maximum temperature of 200 °C (b and e), and after experiment subjected to a maximum temperature of 363 °C (c and f). Applied pressure of 300 kPa for all cases.

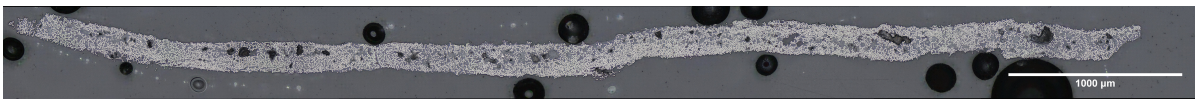


(a) Pre-intimate contact experiment.

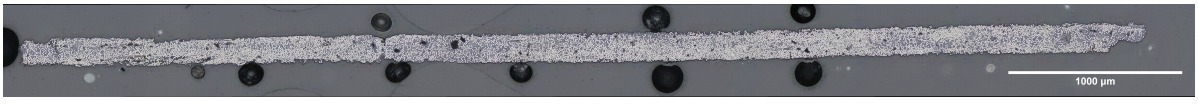


(b) Post-intimate contact experiment

Figure 6.25: Highly laser deconsolidated cross-section pre- and post-intimate contact test of 200 °C maximum temperature at 300 kPa pressure.

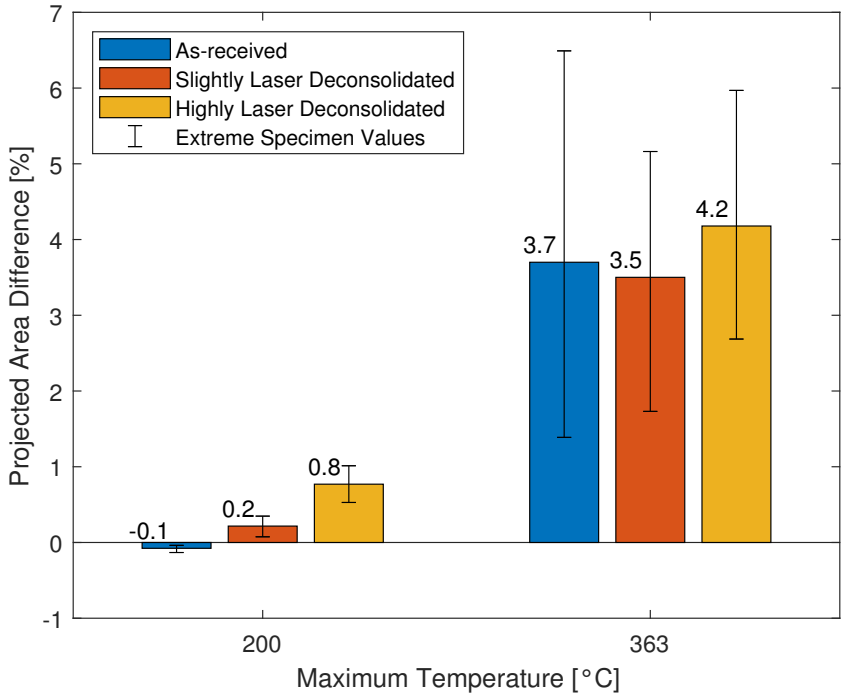


Figure 6.26: Projected area percentage difference post-intimate contact over pre-intimate contact experiment of different laser deconsolidated specimens subjected to maximum temperatures of 200 and 363 °C at 300 kPa pressure.

### Roughness

The root-mean-square roughness of the laser exposed (top) side of the specimens post-intimate contact test are shown in Figure 6.28a. There is no significant difference between the top and bottom side values for the low temperature setting, hence only the top (laser exposed) side is presented. In both cases, the higher the state of deconsolidation, the higher the roughness after the intimate contact experiment. The high temperature setting resulted in a significantly lower roughness of the specimens. Comparing the roughness after the experiment with its state before the experiment, see Figure 6.28b, shows that at the low temperature setting the as-received specimens slightly increased in roughness, whereas the laser deconsolidated specimens decreased in roughness by 20 and 40 % for the slightly and highly laser deconsolidated specimens, respectively. Albeit this significant reduction in roughness, the magnitude is still higher than its lower degree of deconsolidation counterparts. When the melting point is reach the roughness reduces more significantly to only 10 to 20 % of its pre-intimate contact experiment state.

### Waviness

For the waviness profiles, both sides of the specimens have been averaged since there is no significant difference between them. The root-mean-square waviness values are reported in Figure 6.29a. At the low temperature setting the as-received specimens have more waviness than the laser deconsolidated tapes whereas at the high temperature setting the as-received tapes' waviness is lower than the laser deconsolidated tapes. The slightly and highly laser deconsolidated tapes perform similar to each other at both low and high temperature configurations. Since the waviness differences between both temperature settings is low with respect to the waviness of the specimens before the test, the waviness ratios of the laser deconsolidated specimens is similar for both temperatures, see Figure 6.29b. The as-received samples increased in waviness with respect to their pristine state. With the 2.5 mm high bandwidth filter applied, the waviness has significantly decreased as well. The values reported in Figure 6.29c show a small, but clear, difference between the two different maximum temperature settings. These values better match the flattening of the highly laser deconsolidated cross-section shown in Figure 6.25.

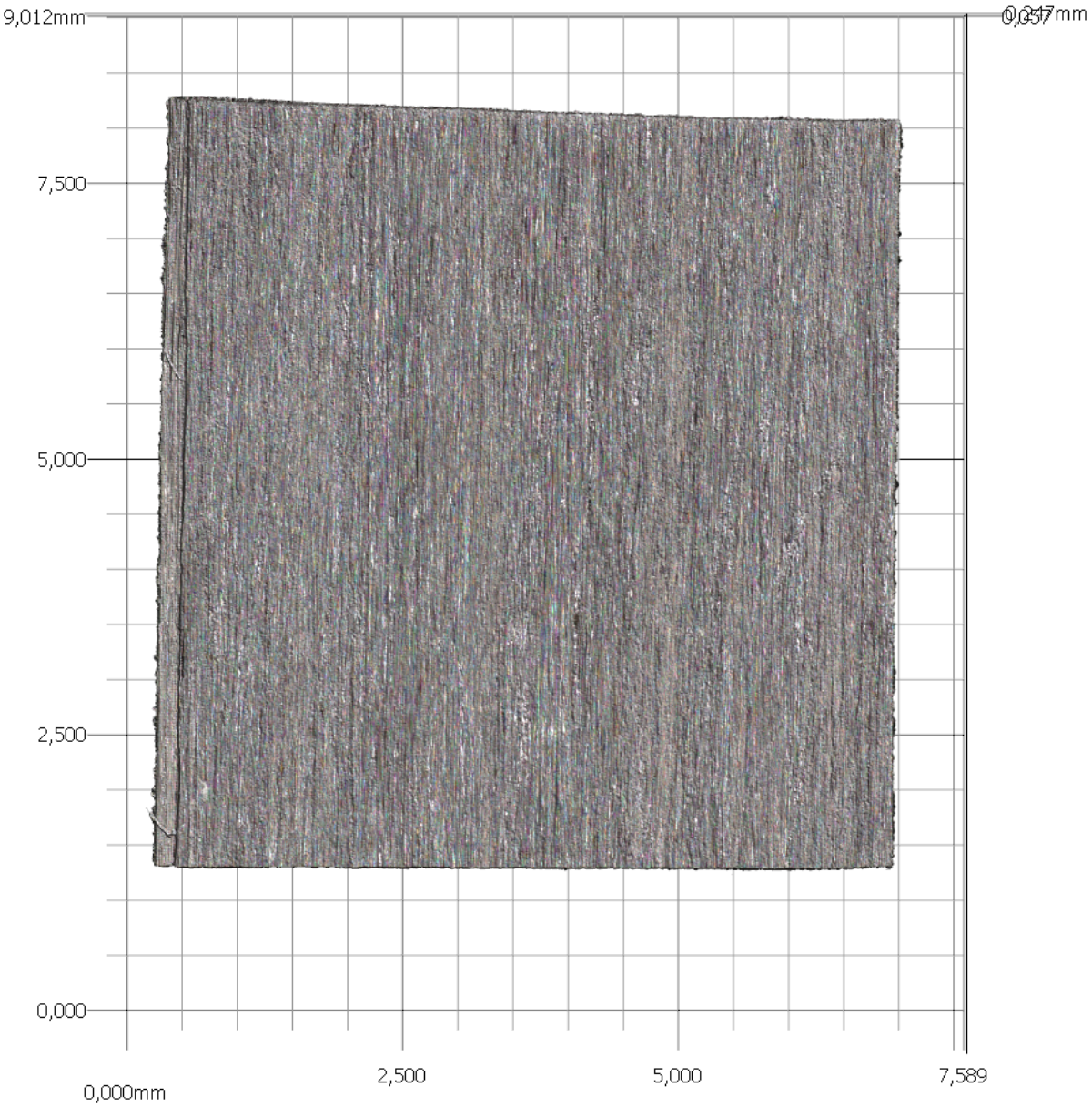


Figure 6.27: Projected area picture of slightly laser deconsolidated specimen subjected to a maximum temperature of 200 °C at 300 kPa pressure.

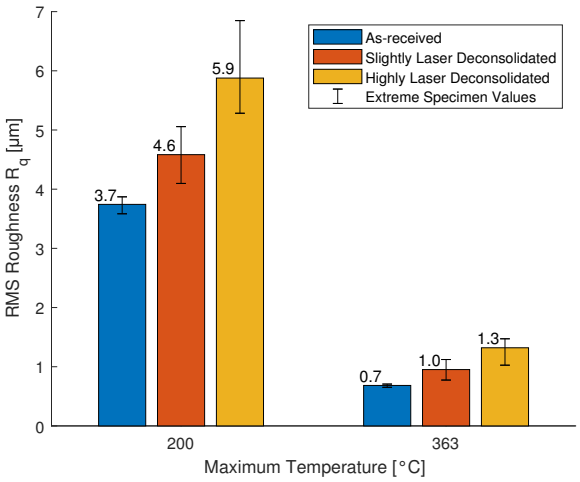


(a) Post-intimate contact experiment

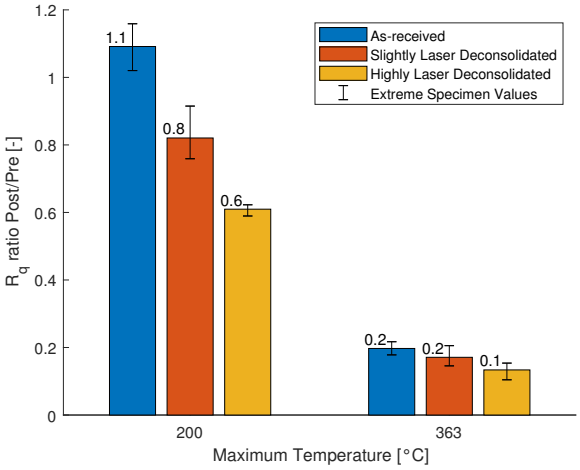


(b) Post- over pre-intimate contact test.

Figure 6.28: Root-mean-square roughness of laser exposed (top) side of different laser deconsolidated states subjected to maximum temperatures of 200 and 363 °C at 300 kPa pressure.

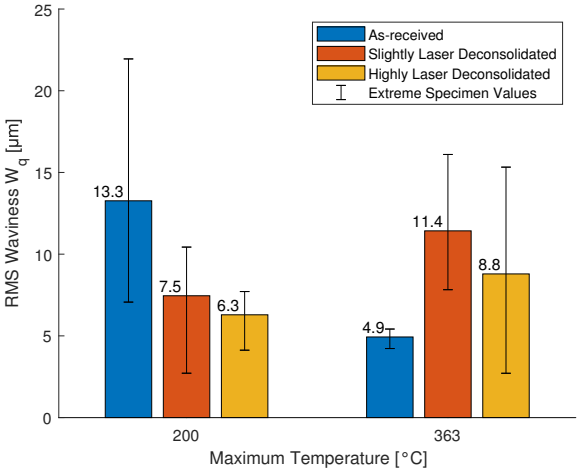


(a) No high bandwidth filter.

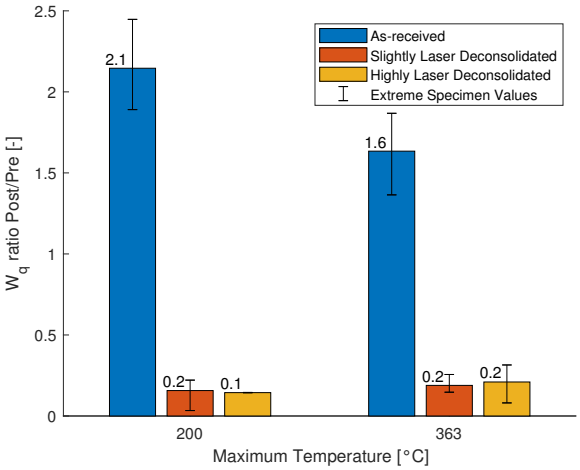


(b) Ratio post- over pre-intimate contact experiment.

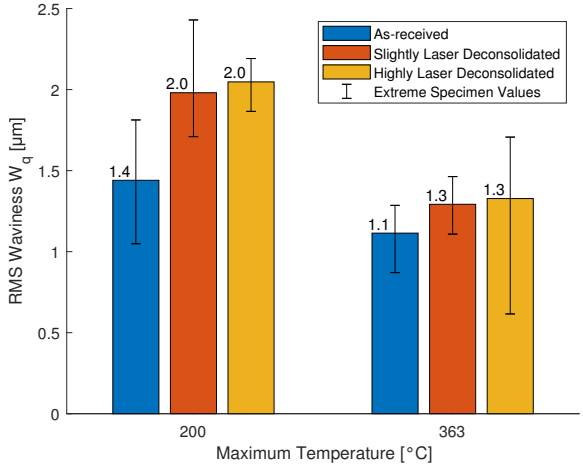


(c) 2.5 mm high bandwidth filter

Figure 6.29: Root-mean-square waviness average of laser exposed (top) and tool (bottom) sides of different laser deconsolidated states subjected to maximum temperatures of 200 and 363 °C at 300 kPa pressure.

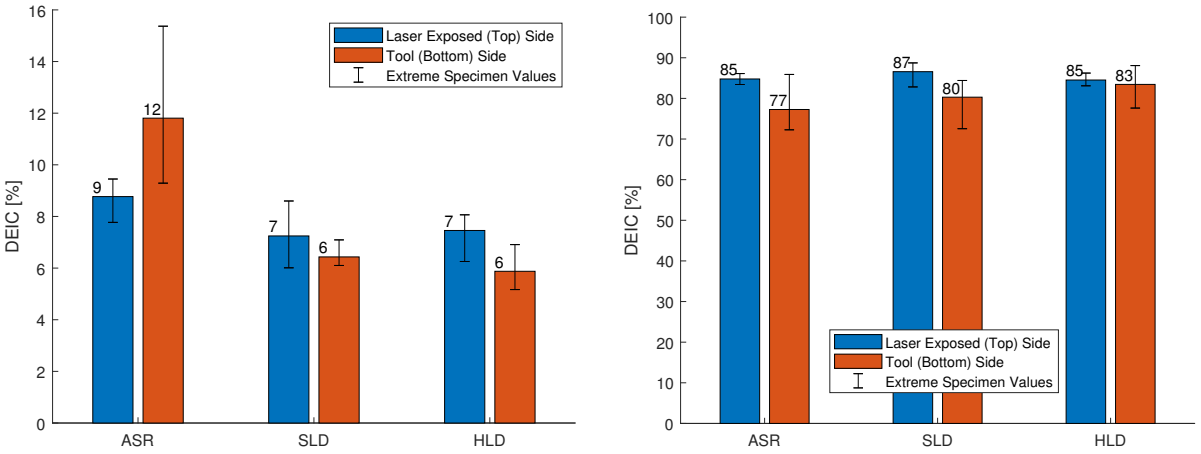


(a) 200 °C Maximum temperature.

(b) 363 °C Maximum temperature.

Figure 6.30: DEIC results of both sides of different laser deconsolidated states subjected to maximum temperatures of 200 and 363 °C at 300 kPa pressure.

### 6.2.5 Developed Degree of Effective Intimate Contact

The DEIC values of the 200 °C maximum temperature, found in Figure 6.30a, shows that all states of deconsolidation result in similar DEIC values for both top and bottom side of the tapes, except the bottom side of the as-received tapes which resulted in a higher DEIC. The DEIC values are very similar to the surface of a pristine tape, found in Table 4.3, and significantly smaller than the higher temperature specimens in Figure 6.30b.

A visual observation of the difference between top and bottom sides of an as-received specimen that was subjected to a maximum temperature of 200 °C is provided in Figure 6.31. The shown specimen was the one with the highest DEIC value of the bottom side. Clearly, the bottom side of the specimen in Figure 6.31c contains significantly more DEIC area than the top surface in Figure 6.31a. Additionally, the grayscale histogram of the bottom side shows an evident peak right of the chosen threshold in Figure 6.31d while the top side does not, see Figure 6.31b.

### 6.2.6 Discussion

Before evaluating Hypothesis HP 3 in Section 6.3.6, the state at glass transition during the intimate contact experimented need to be analyzed. For the laser deconsolidated specimens, a significant reduction of the void content (Figure 6.23) and flattening of the surface (Figures 6.26, 6.28, and 6.29) has been observed when subjected to a maximum temperature of 200 °C while the as-received specimens remained constant. Apparently, the pressure and polymer mobility are high enough to plastically deform the smallest and highest surface asperities of the laser deconsolidated specimens from Figure 6.24d to Figure 6.24e, but asperity size of the as-received specimens is too large to subject to plastic deformation at a nominal pressure of 300 kPa. These changes can all be related to the glass transition of PEEK which occurs around 143 °C and increases polymer mobility. At that temperature, a significant reduction in gap length took place place which relates with the loss of stiffness, see Weiler [78] for a stiffness modulus relation of CF/PEEK versus temperature, flattening the out-of-plane features and reducing the void content.

During the cooling phase, a ‘bump’ was identified (Figures 6.1d and 6.1f) that occurs at a temperature between 290 and 310 °C. Krämer [79] showed with Differential Scanning Calorimetry (DSC) results that the crystallization temperature is around a similar range (between 285 and 305 °C) and suggests that below this temperature no further waviness is being developed. Krämer [79] and Kugler [80] showed that the primary cause for waviness was due to the mismatch of thermal expansion of the composite material and the tool in experiments where a laminate was being cooled down from its molten state. The waviness results (Figure 6.29) and cross-section illustration (Figure 6.24), however, show that significant waviness reduction can be achieved when heating up to temperatures below the crystallization point.

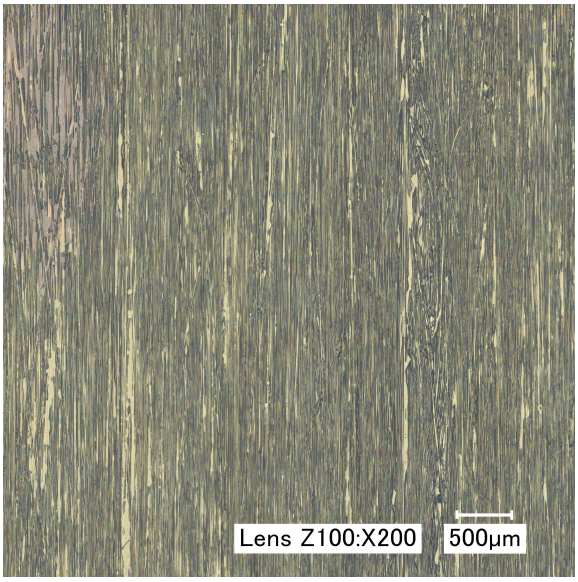


(a) Top side surface.

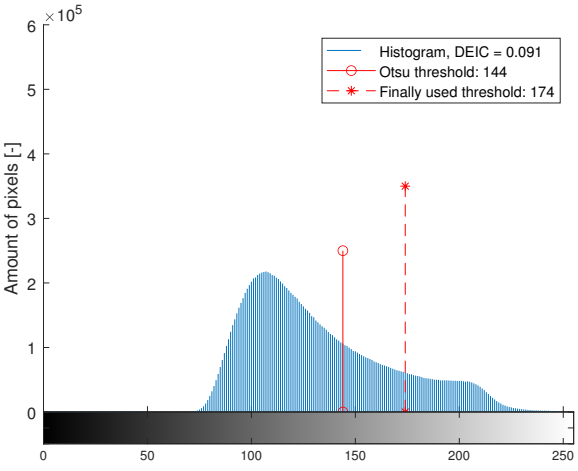


(b) Top side grayscale histogram.

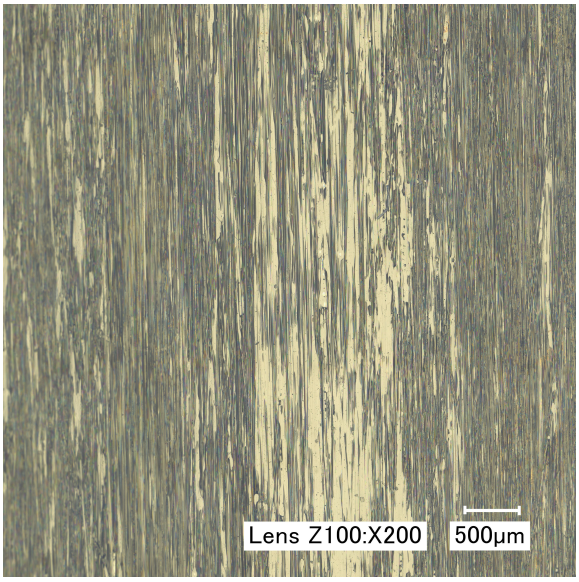


(c) Bottom side surface.

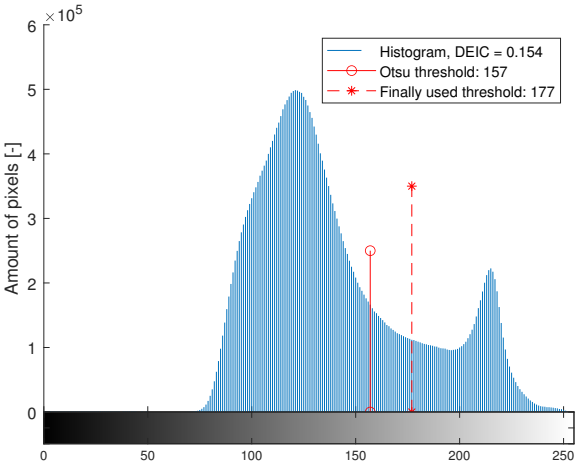


(d) Bottom side grayscale histogram.

Figure 6.31: Top versus bottom side differences of as-received specimens subjected to 300 kPa and a maximum temperature of 200 °C.

Table 6.1: Temperature variation characterization thickness, void content, roughness and DEIC results, subjected to different temperatures at 300 kPa pressure.

| Characterization | | Maximum temperature | | | | Unit |
|---|---|---|---|---|---|---|
| | | 301 °C | 311 °C | 331 °C | 343 °C | |
| Thickness | | 152 | 151 | 151 | – | µm |
| Void content | | 0.22 | 0.21 | 0.21 | – | % |
| Roughness | Top | 4.1 | 3.4 | 3.2 | 1.4 | µm |
| | Bottom | 3.9 | 3.2 | 3.4 | 1.3 | µm |
| DEIC | Top | 9 | 8 | 17 | 79 | % |
| | Bottom | 8 | 9 | 8 | 84 | % |

Despite the reduction of out-of-plane features below melt, the DEIC does not appear to be affected and is still similar to a pristine tape. Hence, DEIC development requires a more free flow of polymer chains than the mobility at rubbery state of 200 °C which was also shown by the lack of resin percolation for the 'low' temperature case in Figure 6.27.

## 6.3 Temperature Variation Near Melt

The temperature difference between the 'low' and 'high' temperature configurations is large in terms of both temperature and time above the glass transition. This section presents results based on individual as-received tape measurements (thus no averaging of repetitions) subjected to increasing temperatures until melt is reached, see Table 4.2 for an overview of the temperature profile settings, to see what happens between the low and high temperature settings at 300 kPa pressure. The results of the characterization of each specimen are shown in Table 6.1. The following sub-sections will discuss each characterization in more detail.

Note that this section compares the temperature variation 301, 311, 331, and 343 °C maximum temperature data in some figures directly with the 200 and 363 °C maximum temperature results. However, the temperature profiles, shown in Figure 6.32, are slightly different since the temperature variation experiments used a 0 s hold time at the maximum temperature in the DMTA machine while the low and high temperature settings employed a 20 s hold time at the maximum temperature resulting in a slightly more shallow temperature profile near the peak. Additionally, the temperature variation results consist of a single specimen for each configuration whereas the 200 and 363 °C maximum temperature experiments were carried out with three repetitions per setting to give better insight to the expected variance.

### 6.3.1 In-situ Gap Length

The gap length measurements in Figure 6.32 show a higher gap length fluctuation over the temperature ramp than the averaged results from the low (Figure 6.18a) and high (Figure 6.2) temperature range, causing a difference of up to 20 µm between the 301 and 311 °C maximum temperature configurations after the glass transition. Considering the thickness increase of the initial state to the post-intimate contact experiment state of the 301 °C maximum temperature sample, there might be some experiment inaccuracy of around 10 µm for that measurement. Anyhow, most importantly is that only the 343 °C maximum temperature setting resulted in a rapid decrease in gap length that is similar to the gap length reduction near the melting point observed in the 363 °C maximum temperature configurations. All other temperature settings exhibit more gradual gap length changes. The behavior of the 343 and 363 °C maximum temperatures are, therefore, very similar to each other despite their difference in hold time. Similarly, for the configurations below the melting temperature: the behavior of the 200 versus 301, 311, and 331 °C maximum temperature curves is similar to each other as well when comparing the global behavior and characteristic point between Figures 6.18b and 6.32.

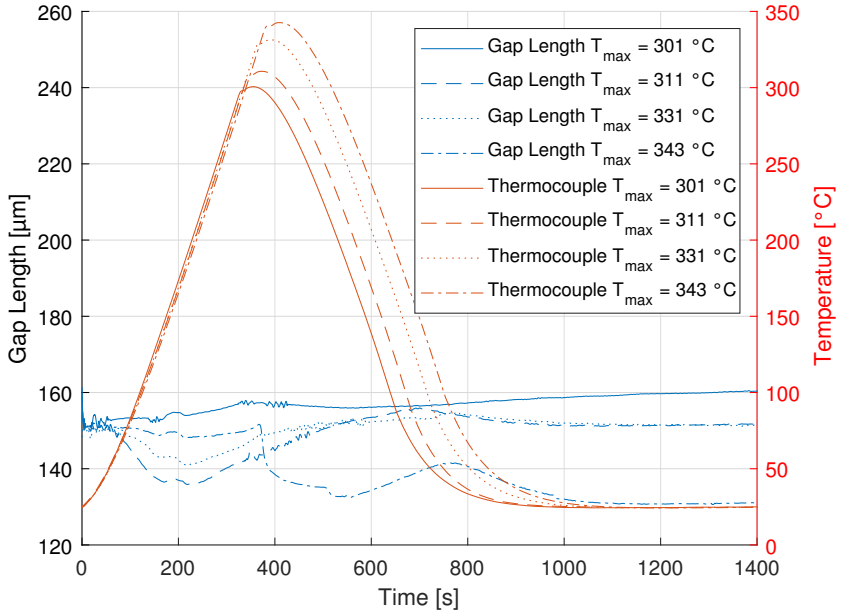


Figure 6.32: Gap length measurements of individual as-received tapes subjected to maximum temperatures of 301, 311, 331, and 343 °C at 300 kPa pressure.

### 6.3.2 Final Thickness

The final thickness values, found in Table 6.1, of the specimens that were subjected to maximum temperatures of 301, 311, and 331 °C is around 150 µm, equal to measurements of the as-received samples subjected to a maximum temperature of 200 °C, shown in Figure 6.20b, as well the nominal thickness of a tape.

Figure 6.33a shows the thickness values after the intimate contact test of all experiments carried out at 300 kPa pressure. The bar chart makes clear that between 200 and 331 °C no change is observed in the final thickness of the specimens.

The cross-section of the 343 °C maximum temperature specimen was not characterized, unfortunately. However, the gap length graph, Figure 6.32, shows a final gap length of around 130 µm for this specimen which matches with the as-received 363 °C maximum temperature gap length and thickness results from Figure 6.20. Hence, all final thickness change seems to happen between 331 and 343 °C and afterwards the final thickness stays constant until at least the 363 °C maximum temperature profile setting.

### 6.3.3 Void Content

The void volume content of the 301, 311, and 331 °C maximum temperature tapes is 0.2 %, see Table 6.1. These values are in-line with the void content results of both 200 and 363 °C maximum temperatures of the as-received tapes in Figure 6.23. Unfortunately, the cross-section of the 343 °C maximum temperature specimen was not prepared, but considering the 363 °C maximum temperature void volume content results of 0.2 % it is assumed that this is also the case for the 343 °C maximum temperature specimen.

### 6.3.4 Surface Roughness Characterization

Only the roughness data is presented for the surface profile characterization. Besides Table 6.1, Figure 6.33b also shows the roughness values and range of the 200 and 363 °C maximum temperature data along with the temperature variation specimens. The roughness values for the 301 °C maximum temperature settings are on the higher side, but in general the roughness does not seem to be affected by the higher temperatures and longer times above the glass transition for the temperatures between 200 and 331 °C.

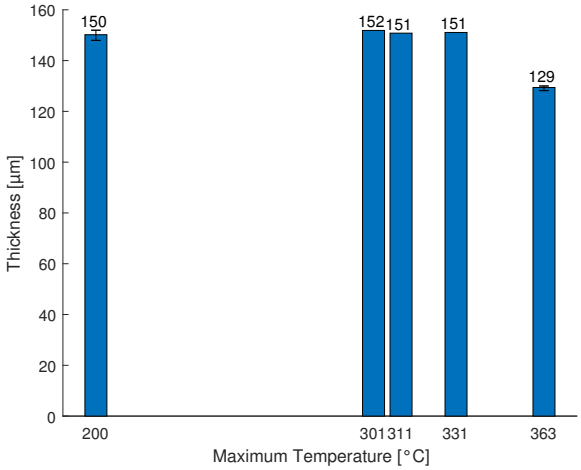


(a) Final thickness from cross-sectional microscopy.

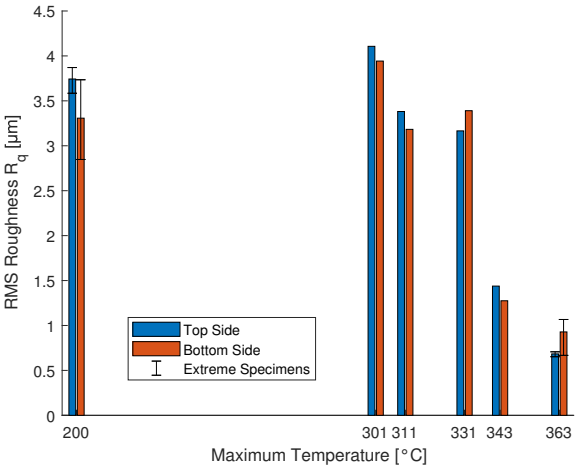


(b) Root-mean-square roughness.

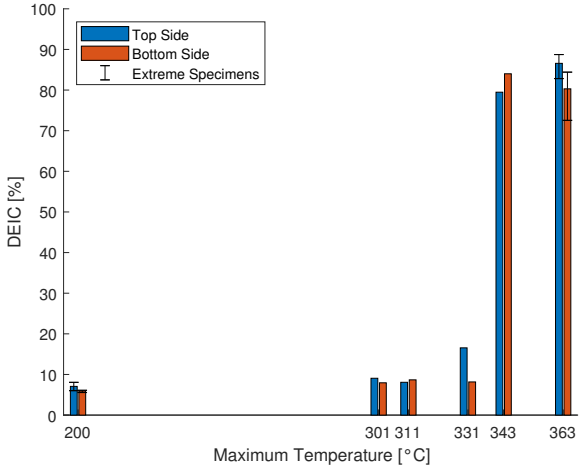


(c) DEIC measurements.

Figure 6.33: Temperature variation results compared with low and high temperature setting experiments of as-received specimens subjected to different maximum temperatures at 300 kPa.

Between the maximum temperatures 331 and 343 °C, there is a steep decrease in roughness whereas from 343 to 363 °C the roughness seems constant.

### 6.3.5 Developed Degree of Effective Intimate Contact

The DEIC values of the 301 and 311 °C maximum temperature specimens in Table 6.1 are in exactly the same range as the top side of the as-received specimens of the 200 °C maximum temperature specimens in Figure 6.30a. The top side measurement of the 331 °C is twice as high as the lower temperature DEIC values, but very similar to the bottom side of the as-received specimens in Figure 6.30a.

When the maximum temperature is increased from 331 to 343 °C, a significant amount of DEIC is developed that is the same as the higher maximum temperature of 363 °C and longer time above melt specimens reach in Figure 6.30b.

### 6.3.6 Discussion

In the gap length graphs (Figure 6.1), a plateau was identified which starts after the glass transition until and stops right before the melting point. This suggests no significant change happens until the PEEK matrix starts to melt. Further exploration of this plateau was conducted with as-received specimens to evaluate Hypothesis HP 3. The as-received specimens showed no significant change with respect to its pristine state when at 200 °C maximum temperature. When being subjected to higher maximum temperatures up to 331 °C, the as-received tapes were still not showing any significant changes in final thickness, void content, roughness, and DEIC, even though the PEEK strength further reduces [81]. Only when the melting point is reached, significant changes happen as is depicted in Figure 6.33. This contradicts with the degree of intimate contact development observations below melt using CF/PEEK around 325 °C by Celik [50], the study from Stokes-Griffin and Compston [37], and below melt Carbon Fiber Reinforced PEKK Thermoplastic Composite (CF/PEKK) observations [82]. Their tests rely on the interface between two tapes, it can be hypothesized that above the glass transition temperature there is more in-situ intimate contact contributed by elastic deformation and if autohesion occurs, the developed intimate contact will remain when cooling down together with tensional residual stress, whereas if no autohesion takes place the polymer will spring back when pressure is released which is the case for the experiments presented in this chapter. This proposed hypothesis thus bases sub-melt intimate contact development on the elastic and plastic deformation of a polymer rich area provided with autohesion to prevent springback during cooling.

The developed DEIC at a maximum temperature of 343 °C took place within seconds, similar to the lower viscosity Carbon Fiber Reinforced Polyamide-6 Thermoplastic Composite (CF/PA6) carbon fiber composite experiments by Schaefer [6] and the CF/PEKK experiments at 290 kPa by Çelik et al. [39]. The 363 °C maximum temperature setting resulted in similar DEIC values as the 343 °C maximum temperature setting while being exposed above melt for a longer time and at higher temperatures. Experiments with a similar time frame were published by Lee and Springer [4], where developed intimate contact remained constant at 85 % between a consolidation time of around 30 to 70 s at 276 kPa pressure and 350 °C. Higher degrees of intimate contact, near 100 %, require either substantial more time or pressure according to the experimental data and models [4, 5].

## 6.4 Conclusion

Three series of intimate contact development series were presented. The first series was performed above the melting temperature ar 363 °C and focused on the effects of pressure between 10 and 300 kPa. Either an increase of the degree of deconsolidation or a decrease of applied pressure caused an overall increase of the in-situ gap length measurement data, increase of roughness, and decrease of DEIC. At 10 kPa, the final thickness and roughness remained very similar to its pristine state, however, a significant amount of intimate contact was developed.

A second series zoomed-in at the behavior near the glass transition temperature. The as-received state of deconsolidation did not change much in roughness value and the cross-section before and after the intimate contact test looked very similar. The rapid laser deconsolidated specimens, however, decreased in void content and roughness. Barely any intimate contact development occurred at this temperature.

A final series further investigated as-received tape between the glass transition temperature and the melting region to see if roughness, void content, or DEIC developed gradually increased. The characterizations remained constant until the melt region was reached, indicating there are no significant changes occurring in between the glass and melt temperatures.

# Chapter 7

# Conclusions

To further adopt the Laser-Assisted Fiber Placement (L-AFP) process under Out-of-autoclave (OOA) conditions, industry demands higher laminate performance while increasing the placement speeds. Intimate contact development is a prerequisite to initiate any load transfer between the placed tapes and plays a key role in the final laminate performance. Recent research showed the effects of thermal deconsolidation due to rapid laser heating are substantial and currently not taken into account in the prediction on intimate contact development. This thesis then defined the term 'Rapid Laser Deconsolidation' to better distinguish thermal deconsolidation due to rapid laser heating from the more conventionally researched (thermal) deconsolidation. Literature demonstrated that characterizing a rapid laser deconsolidated tape surface resulted in better prediction of developed intimate contact than using an pristine tape surface as input in the widely adopted squeeze flow of surface asperity based intimate contact models. Additionally, the rapid laser deconsolidation observations led to the proposal of an intimate contact development theory based on the re-impregnation of dry fibers. However, many consequences of rapid laser deconsolidation are not in-depth investigated and it is not yet widely considered in the latest publications.

An approach was presented to study the L-AFP process via two separate experiments, (1) a rapid laser deconsolidation set-up and (2) an intimate contact development experiment, allowing to investigate the effect of different degrees of deconsolidation onto the developed intimate contact. The rapid laser deconsolidation part functioned as a preparatory phase where Carbon Fiber Reinforced PEEK Thermoplastic Composite (CF/PEEK) tape specimens of three degrees of deconsolidation were produced: (1) as-received, (2) slightly laser deconsolidated which reached temperatures between glass transition and melting point, and (3) highly laser deconsolidated reaching temperatures well above the melting point. Going from as-received, to slightly, to highly laser deconsolidated tapes; the tape 'quality' decreased consecutively which was characterized at its cooled-down state at room temperature by the increased roughness, waviness, and void content. A qualitative inspection of the cross-sections also clearly showed the degradation of these laminate quality parameters. For L-AFP, this showed that the characterization of the as-received tape surface for the purpose of input for intimate contact development models misrepresents the state of the tape right before nip-point. This also raises the question if tapes that exhibit less void content in their pristine state will results in better L-AFP placed laminates.

The intimate contact development experiment, performed by compressing between two platens, subjected the specimens to a temperature profile at constant pressures of 10, 50, 100, and 300 kPa. A significant compaction of the laser deconsolidated samples occurs at the glass transition temperature, when the matrix loses part of its stiffness properties. As-received tapes subjected to a maximum temperature of 200 °C, which is above its glass transition, at 300 kPa pressure barely changed in thickness, void content, roughness, and Degree of Effective Intimate Contact (DEIC). The laser deconsolidated tapes, however, significantly reduced in thickness while still 17 to 22 µm thicker after the test than a pristine tape. The void content was decreased, but still significantly higher than a pristine tape and the roughness decreased to values slightly above the pristine tape measurements. Therefore, under sub-melt temperatures and 300 kPa pressure, the rapid laser deconsolidation induced tape quality characteristics can only be partly brought back to pristine tape conditions.

To understand around which temperature the thickness and roughness changes, and significant amount of DEIC develops, a set of experiments with varying temperature was set up. Between 200 to 331 °C maximum temperatures; the thickness, roughness, and void content remained constant, indicating that no further change happens below melt. Only when 343 °C, which is the melting temperature of the matrix, is reached, a vast change in properties is observed. The DEIC also remained constant from 200 to 331 °C at 300 kPa pressure (except for the top side of the 331 °C setting) which contradicts with two recent publications that observed sub-melt bonding. Since the aforementioned literature employed two tapes, autohesion was possible. Whereas in the experiments presented in the previous chapter, all elastic deformation will spring back to its nominal shape when pressure is released. This led to the hypothesis that sub-melt bonding can occur when autohesion solidifies elastically deformation based developed intimate contact area. This will, however, lead to residual stresses when the elastically deformed matrix tries to springback due to thermal expansion deformations during cooling. Hence, sub-melt bonding might be a key driver for the higher amount of residual tresses in L-AFP created laminates than autoclave consolidated ones.

In contrast to the sub-melt intimate contact development reported in other literature, DEIC requires flow of the matrix material which is not possible in the rubbery state. When the melting point is reached, the DEIC is being developed with a strong favor in the fiber direction. Showing that matrix flow along the fibers is significant. For all degrees of deconsolidation, a significant amount of resin percolation was observed. These observations indicate that a fiber re-impregnation based intimate contact model would benefit from taking matrix flow along the fiber into account.

All three degrees of deconsolidation were also tested at a maximum temperature of 363 °C which is above the melting temperature of the matrix. At 300 kPa and almost 108 s above melt, the differences between the degrees of deconsolidation were insignificant. However, when decreasing the pressure to 10, 50, and 100 kPa, clear trends were observed: higher degrees of deconsolidation lead to larger final thickness, higher roughness, and less DEIC. Vice-versa, a lower pressure level configurations, for a set degree of deconsolidation, also results in a larger final thickness, higher roughness, and less DEIC. At 10 kPa, the tape ends up in a state close to its pristine condition, but also develops a significant amount of DEIC. From these results, it appears that below a certain pressure the rapid laser deconsolidation has a significant effect on the tape quality in L-AFP. When a certain pressure level is met and the material reached the melting temperature, the effects of rapid laser deconsolidation can be reversed.

The findings have shown that the simulation of L-AFP placed laminates would benefit from taking the effects of rapid laser deconsolidation into account since the rapid laser deconsolidated tapes significantly changed in shape, void content, and fiber-matrix composition. Being able to reduce the degree of deconsolidation of the tape that arrives at the nip-point, improves the laminate quality in terms of more DEIC, less void content, lower thickness, and less roughness. Provided with enough pressure and time the developed DEIC, roughness, void content, and thickness properties of a rapid laser deconsolidated placed tape, can all be reverted back the to the levels of an as-received tape. The knowledge of sub-melt bonding can be used for strategy regarding second-pass consolidation rolling steps and to understand the source of the residual stresses present in L-AFP produced laminates.

# Chapter 8

# Recommendations

Recommendations for future work are elaborated on in this chapter, the topics are structured into three sections. Using the same or similar set-up as the current work allows for several improvements and additional tests which are presented in Section 8.1. Two possibilities with the currently available data are discussed in Section 8.2. Some differences between the current set-up and L-AFP are pointed out in Section 8.3 which can aid in the design choices for new intimate contact development experimental set-ups.

## 8.1 Same Set-up

Using the same or similar set-up a number of things can be changed or improved. First of all, the current work was exploratory and three repetitions per setting does not allow to assess statistical significance. In creasing the repetitions will provide better insight into the variations and differences can be accredited with more confidence.

Near, but below, melt temperature tests of rapid laser deconsolidated can confirm the current assumptions that no significant change in roughness, void content, and DEIC occurs between glass transition and melting temperatures. The current specimens consisted of only as-received tapes. It would be interesting to ascertain whether the same observations hold true of the rapid laser deconsolidated specimens, especially regarding the void content.

Also testing tapes from different suppliers, especially resin rich tapes versus equally fiber-matrix distribution will add valuable results to the effects on intimate contact development. Will there still be a significant difference between as-received and rapid laser deconsolidated tapes if sufficient resin is near the surface of the rapid laser deconsolidated tape? The current set-up is ideal to make comparisons between different compositions of composite tapes and compare how roughness, void content, and DEIC develop, while also being able to qualitatively assess the cross-sections of the specimens.

The crystallization temperatures were compared with literature data. Performing DSC tests at 60 °C/s of the actually used material will help to further validate and correlate the in-situ gap length behavior observed during cooling.

## 8.2 Deep Dive Current Data

Due to time limitations and setting the scope of the current research some interesting or complementary actions can be taken to further broaden the scope of the research using the currently available data. With the current data, the fiber-matrix density along the thickness of multiple sections of the tapes can be extracted to obtain the average dry fiber length. This can quantitatively express the observations of fibers sticking out of the fiber bed. Subsequently, intimate contact simulations using the fiber re-impregnation model [7] can be performed with the current data to further study the effect of taking rapid laser deconsolidation.

Based on the in-situ gap length data, the viscosity can be calculated in a similar fashion to Khan [34]. The gap length plots in Figure 6.1a show a clear onset of the melting point for the as-received specimens, the gap length data during that first gap length reduction can then be used to calculate the viscosity. The slightly and highly laser deconsolidated specimens can also be characterized, but picking the melting onset point is less straightforward. Downside is that the viscosity characterization takes place at melting temperature of 343 °C whereas viscosity values at multiple temperatures are often preferred in order to describe its temperature relationship in the L-AFP simulation. Most interesting is whether the rapid laser deconsolidated tapes exhibit a different apparent viscosity than the as-received tapes due to the changes in their meso- and macroscopic properties. Especially, for squeeze flow based intimate contact models, a viscosity expression that includes certain rapid laser deconsolidation effects might prove more accurate than the viscosity obtained from as-received tapes that are elevated to measurement temperature while being pressurized.

## 8.3 Similarity to L-AFP

The current time above melting temperature was 107.7 s whereas L-AFP processing conditions are <1 s. If the time above melt can be reduced, the experimental conditions will be more comparable to the L-AFP process. Exploratory trial runs can show if the test conditions and machine are repeatable enough that multiple repetitions will undergo the same temperature cycle. The exact time above melt is not necessarily required to be known as qualitative time steps already provide a lot of knowledge about intimate contact development.

During the rapid laser deconsolidation experiments, the currently highly deconsolidated tapes reached averaged maximum temperatures of 395 to 511 °C which is well above recommended processing temperature range of 370 to 400 °C. Further experiments with more realistic laser settings can be more relevant to the L-AFP process.

Currently the pressure was applied during the whole experiment. With the DMTA machine it was difficult to apply an ‘instantaneous’ pressure as the force application would first overshoot. It could be interesting to start with a very low pressure during the heating phase to allow a specimen to deconsolidate and apply a more significant pressure when melting is reached or at another higher temperature point. Also, testing the difference between releasing pressure during cooling right before and after the recrystallization point to further investigate its impact on tape laying. This will also yield interesting understanding for what happens to plies below the top layer of the substrate and second passes with the laser and roller to enhance the substrate.

# Bibliography


[1] Christopher Mark Stokes-Griffin and Paul Compston. An inverse model for optimisation of laser heat flux distributions in an automated laser tape placement process for carbon-fibre/PEEK. *Composites Part A: Applied Science and Manufacturing*, 88:190–197, sep 2016. URL https://www.sciencedirect.com/science/article/pii/S1359835X16301713.

[2] Christopher Mark Stokes-Griffin and Paul Compston. The effect of processing temperature and placement rate on the short beam strength of carbon fibre–PEEK manufactured using a laser tape placement process. *Composites Part A: Applied Science and Manufacturing*, 78:274–283, nov 2015. URL https://www.sciencedirect.com/science/article/pii/S1359835X15002791.

[3] Philip H. Dara and Alfred C. Loos. Thermoplastic matrix composite processing model. Technical report, Virginia Polytechnic Institute and State University, Blacksburg, Virginia, 1985.

[4] Woo Il Lee and George S. Springer. A Model of the Manufacturing Process of Thermoplastic Matrix Composites. *Journal of Composite Materials*, 21(11):1017–1055, nov 1987. ISSN 0021-9983. doi: 10.1177/002199838702101103. URL http://journals.sagepub.com/doi/10.1177/002199838702101103.

[5] F. Yang and Ranga Pitchumani. A fractal Cantor set based description of interlaminar contact evolution during thermoplastic composites processing. *Journal of Materials Science*, 36(19):4661–4671, 2001. doi: 10.1023/A:1017950215945.

[6] Philipp M. Schaefer, T. Guglhoer, M. G. R Sause, and Klaus Drechsler. Development of intimate contact during processing of carbon fiber reinforced Polyamide-6 tapes. *Journal of Reinforced Plastics and Composites*, 36(8):593–607, apr 2017. ISSN 0731-6844. doi: 10.1177/0731684416687041. URL http://journals.sagepub.com/doi/10.1177/0731684416687041.

[7] Thijs Kok. *On the consolidation quality in laser assisted fiber placement: the role of the heating phase*. Phd, University of Twente, Enschede, sep 2018. URL http://purl.org/utwente/doi/10.3990/1.9789036546065.

[8] Philips Photonics GmbH. Laser System with Laser Module PPM412-12-980-24 with Driver Unit PPU104-12: Reference and Installation Manual. Technical Report Version 1.0, Philips, Aachen, 2017.

[9] Harald E.N. Bersee. Composite Aerospace Manufacturing Processes. In *Encyclopedia of Aerospace Engineering*. John Wiley & Sons, Ltd, Chichester, UK, dec 2010. doi: 10.1002/9780470686652.eae365. URL http://doi.wiley.com/10.1002/9780470686652.eae365.

[10] Guy Hellard. A Long Story of Innovations and Experiences Composites in Airbus Table of Content. In *Global Investor Forum by Dr Roland Thévenin*, 2008.

[11] AG Miller. The Boeing 787 Dreamliner, Keynote Address. In *22nd American society for composites technical conference, Seattle, WA*, may 2007.

[12] Suong Van Hoa, Minh Duc Hoang, and Jeff Simpson. Manufacturing procedure to make flat thermoplastic composite laminates by automated fibre placement and their mechanical properties. *Journal of Thermoplastic Composite Materials*, 30(12):1693–1712, dec 2017. ISSN 0892-7057. doi: 10.1177/0892705716662516. URL http://journals.sagepub.com/doi/10.1177/0892705716662516.

[13] Anthony J. Comer, Dipa Ray, Winifred O. Obande, D. Jones, J. Lyons, I. Rosca, R.M. O' Higgins, and M.A. McCarthy. Mechanical characterisation of carbon fibre–PEEK manufactured by laser-assisted automated-tape-placement and autoclave. *Composites Part A: Applied Science and Manufacturing*, 69:10–20, feb 2015. ISSN 1359-835X. doi: 10.1016/J.COMPOSITESA.2014.10.003. URL https://www.sciencedirect.com/science/article/pii/S1359835X14003133.

[14] John Tierney and John W. Gillespie. Modeling of in Situ strength development for the thermoplastic composite tow placement process. *Journal of Composite Materials*, 40(16):1487–1506, 2006. ISSN 00219983. doi: 10.1177/0021998306060162.

[15] Muhammad Amir Khan, Peter Mitschang, and Ralf Schledjewski. Tracing the void content development and identification of its effecting parameters during in situ consolidation of thermoplastic tape material. *Polymers and polymer composites*, 18(1), 2010. URL https://www.proquest.com/openview/c75c02fd25743a8152100a2c04dc62e8/.

[16] John M. Haake. High power diode laser-assisted fiber placement of composite structure. In *24th International Congress on Applications of Lasers and Electro-Optics, ICALEO 2005 - Congress Proceedings*, pages 437–443, 2005. doi: 10.2351/1.5060524.

[17] D. Modi, Anthony J. Comer, Ronan M. O'Higgins, and Michael A. McCarthy. Thermoplastic Composites: In-Situ COnsolidation or In-Situ Welding? In *Proceedings of the 19th international conference on composite materials (ICCM 19)*, volume 28, Montreal, 2013. URL http://confsys.encs.concordia.ca/ICCM19/AllPapers/FinalVersion/MOD81592.pdf.

[18] Eric Beyeler, Walter Phillips, and Selçuk I. Güçeri. Experimental Investigation of Laser-Assisted Thermoplastic Tape Consolidation. *Journal of Thermoplastic Composite Materials*, 1(1):107–121, 1988. ISSN 15307980. doi: 10.1177/089270578800100109.

[19] F. Yang and Ranga Pitchumani. Healing of thermoplastic polymers at an interface under nonisothermal conditions. *Macromolecules*, 35(8):3213—-3224, 2002. ISSN 00249297. doi: 10.1021/ma010858o. URL https://pubs-acs-org.tudelft.idm.oclc.org/doi/10.1021/ma010858o.

[20] F. Yang and Ranga Pitchumani. Nonisothermal healing and interlaminar bond strength evolution during thermoplastic matrix composites processing. *Polymer Composites*, 24(2):263–278, apr 2003. ISSN 02728397. doi: 10.1002/pc.10027. URL http://doi.wiley.com/10.1002/pc.10027.

[21] L. J. Bastien and J. W. Gillespie. A non-isothermal healing model for strength and toughness of fusion bonded joints of amorphous thermoplastics. *Polymer Engineering and Science*, 31(24):1720–1730, dec 1991. ISSN 0032-3888. doi: 10.1002/pen.760312406. URL http://doi.wiley.com/10.1002/pen.760312406.

[22] Firas Awaja. Autohesion of polymers. *Polymer*, 97:387–407, aug 2016. ISSN 00323861. doi: 10.1016/j.polymer.2016.05.043.

[23] Susan C. Mantell and George S. Springer. Manufacturing Process Models for Thermoplastic Composites. *Journal of Composite Materials*, 26(16):2348–2377, 1992. doi: 10.1177/002199839202601602.

[24] Susan C. Mantell, Qiuling Wang, and George S. Springer. Processing Thermoplastic Composites in a Press and by Tape Laying—Experimental Results. *Journal of Composite Materials*, 26(16):2378–2401, 1992. ISSN 1530793x. doi: 10.1177/002199839202601603. URL https://doi.org/10.1177/002199839202601603.

[25] Fazil O. Sonmez and H Thomas Hahn. Analysis of the On-Line Consolidation Process in Thermoplastic Composite Tape Placement. *Journal of Thermoplastic Composite Materials*, 10(6):543–572, 1997. doi: 10.1177/089270579701000604.

[26] Christophe Ageorges, Lin Ye, Yiu Wing Mai, and Meng Hou. Characteristics of resistance welding of lap shear coupons. Part II. Consolidation. *Composites Part A: Applied Science and Manufacturing*, 29(8):911–919, aug 1998. ISSN 1359835X. doi: 10.1016/S1359-835X(98)00023-2.

[27] Shao Cong Dai and Lin Ye. Characteristics of CF/PEI tape winding process with on-line consolidation. *Composites Part A: Applied Science and Manufacturing*, 33(9):1227–1238, sep 2002. ISSN 1359835X. doi: 10.1016/S1359-835X(02)00083-0.

[28] Fazil O. Sonmez and Mustafa Akbulut. Process optimization of tape placement for thermoplastic composites. *Composites Part A: Applied Science and Manufacturing*, 38(9):2013–2023, sep 2007. URL http://linkinghub.elsevier.com/retrieve/pii/S1359835X07000814.

[29] Wouter Johannes Bernardus Grouve, L. L. Warnet, B. Rietman, H. A. Visser, and R. Akkerman. Optimization of the tape placement process parameters for carbon–PPS composites. *Composites Part A: Applied Science and Manufacturing*, 50:44–53, 2013. ISSN 1359835X. doi: 10.1016/j.compositesa.2013.03.003.

[30] Arthur Levy, Dirk Heider, John Tierney, and John W. Gillespie. Inter-layer thermal contact resistance evolution with the degree of intimate contact in the processing of thermoplastic composite laminates. *Journal of Composite Materials*, 48(4):491–503, 2014. doi: 10.1177/0021998313476318. URL https://doi.org/10.1177/0021998313476318.

[31] Arthur Levy, Steven Le Corre, and Irene Fernandez Villegas. Modeling of the heating phenomena in ultrasonic welding of thermoplastic composites with flat energy directors. *Journal of Materials Processing Technology*, 214(7):1361–1371, jul 2014. ISSN 0924-0136. doi: 10.1016/J.JMATPROTEC.2014.02.009. URL https://www.sciencedirect.com/science/article/pii/S0924013614000508.

[32] M. Amir Khan and Ralf Schledjewski. Influencing factors for an online consolidating thermoplastic tape placement process. In *Processing 17th international conference on composite materials*, pages 27–31, Edinburgh, 2009.

[33] J. S.U. Schell, J. Guilleminot, C. Binetruy, and P. Krawczak. Computational and experimental analysis of fusion bonding in thermoplastic composites: Influence of process parameters. *Journal of Materials Processing Technology*, 209(11):5211–5219, jun 2009. ISSN 09240136. doi: 10.1016/j.jmatprotec.2009.03.008.

[34] Muhammad Amir Khan, Peter Mitschang, and Ralf Schledjewski. Identification of some optimal parameters to achieve higher laminate quality through tape placement process. *Advances in Polymer Technology*, 29(2):98–111, jul 2010. ISSN 1098-2329. doi: 10.1002/adv.20177. URL http://dx.doi.org/10.1002/adv.20177http://doi.wiley.com/10.1002/adv.20177.

[35] Muhammad Amir Khan, Peter Mitschang, and Ralf Schledjewski. Parametric study on processing parameters and resulting part quality through thermoplastic tape placement process. *Journal of Composite Materials*, 47(4):485–499, feb 2013. ISSN 0021-9983. doi: 10.1177/0021998312441810. URL http://journals.sagepub.com/doi/10.1177/0021998312441810.

[36] M. Narnhofer, Ralf Schledjewski, Peter Mitschang, and L. Perko. Simulation of the Tape-Laying Process for Thermoplastic Matrix Composites. *Advances in Polymer Technology*, 32(S1):E705–E713, mar 2013. ISSN 07306679. doi: 10.1002/adv.21312. URL http://doi.wiley.com/10.1002/adv.21312.

[37] Christopher Mark Stokes-Griffin and Paul Compston. Investigation of sub-melt temperature bonding of carbon-fibre/PEEK in an automated laser tape placement process. *Composites Part A: Applied Science and Manufacturing*, 84:17–25, 2016. ISSN 1359-835X. doi: https://doi.org/10.1016/j.compositesa.2015.12.019. URL http://www.sciencedirect.com/science/article/pii/S1359835X16000038.

[38] Philipp M. Schaefer, Michael Von Staden, Swen Zaremba, and Klaus Drechsler. Materialcharacterization for determining the consolidation properties of carbon fiber tapes with PA 6 matrix. In *ICCM International Conferences on Composite Materials*, Copenhagen, 2015.

[39] Ozan Çelik, Daniël Peeters, Clemens Dransfeld, and Julie Teuwen. Intimate contact development during laser assisted fiber placement: Microstructure and effect of process parameters. *Composites Part A: Applied Science and Manufacturing*, 134:105888, jul 2020. ISSN 1359835X. doi: 10.1016/j.compositesa.2020.105888.

[40] J. A. Barnes and F. N. Cogswell. Transverse flow processes in continuous fibre-reinforced thermoplastic composites. *Composites*, 20(1):38–42, jan 1989. ISSN 0010-4361. doi: 10.1016/0010-4361(89)90680-0. URL https://www.sciencedirect.com/science/article/pii/0010436189906800.

[41] R. Balasubramanyam, R.S. Jones, and A.B. Wheeler. Modelling transverse flows of reinforced thermoplastic materials. *Composites*, 20(1):33–37, jan 1989. ISSN 0010-4361. doi: 10.1016/0010-4361(89)90679-4. URL https://www.sciencedirect.com/science/article/pii/0010436189906794.

[42] E.L. Wang and Timothy G. Gutowski. Laps and gaps in thermoplastic composites processing. *Composites Manufacturing*, 2(2):69–78, jan 1991. ISSN 0956-7143. doi: 10.1016/0956-7143(91)90182-G. URL https://www.sciencedirect.com/science/article/pii/095671439190182G.

[43] S. F. Shuler and Suresh G. Advani. Transverse squeeze flow of concentrated aligned fibers in viscous fluids. *Journal of Non-Newtonian Fluid Mechanics*, 65(1):47–74, jul 1996. ISSN 0377-0257. doi: 10.1016/0377-0257(96)01440-1. URL https://www.sciencedirect.com/science/article/pii/0377025796014401.

[44] Hong-Ru Ru Lin and Suresh G. Advani. Processing models and characterization of thermoplastic composite wound parts. *Polymer Composites*, 18(3):405–411, jun 1997. ISSN 02728397. doi: 10.1002/pc.10291. URL http://doi.wiley.com/10.1002/pc.10291.

[45] D. J. Groves, A. M. Bellamy, and D. M. Stocks. Anisotropic rheology of continuous fibre thermoplastic composites. *Composites*, 23(2):75–80, mar 1992. ISSN 0010-4361. doi: 10.1016/0010-4361(92)90107-6. URL https://www.sciencedirect.com/science/article/pii/0010436192901076.

[46] A. Deignan, W. F. Stanley, and M. A. McCarthy. Insights into wide variations in carbon fibre/polyetheretherketone rheology data under automated tape placement processing conditions. *Journal of Composite Materials*, page 002199831774073, nov 2017. ISSN 0021-9983. doi: 10.1177/0021998317740733. URL http://journals.sagepub.com/doi/10.1177/0021998317740733.

[47] G. B. McGuinness and C. M. ÓBrádaigh. Characterisation of thermoplastic composite melts in rhombus-shear: the picture-frame experiment. *Composites Part A: Applied Science and Manufacturing*, 29(1-2):115–132, jan 1998. ISSN 1359-835X. doi: 10.1016/S1359-835X(97)00061-4. URL https://www.sciencedirect.com/science/article/pii/S1359835X97000614.

[48] W.F. Stanley and P.J. Mallon. Intraply shear characterisation of a fibre reinforced thermoplastic composite. *Composites Part A: Applied Science and Manufacturing*, 37(6):939–948, jun 2006. ISSN 1359-835X. doi: 10.1016/J.COMPOSITESA.2005.03.017. URL https://www.sciencedirect.com/science/article/pii/S1359835X05001247.

[49] Abhas Choudhary. *Thermal deconsolidation of thermoplastic prepreg tapes during Laser-Assisted Fiber Placement*. Msc thesis, Delft University of Technology, Delft, jul 2019.

[50] Ozan Çelik, S. M. Amin Hosseini, Ismet Baran, Wouter Johannes Bernardus Grouve, Remko Akkerman, Daniël M.J. Peeters, Julie J.E. Teuwen, and Clemens A. Dransfeld. The influence of inter-laminar thermal contact resistance on the cooling of material during laser assisted fiber placement. *Composites Part A: Applied Science and Manufacturing*, 145:106367, jun 2021. ISSN 1359835X. doi: 10.1016/j.compositesa.2021.106367.

[51] C. Santulli, R. Garcia Gil, A. C. Long, and M. J. Clifford. Void content measurements in commingled E-glass/polypropylene composites using image analysis from optical micrographs. *Science and Engineering of Composite Materials*, 10(2):77–90, 2002. ISSN 0334181X. doi: 10.1515/secm.2002.10.2.77.

[52] Lin Ye, Meng Lu, and Yiu Wing Mai. Thermal de-consolidation of thermoplastic matrix composites-I. Growth of voids. *Composites Science and Technology*, 62(16):2121–2130, dec 2002. ISSN 02663538. doi: 10.1016/S0266-3538(02)00144-6.

[53] Markus Brzeski and Peter Mitschang. Deconsolidation and Its Interdependent Mechanisms of Fibre Reinforced Polypropylene. *Polymers and Polymer Composites*, 23(8):515–524, oct 2015. ISSN 0967-3911. doi: 10.1177/096739111502300801. URL http://journals.sagepub.com/doi/10.1177/096739111502300801.

[54] Andrew Beehag and Lin Ye. Role of cooling pressure on interlaminar fracture properties of commingled CF/PEEK composites. *Composites Part A: Applied Science and Manufacturing*, 27(3):175–182, jan 1996. ISSN 1359-835X. doi: 10.1016/1359-835X(95)00027-Y. URL https://www.sciencedirect.com/science/article/pii/1359835X9500027Y.

[55] Lin Ye, Zuo Rong Chen, Meng Lu, and Meng Hou. De-consolidation and re-consolidation in CF/PPS thermoplastic matrix composites. *Composites Part A: Applied Science and Manufacturing*, 36(7):915–922, 2005. ISSN 1359835X. doi: 10.1016/j.compositesa.2004.12.006.

[56] Sridhar Ranganathan, Suresh G. Advani, and Mark A. Lamontia. A Non-Isothermal Process Model for Consolidation and Void Reduction during In-Situ Tow Placement of Thermoplastic Composites. *Journal of Composite Materials*, 29(8):1040–1062, may 1995. ISSN 0021-9983. doi: 10.1177/002199839502900803. URL http://journals.sagepub.com/doi/10.1177/002199839502900803.

[57] J. Wolfrath, V. Michaud, and J.-A.E. Månson. Deconsolidation in glass mat thermoplastics: Influence of the initial fibre/matrix configuration. *Composites Science and Technology*, 65(10):1601–1608, aug 2005. ISSN 0266-3538. doi: 10.1016/J.COMPSCITECH.2005.02.001. URL https://www.sciencedirect.com/science/article/pii/S0266353805000527.

[58] Christopher Mark Stokes-Griffin, Paul Compston, Timothy I Matuszyk, and Michael J Cardew-Hall. Thermal modelling of the laser-assisted thermoplastic tape placement process. *Journal of Thermoplastic Composite Materials*, 28(10):1445–1462, oct 2015. ISSN 0892-7057. doi: 10.1177/0892705713513285. URL http://journals.sagepub.com/doi/10.1177/0892705713513285.

[59] F. Yang and Ranga Pitchumani. Interlaminar contact development during thermoplastic fusion bonding. *Polymer Engineering & Science*, 42(2):424–438, feb 2002. ISSN 0032-3888. doi: 10.1002/pen.10960. URL http://doi.wiley.com/10.1002/pen.10960.

[60] J. Wolfrath, V. Michaud, and J. A.E. Månson. Deconsolidation in glass mat thermoplastic composites: Analysis of the mechanisms. *Composites Part A: Applied Science and Manufacturing*, 36(12):1608–1616, dec 2005. ISSN 1359835X. doi: 10.1016/j.compositesa.2005.04.001.

[61] Tjitse K. Slange, L.L. Warnet, Wouter Johannes Bernardus Grouve, and R. Akkerman. Deconsolidation of C/PEEK blanks: on the role of prepreg, blank manufacturing method and conditioning. *Composites Part A: Applied Science and Manufacturing*, 113:189–199, oct 2018. ISSN 1359-835X. doi: 10.1016/J.COMPOSITESA.2018.06.034. URL https://www.sciencedirect.com/science/article/pii/S1359835X18302628.

[62] Mark B. Gruber, Ira Z. Lockwood, Tracy L. Dolan, Steven B. Funck, John J. Tierney, Pavel Simacek, John W. Gillespie Jr, Suresh G. Advani, Brian J. Jensen, Roberto J. Cano, and Others. Thermoplastic in-situ placement requires better impregnated tapes and tows. In *Proceedings of the 2012 SAMPE Conference and Exhibition, Baltimore, MD*, 2012.

[63] Qiuyu Miao, Zhihong Dai, Guangyi Ma, Fangyong Niu, and Dongjiang Wu. Effect of consolidation force on interlaminar shear strength of CF/PEEK laminates manufactured by laser-assisted forming. *Composite Structures*, 266:113779, jun 2021. ISSN 02638223. doi: 10.1016/j.compstruct.2021.113779.

[64] Tjitse K. Slange, Wouter Johannes Bernardus Grouve, Laurent L. Warnet, S. Wijskamp, and Remko Akkerman. Towards the combination of automated lay-up and stamp forming for consolidation of tailored composite components. *Composites Part A: Applied Science and Manufacturing*, 119:165–175, apr 2019. ISSN 1359-835X. doi: 10.1016/J.COMPOSITESA.2019.01.016. URL https://www.sciencedirect.com/science/article/pii/S1359835X19300181.

[65] V. Michaud and J. A. E. Månson. Impregnation of Compressible Fiber Mats with a Thermoplastic Resin. Part I: Theory. *Journal of Composite Materials*, 35(13):1150–1173, jul 2001. ISSN 0021-9983. doi: 10.1177/002199801772662271. URL http://journals.sagepub.com/doi/10.1177/002199801772662271.

[66] Timothy G. Gutowski, Z. Cai, S. Bauer, D. Boucher, J. Kingery, and S. Wineman. Consolidation Experiments for Laminate Composites. *Journal of Composite Materials*, 21(7):650–669, 1987. ISSN 1530793x. doi: 10.1177/002199838702100705.

[67] Timothy G. Gutowski, Tadahiko Morigaki, and Zhong Zhong Cai. The Consolidation of Laminate Composites. *Journal of Composite Materials*, 21(2):172–188, feb 1987. ISSN 0021-9983. doi: 10.1177/002199838702100207. URL http://journals.sagepub.com/doi/10.1177/002199838702100207.

[68] B.R. Gebart. Permeability of Unidirectional Reinforcements for RTM. *Journal of Composite Materials*, 26(8):1100–1133, aug 1992. ISSN 0021-9983. doi: 10.1177/002199839202600802. URL http://journals.sagepub.com/doi/10.1177/002199839202600802.

[69] Z. Cai and A. L. Berdichevsky. An improved self-consistent method for estimating the permeability of a fiber assembly. *Polymer Composites*, 14(4):314–323, 1993. ISSN 15480569. doi: 10.1002/pc.750140407.

[70] Timothy G. Gutowski and G. Dillon. The Elastic Deformation of Lubricated Carbon Fiber Bundles: Comparison of Theory and Experiments. *Journal of Composite Materials*, 26(16):2330–2347, jan 1992. ISSN 0021-9983. doi: 10.1177/002199839202601601. URL http://journals.sagepub.com/doi/10.1177/002199839202601601.

[71] Ebrahim Oromiehie, B. Gangadhara Prusty, Paul Compston, and Ginu Rajan. Automated fibre placement based composite structures: Review on the defects, impacts and inspections techniques, sep 2019. ISSN 02638223.

[72] Diego Saenz-Castillo, María I Martín, Vanessa García-Martínez, Abhiram Ramesh, Mark Battley, and Alfredo Güemes. A comparison of mechanical properties and X-ray tomography analysis of different out-of-autoclave manufactured thermoplastic composites. *Journal of Reinforced Plastics and Composites*, 39(19-20):703–720, oct 2020. ISSN 0731-6844. doi: 10.1177/0731684420924081. URL http://journals.sagepub.com/doi/10.1177/0731684420924081.

[73] Holger Moench and Günther Derra. High Power VCSEL Systems. *Laser Technik Journal*, 11(2):43–47, 2014. doi: 10.1002/latj.201400024.

[74] Khaled Yassin and Mehdi Hojjati. Processing of thermoplastic matrix composites through automated fiber placement and tape laying methods. *Journal of Thermoplastic Composite Materials*, 31(12):1676–1725, dec 2018. ISSN 0892-7057. doi: 10.1177/0892705717738305. URL http://journals.sagepub.com/doi/10.1177/0892705717738305.

[75] Thomas Weiler, Philipp Striet, Annika Voell, Michael Emonts, Jochen Stollenwerk, and Henning Janssen. Tailored irradiation by VCSEL for controlled thermal states in thermoplastic tape placement. In Henry Helvajian, Alberto Piqué, and Bo Gu, editors, *Laser 3D Manufacturing V*, volume 10523, page 15. SPIE, feb 2018. ISBN 9781510615311. doi: 10.1117/12.2291015. URL https://www.spiedigitallibrary.org/conference-proceedings-of-spie/10523/2291015/Tailored-irradiation-by-VCSEL-for-controlled-thermal-states-in-thermoplastic/10.1117/12.2291015.full.

[76] Pavel Simacek, Suresh G. Advani, Mark Gruber, and Brian Jensen. A non-local void filling model to describe its dynamics during processing thermoplastic composites. *Composites Part A: Applied Science and Manufacturing*, 46:154–165, mar 2013. ISSN 1359-835X. doi: 10.1016/J.COMPOSITESA.2012.10.015. URL https://www.sciencedirect.com/science/article/pii/S1359835X1200334X.

[77] Christophe Ageorges, Lin Ye, and Meng Hou. Experimental investigation of the resistance welding of thermoplastic-matrix composites. Part II: optimum processing window and mechanical performance. *Composites Science and Technology*, 60(8):1191–1202, jun 2000. ISSN 02663538. doi: 10.1016/S0266-3538(00)00025-7. URL http://linkinghub.elsevier.com/retrieve/pii/S0266353800000257.

[78] Thomas Weiler. *Thermal Skin Effect in Laser-Assisted Tape Placement of Thermoplastic Composites*. PhD thesis, RWTH Aachen University, Aachen, 2019.

[79] E. T. M. Krämer, Wouter Johannes Bernardus Grouve, S. Koussios, L. L. Warnet, and R. Akkerman. Real-time observation of waviness formation during C/PEEK consolidation. *Composites Part A: Applied Science and Manufacturing*, 133:105872, jun 2020. ISSN 1359835X. doi: 10.1016/j.compositesa.2020.105872.

[80] Danielle Kugler and Tess J. Moon. Identification of the Most Significant Processing Parameters on the Development of Fiber Waviness in Thin Laminates. *Journal of Composite Materials*, 36 (12):1451–1479, jun 2002. ISSN 0021-9983. doi: 10.1177/0021998302036012575. URL http://journals.sagepub.com/doi/10.1177/0021998302036012575.

[81] Bing Zheng, Xiping Gao, Maoyuan Li, Tianzhengxiong Deng, Zhigao Huang, Huamin Zhou, and Dequn Li. Formability and failure mechanisms of woven CF/PEEK composite sheet in solid-state thermoforming. *Polymers*, 11(6), 2019. ISSN 20734360. doi: 10.3390/polym11060966.

[82] Florence Saffar, Camille Sonnenfeld, Pierre Beauchêne, and Chung Hae Park. In-situ Monitoring of the Out-Of-Autoclave Consolidation of Carbon / Poly-Ether-Ketone-Ketone Prepreg Laminate. 7(June):1–12, 2020. doi: 10.3389/fmats.2020.00195.

[83] Mattia Di Francesco, Laura Veldenz, Giuseppe Dell'Anno, and Kevin Potter. Heater power control for multi-material, variable speed Automated Fibre Placement. *Composites Part A: Applied Science and Manufacturing*, 101:408–421, oct 2017. ISSN 1359-835X. doi: 10.1016/J.COMPOSITESA.2017.06.015. URL https://www.sciencedirect.com/science/article/pii/S1359835X17302427.

# Appendix A

# Experiment Settings

This appendix contains the settings applied to the specimens. Table A.1 contains the as-received specimens of the temperature variation series which was performed without repetition of the configurations, the 'low' intimate contact peak temperature specimens are shown in Table A.2, and Table A.3 lists the 'high' intimate contact peak temperature settings. The abbreviations ASR, SLD, and HLD are used for the as-received, slightly laser deconsolidated, and highly laser deconsolidated specimens, respectively.

A description of the laser settings and presented values is provided in Section A.1. In similar fashion, Section A.2, covers the used settings and presented values of the intimate contact development experiment.

## A.1 Laser Settings

The laser deconsolidation phase was carried out with a VCSEL laser, mounted 5 cm parallel above the specimen. The amount of zones, power per zone, and duration of the laser heating could be controlled with the basic software tool. During the experiments, all zones were set to an equal amount of power.

Temperature measurement during the laser deconsolidation was performed by a FLIR thermal camera. The tables report the peak temperature, that is the highest temperature during the heating time, see Figure 5.2. Here, the average temperature is with respect to the tape area from which the specimens will be cut and the maximum temperature was determined by averaging a 3 by 3 pixel grid at the location with the maximum temperature during peak temperature.

Table A.1 does not contain any laser settings since the temperature variation configurations conists of only as-received tape specimens. The laser settings for the as-received specimens are blank in Tables A.2 and A.3 as these were not subjected to the rapid laser deconsolidation experiment.

## A.2 Intimate Contact Experiment Settings

The intimate contact experiment was performed in a RSA-G2 DMTA machine. All configurations used heating and cooling rates of 60 °C/s with start and end temperatures of 25 °C. The tables report the set maximum temperature, the soak time at this temperature and the amount of force to be applied during the experiment. Before the intimate contact experiment, the area was measured, described in Section 4.4.2, based on that measurement and the desired pressure level, the amount of force was determined. Due to some small changes in the threshold for the area measurement, the applied pressure is not exactly at the desired value using the final area measurement method. Note that the report assumes the pressures to be exactly 10, 50, 100, or 300 kPa.

Table A.1: DMTA machine settings per specimen with corresponding peak thermocouple measurement for temperature variation experiments.

| Peak Thermocouple Temperature ˚C | DMTA Settings Temperature ˚C | Soak s | Force N | Measured Area $mm^2$ | Calculated Pressure kPa |
|---|---|---|---|---|---|
| 301 | 350 | 0 | 12.129 | 40.4 | 300.0 |
| 311 | 365 | 0 | 13.860 | 46.2 | 300.0 |
| 331 | 385 | 0 | 13.629 | 45.4 | 300.2 |
| 343 | 400 | 0 | 14.163 | 48.4 | 292.6 |

Table A.2: VCSEL and DMTA machine settings per specimen of the maximum 200 ˚C temperature configurations.

| | Laser Settings | | | Meas Peak Temp | | DMTA Settings | | | Meas | Calc |
|---|---|---|---|---|---|---|---|---|---|---|
| | Zones | Power W | Time ms | Avg ˚C | Max ˚C | Temp ˚C | Soak s | Force N | Area $mm^2$ | Pressure kPa |
| ASR | | | | | | 245 | 20 | 12.648 | 42.5 | 297.8 |
| ASR | | | | | | 245 | 20 | 12.762 | 42.9 | 297.7 |
| ASR | | | | | | 245 | 20 | 11.814 | 39.6 | 298.1 |
| SLD | 1–11 | 286 | 800 | 257.5 | 285.4 | 245 | 20 | 12.846 | 42.8 | 300.0 |
| SLD | 1–11 | 286 | 800 | 280.4 | 332.9 | 245 | 20 | 13.851 | 46.2 | 300.0 |
| SLD | 1–11 | 286 | 800 | 263.4 | 291.1 | 245 | 20 | 13.794 | 46.0 | 300.0 |
| HLD | 1–11 | 550 | 800 | 459.6 | 529.5 | 245 | 20 | 13.785 | 45.9 | 300.0 |
| HLD | 1–11 | 550 | 800 | 511.4 | 563.7 | 245 | 20 | 13.443 | 44.8 | 300.0 |
| HLD | 1–11 | 550 | 800 | 458.4 | 520.5 | 245 | 20 | 13.104 | 43.7 | 300.0 |

Table A.3: VCSEL and DMTA machine settings per specimen of the maximum 363 °C temperature configurations.

| | Laser Settings | | | Meas Peak Temp | | DMTA Settings | | | Meas | Calc |
|---|---|---|---|---|---|---|---|---|---|---|
| | Zones | Power | Time | Avg | Max | Temp | Soak | Force | Area | Pressure |
| | | W | ms | °C | °C | °C | s | N | $mm^2$ | kPa |
| ASR | | | | | | 400 | 20 | 0.4275 | 43.0 | 9.9 |
| ASR | | | | | | 400 | 20 | 0.4570 | 46.0 | 9.9 |
| ASR | | | | | | 400 | 20 | 0.4574 | 46.0 | 9.9 |
| SLD | 1–11 | 286 | 800 | 272.2 | 324.3 | 400 | 20 | 0.4485 | 45.0 | 10.0 |
| SLD | 1–11 | 286 | 800 | 281.8 | 305.6 | 400 | 20 | 0.4270 | 42.9 | 10.0 |
| SLD | 1–11 | 286 | 800 | 295.8 | 329.0 | 400 | 20 | 0.4418 | 44.2 | 10.0 |
| HLD | 1–11 | 550 | 800 | 445.3 | 505.6 | 400 | 20 | 0.4469 | 45.0 | 9.9 |
| HLD | 1–11 | 550 | 800 | 446.7 | 513.4 | 400 | 20 | 0.4266 | 42.8 | 10.0 |
| HLD | 1–11 | 550 | 800 | 394.9 | 447.6 | 400 | 20 | 0.4570 | 45.7 | 10.0 |
| ASR | | | | | | 400 | 20 | 2.0720 | 41.6 | 49.8 |
| ASR | | | | | | 400 | 20 | 2.2905 | 46.1 | 49.7 |
| ASR | | | | | | 400 | 20 | 2.2645 | 45.8 | 49.4 |
| SLD | 1–11 | 286 | 800 | 291.0 | 326.6 | 400 | 20 | 2.3310 | 46.6 | 50.0 |
| SLD | 1–11 | 286 | 800 | 231.5 | 268.5 | 400 | 20 | 2.2975 | 46.0 | 50.0 |
| SLD | 1–11 | 286 | 800 | 296.2 | 317.0 | 400 | 20 | 2.3805 | 47.6 | 50.0 |
| HLD | 1–11 | 550 | 800 | 496.0 | 548.8 | 400 | 20 | 2.1675 | 43.5 | 49.9 |
| HLD | 1–11 | 550 | 800 | 476.6 | 565.3 | 400 | 20 | 2.1775 | 43.7 | 49.8 |
| HLD | 1–11 | 550 | 800 | 484.5 | 566.2 | 400 | 20 | 2.2135 | 44.4 | 49.9 |
| ASR | | | | | | 400 | 20 | 4.5160 | 46.5 | 97.0 |
| ASR | | | | | | 400 | 20 | 4.4920 | 45.4 | 98.9 |
| ASR | | | | | | 400 | 20 | 4.2720 | 43.0 | 99.4 |
| SLD | 1–11 | 286 | 800 | 241.1 | 285.4 | 400 | 20 | 4.5930 | 46.1 | 99.7 |
| SLD | 1–11 | 286 | 800 | 245.8 | 296.9 | 400 | 20 | 4.3830 | 44.0 | 99.7 |
| SLD | 1–11 | 286 | 800 | 272.1 | 293.9 | 400 | 20 | 4.7270 | 45.1 | 104.8 |
| HLD | 1–11 | 550 | 800 | 452.8 | 483.9 | 400 | 20 | 4.2260 | 42.3 | 100.0 |
| HLD | 1–11 | 550 | 800 | 505.9 | 556.9 | 400 | 20 | 4.5100 | 45.2 | 99.7 |
| HLD | 1–11 | 550 | 800 | 506.0 | 561.8 | 400 | 20 | 4.3500 | 43.6 | 99.7 |
| ASR | | | | | | 400 | 20 | 13.5120 | 45.3 | 298.0 |
| ASR | | | | | | 400 | 20 | 12.9570 | 43.7 | 296.8 |
| ASR | | | | | | 400 | 20 | 12.2550 | 41.1 | 297.9 |
| SLD | 1–11 | 286 | 800 | 272.0 | 341.1 | 400 | 20 | 14.1810 | 47.4 | 299.0 |
| SLD | 1–11 | 286 | 800 | 268.3 | 321.2 | 400 | 20 | 13.0320 | 43.6 | 298.9 |
| SLD | 1–11 | 286 | 800 | 286.1 | 324.0 | 400 | 20 | 13.2450 | 44.3 | 298.9 |
| HLD | 1–11 | 550 | 800 | 479.0 | 516.1 | 400 | 20 | 12.9240 | 43.2 | 299.2 |
| HLD | 1–11 | 550 | 800 | 436.8 | 498.0 | 400 | 20 | 13.0650 | 43.7 | 299.0 |
| HLD | 1–11 | 550 | 800 | 505.6 | 528.2 | 400 | 20 | 12.3870 | 41.4 | 299.1 |

# Appendix B

# Emissivity Calibration

This appendix shows how the emissivity for the FLIR A655sc thermal camera was obtained. Similar to the ASTM E1933 standard, the laser was used to heat two separate spot by enabling zones 5, 6, 10, and 11. A K-type thermocouple was attached to the heated area on the left using an ultrasonic spot welder with a small piece of Kapton tape in between, Figure B.1 shows the size of Kapton tape that was used to cover the thermocouple. The heated area on the CF/PEEK tape at the right hand side was left untouched as reference measurement of the thermal camera. The left and right heated areas are within the two Kapton tapes used to attach the CF/PEEK tape onto the tool as is indicated in Figure B.1. From the thermal camera reading, the 3x3 pixel averaged maximum temperature is used for the reading. The thermocouple measurement and thermal camera measurement were then matched by tuning the emissivity value.

Additionally, the distance to object was set to 0.25 m and the other settings kept at factory level: the reflected object, atmosphere, and external objects temperatures and at 20 °C, the relative humidity of the atmosphere at 50 %, the atmosphere transmission at 0.99, and the external object transmission to 1.00.

At higher temperatures, near and above the melting point, the thermocouple sometimes detached from the CF/PEEK tape and the temperature variation between the left and right areas increased. Therefore, the laser power was lowered to 200 W for 500 ms, at which point the thermocouple did not detach anymore and the left and right area temperatures seemed to be more consistent. This resulted in temperatures around 200 °C which is significantly lower than the temperatures experienced by the highly laser deconsolidated samples. It is assumed that the emissivity of the material will not change significantly between 200 and 470–530 °C.

The average from five repetitions was used as final emissivity value which is 0.80 with the individual measurements ranging from 0.768 to 0.846. The individual measurement curves are shown in Figure B.2. The thermocouple measurement in Figure B.2c follows the thermal camera reading better than the other measurements. It is not known why the other measurements, Figures B.2a, B.2b, and B.2d, under-represent the temperature during heating and over-represent the temperature during cooling.

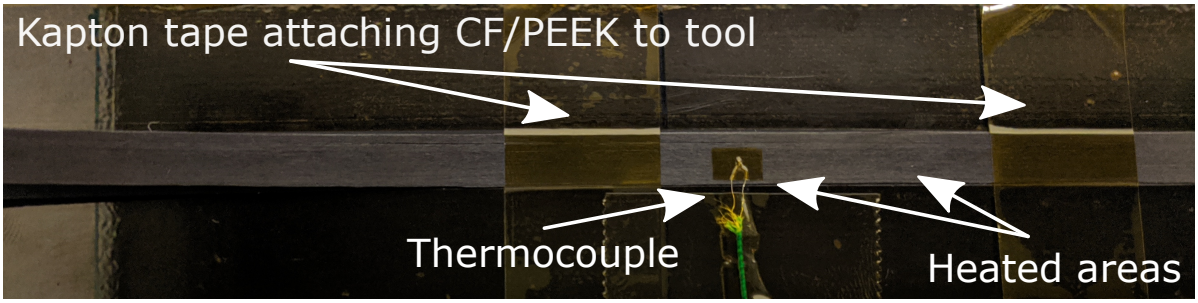


Figure B.1: Thermocouple attachment to CF/PEEK tape.

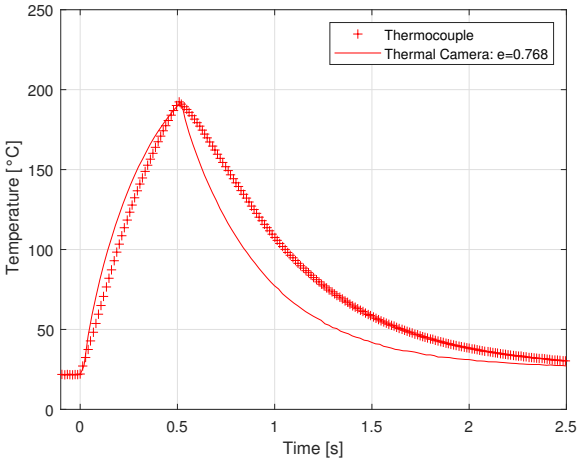


(a) Emissivity 0.768

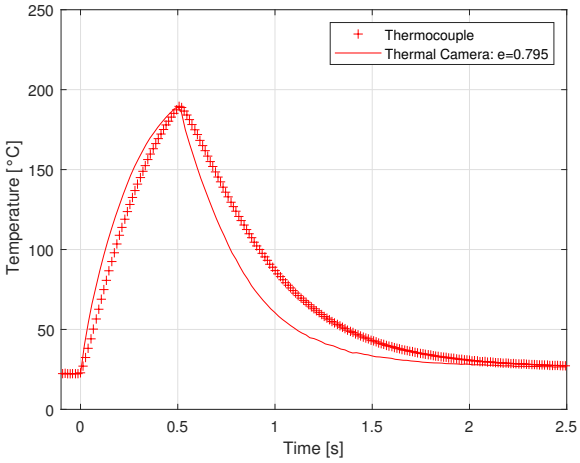


(b) Emissivity 0.795

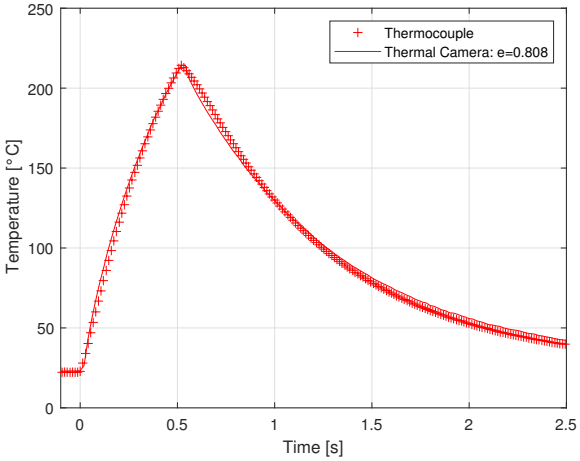


(c) Emissivity 0.808

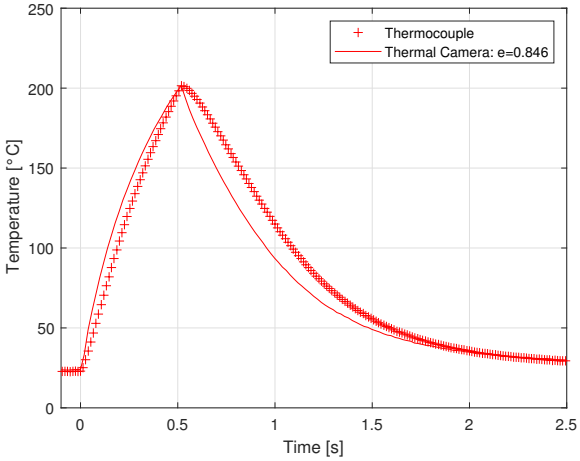


(d) Emissivity 0.846

Figure B.2: Emissivity calibration curves, repeated four times, of thermocouple measured zone and thermal camera zone, emissivity tuned to match peak temperature.

Using the same procedure, except for the ultrasonic welding step, Choudhary [49] obtained an emissivity of 0.84 for half inch CF/PEEK tape from the same supplier. In that experiment, temperatures above melt were reached, the thermocouple and thermal camera temperature are aligned well similar to the measurement in Figure B.2c, but it is unclear which camera to object distance was used. The results in Figure B.2 used a 0.25 m distance as explained in Section 4.2.2. Choudhary [49] obtained an emissivity value of 0.855 for quarter inch CF/PEKK and Çelik et al. found an emissivity of 0.85 for that material at 220 °C which should perform similar to CF/PEEK. Based on these publications it is assumed that the emissivity of CF/PEEK is constant. Di Francesco et al. [83] obtained an emissivity of 0.80 for CF/PEEK using the ASTM E1933 methodology with the thermal camera placed 0.3 m away, at a 20 deg angle, evaluated between 350–450 °C.